

Micelles and Interpolyelectrolyte Complexes formed  
by Polyisobutylene-*block*-Poly([meth]acrylic acid) -  
Synthesis of Polymers and Characterization in  
Aqueous Solutions

Dissertation

zur Erlangung des akademischen Grades eines Doktors der  
Naturwissenschaften (Dr. rer. nat.) in der Fakultät für Biologie,  
Chemie und Geowissenschaften der Universität Bayreuth

vorgelegt von  
Markus Burkhardt  
aus Coburg

Bayreuth, Juni 2007

Wenn wir alles erforschen,  
werden wir die Wahrheit manchmal da finden,  
wo wir sie am wenigsten erwarten.

Quintillian

für meine Familie

Die vorliegende Arbeit wurde in der Zeit von August 2003 bis Juni 2007 in Bayreuth am Lehrstuhl Makromolekulare Chemie II unter der Betreuung von Herrn Prof. Dr. Axel H. E. Müller in Zusammenarbeit mit dem Stranski Laboratorium, Institut für Chemie, Technische Universität Berlin unter der Betreuung von Herrn Prof. Dr. Michael Gradzielski angefertigt.

Vollständiger Abdruck der von der Fakultät für Biologie, Chemie und Geowissenschaften der Universität Bayreuth zur Erlangung des akademischen Grades eines Doktors der Naturwissenschaften genehmigten Dissertation.

Dissertation eingereicht am: 28. Juni 2007

Zulassung durch die Promotionskommission: August 2007

Wissenschaftliches Kolloquium: 03. Dezember 2007

Amtierender Dekan: Prof. Dr. Axel Müller

Prüfungsausschuss:

Prof. Dr. A. H. E. Müller (Erstgutachter, Universität Bayreuth)

Prof. Dr. M. Gradzielski, (Zweitgutachter, Stranski Laboratorium, Institut für Chemie, Technische Universität Berlin)

Prof. Dr. H. Alt (Prüfungsvorsitzender, Universität Bayreuth)

Prof. Dr. K.-H. Seifert (Universität Bayreuth)

# CONTENTS

1. <i>Introduction</i> . . . . .	8
1.1 Cationic Polymerization . . . . .	9
1.1.1 General Concepts of Controlled/Living Cationic Polymerization	9
1.1.2 Monomers . . . . .	12
1.1.3 Initiating Systems . . . . .	12
1.1.4 Solvents . . . . .	13
1.1.5 Additives . . . . .	13
1.2 Anionic Polymerization . . . . .	14
1.2.1 General Concepts of Controlled/Living Anionic Polymerization	14
1.2.2 Monomers . . . . .	15
1.2.3 Initiators . . . . .	15
1.2.4 Additives . . . . .	17
1.2.5 Combination of Living Cationic and Living Anionic Polymer- ization . . . . .	17
1.3 Architectures of Copolymers . . . . .	18
1.4 Solution Behavior of Amphiphilic Block Copolymers . . . . .	18
1.4.1 Characterization of Block Copolymers in Solution . . . . .	20
1.4.2 Complexation of PIB <sub>x</sub> - <i>b</i> -PMAA <sub>y</sub> . . . . .	22
1.4.3 Decomposition of PIB <sub>x</sub> - <i>b</i> -PMAA <sub>y</sub> based Complexes . . . . .	23
2. <i>Aim and Strategy</i> . . . . .	24
3. <i>Overview of the Thesis</i> . . . . .	25
3.1 Polyisobutylene- <i>block</i> -poly(methacrylic acid) Diblock Copolymers: Self- Assembly in Aqueous Media . . . . .	25
3.2 Water-Soluble Interpolyelectrolyte Complexes of Polyisobutylene- <i>block</i> - Poly(methacrylic acid) Micelles: Formation and Properties . . . . .	28
3.3 Aqueous Solutions of Polyisobutylene- <i>block</i> -Poly(acrylic acid) Diblock Copolymers: Path Dependent Formation of Non-Equilibrium Assem- blies . . . . .	31
3.4 Individual Contributions to Joint Publications . . . . .	33
4. <i>Experimental Part and Methods</i> . . . . .	35
4.1 Materials . . . . .	35
4.1.1 Cationic Polymerization . . . . .	35
4.1.2 Anionic Polymerization . . . . .	35
4.1.3 Preparation of Solutions . . . . .	36
4.2 Cationic Polymerization . . . . .	36
4.3 Anionic Polymerization . . . . .	36
4.4 Synthesis of Polycation . . . . .	37
4.5 Hydrolysis of PIB <sub>x</sub> - <i>b</i> -PtBMA <sub>y</sub> and PIB <sub>x</sub> - <i>b</i> -PtBA <sub>y</sub> . . . . .	38

---

4.6	Preparation of Micelles and Complexes . . . . .	38
4.7	Light Scattering . . . . .	38
4.7.1	Static Light Scattering (SLS)[70, 71] . . . . .	39
4.7.2	Refractive Index Increment $dn/dc$ . . . . .	42
4.7.3	Dynamic Light Scattering (DLS) . . . . .	42
4.8	Small Angle Neutron Scattering (SANS) . . . . .	44
4.9	Potentiometric Titration . . . . .	48
4.10	Flourescence Measurements . . . . .	48
4.11	UV-Vis-Spectroscopy . . . . .	49
4.12	Cryogenic Transmission Electron Microscopy (Cryo-TEM)[94] . . . . .	49
5.	<i>PIB<sub>x</sub>-b-PMAA<sub>y</sub> Diblock Copolymers: Self-Assembly in Aqueous Media</i> . . . . .	55
5.1	Introduction . . . . .	56
5.2	Experimental Part . . . . .	58
5.2.1	Materials . . . . .	58
5.2.2	Methods . . . . .	58
5.3	Results and Discussion . . . . .	61
5.3.1	Determination of cmc . . . . .	61
5.3.2	Potentiometric Titration . . . . .	63
5.3.3	Cryo-TEM . . . . .	66
5.3.4	Dynamic Light Scattering . . . . .	68
5.3.5	Static Light Scattering . . . . .	71
5.3.6	Small Angle Neutron Scattering . . . . .	75
5.4	Conclusion . . . . .	83
5.5	Supporting Information . . . . .	87
5.5.1	Synthesis . . . . .	87
6.	<i>Water-Soluble IPECs of PIB<sub>x</sub>-b-PMAA<sub>y</sub> Micelles: Formation and Properties</i> 90	
6.1	Introduction . . . . .	91
6.2	Experimental Part . . . . .	93
6.2.1	Materials . . . . .	93
6.2.2	Sample Preparation . . . . .	94
6.2.3	Methods . . . . .	95
6.3	Results and Discussion . . . . .	97
6.3.1	Complexation . . . . .	97
6.3.2	Salt-Induced Dissociation of Complexes . . . . .	106
6.4	Conclusion . . . . .	111
7.	<i>Solutions of PIB-b-PAA: Formation of Non-Equilibrium Assemblies</i> . . . . .	116
7.1	Introduction . . . . .	118
7.2	Experimental Part . . . . .	119
7.2.1	Materials . . . . .	119
7.2.2	Methods . . . . .	120
7.3	Results and Discussion . . . . .	121
7.3.1	Cryo-TEM of CsCl-solutions . . . . .	121
7.3.2	Small Angle Neutron Scattering . . . . .	123
7.3.3	Dynamic Light Scattering . . . . .	124
7.3.4	Cryo-Transmission Electron Microscopy of H <sub>2</sub> O/NaCl-solutions	127
7.3.5	Influence of Solvent and Counterion . . . . .	129

---

7.3.6	Comparison to $\text{PIB}_x\text{-}b\text{-PMAA}_y$ . . . . .	130
7.4	Conclusion . . . . .	130
8.	<i>Summary / Zusammenfassung</i> . . . . .	134
9.	<i>Acknowledgment</i> . . . . .	140
10.	<i>List of Publications</i> . . . . .	141

## 1. INTRODUCTION

Amphiphilic block copolymers are of great interest in various research fields. Due to the large variety of different monomers for the blocks, materials with tailored properties like responsiveness to changes in pH, temperature or ionic strength can be easily obtained [1]. Nowadays different controlled polymerization techniques, e.g. radical, anionic or cationic methods are used to design polymers. Also combinations of them aiming at di-, tri- or even multi-block copolymers can be utilized to combine different properties of monomers, that are not polymerizable by one technique. Industry is interested in amphiphilic block copolymers due to their use as lubricants [2], e.g. for oil drilling, as well as in pharmaceuticals or as carriers for drugs [3]. Also the use as micro- or nanocontainers for reactions as applied for surfactant systems [4] is reported very frequently. Especially polymers based on weak polyelectrolytes such as poly(acrylic acid) (PAA) or poly(methacrylic acid) (PMAA) have attracted attention due to the ability to influence the system strongly upon changes in pH and ionic strength of the solution [5].

Therefore an insight into the effect of the block lengths of stimuli-responsive block copolymers on properties and the structure of the polymeric assemblies in aqueous solutions is desirable. Several reports describing the micellization of block copolymers obtained via sequential living anionic polymerization with a hydrophobic polystyrene (PS) block and properties of the resulting micelles have been published. In pure aqueous solutions these polymers appear to exist in a non-dynamic or "frozen" state [6], as the glass transition temperature of PS is  $T_g = 104^\circ\text{C}$ . These frozen aggregates recover their dynamic behavior in water-dioxane mixtures. For aqueous polymer solutions with aggregates, which should behave dynamic, block copolymers with a hydrophobic block with a  $T_g$  below room temperature (RT) are of great interest. In this work we have used polyisobutylene (PIB) as the hydrophobic part. The polymers were synthesized via living cationic polymerization and end-capped with thiophene [7]. The PIB macroinitiator was then used to initiate the anionic polymerization of *t*-butyl-methacrylate (*t*BMA) and *t*-butyl-acrylate (*t*BA). After hydrolysis of the *t*-butyl groups resulting in (meth)acrylic acid moieties, the block copolymers were dissolved in aqueous media and the formed assemblies were characterized above the *cmc* by means of DLS, SLS, SANS and cryo-TEM. In this work the properties of assemblies formed by block copolymers of different block length ratios are reported and compared to those formed by similar block copolymers studied by Pergushov *et al.* [8, 9] and Schuch *et al.* [10].

Additionally complexation of the negative charges on the polymer chain is possible. Several attempts are reported to obtain polyelectrolyte complexes (PECs) of homopolymers with oppositely charged surfactants [11, 12]. Babak *et al.* reported on chitosan capsules stabilized by a shell formed by an electrostatic complex. The complex is formed by chitosan as a semi rigid positively charged polyelectrolyte and sodium dodecyl sulfate (SDS) as anionic surfactant. They report that the shell con-

sists of a network containing anionic surfactant micelles that somehow can cross-link the cationic polymer chains.

Also special architectures like brushes were investigated [13]. Except for surfactants, also complexes with enzymes [14] or DNA [15] and their possible applications as carriers were reported [16]. Another attempt is to form complexes containing polyelectrolytes with opposite charges. Several groups report on complexation phenomena between homopolymers, resulting in interpolyelectrolyte complexes (IPECs). Especially the layer-by-layer approach for homopolymers [17] and even micelles [18] are of interest.

In the last few years, the formation of complexes of amphiphilic block copolymers and homo polyelectrolytes as well as block copolymers has attracted more and more attention. Especially the complexation of linear amphiphilic diblock copolymers with oppositely charged polymers (synthetic and natural ones) is interesting for drug delivery and drug release. In this work we investigate the complexes formed by micelles consisting of polyisobutylene-*b*-poly(methacrylic acid) (PIB<sub>*x*</sub>-*b*-PMAA<sub>*y*</sub>) and positively charged poly(N-ethyl-4-vinylpyridinium bromide) (P4VPQ) [8, 9].

Additionally, the investigations were extended to a new block copolymer based on PIB, namely polyisobutylene-*b*-poly(acrylic acid) (PIB<sub>*x*</sub>-*b*-PAA<sub>*y*</sub>). This polymer was intended to have properties comparable to those of PIB<sub>*x*</sub>-*b*-PMAA<sub>*y*</sub>). Especially the influence of the missing methyl group within the polyelectrolyte chain on the structure and properties is interesting. Up to now, already investigation on differences of the two homopolymers, PAA and PMAA, with respect to potentiometric titrations were reported. It turned out that the methyl group slightly changes the behavior, as a kink in the pH titration curve was observed, which is explained by a change in the conformation of the chain due to hydrophobic interactions. Furthermore, Colombani *et al.* [19] investigated an interesting behavior of their system. They investigated the salt dependence of poly(*n*-butyl acrylate)-*block*-poly(acrylic acid) (P*n*BA-*b*-PAA). They found out, that depending on the point of time of addition of salt to their polymer and polymer solution, respectively, different micellar assemblies were formed in aqueous solutions. They explained it with a partially frozen system, that can equilibrate in the absence of salt. Upon addition of salt, the requirement of equilibrium structure, the exchange of unimers between micelles is at least partially hindered. Therefore, in this work we investigated the influence of a change of the hydrophobic block from P*n*BA to PIB. The results obtained are compared to the results from Colombani.

In the following sections, the basics of the different techniques used for polymerization of the diblock copolymers investigated in this work as well as the characterization techniques applied during this work are explained.

## 1.1 Cationic Polymerization

### 1.1.1 General Concepts of Controlled/Living Cationic Polymerization

For polymerizations of monomers like isobutylene (IB) there exist different steps having their own characteristic rate constants (Figure 1.1). Besides propagation there is always a certain probability that the living chain ends undergo side reactions like transfer (Figure 1.2) or termination. The probability of these unwanted reactions depends on the ratio of rate constants of the side reactions and the propagation.

These ratios also define whether a polymerization is controlled and living or just a normal cationic polymerization.

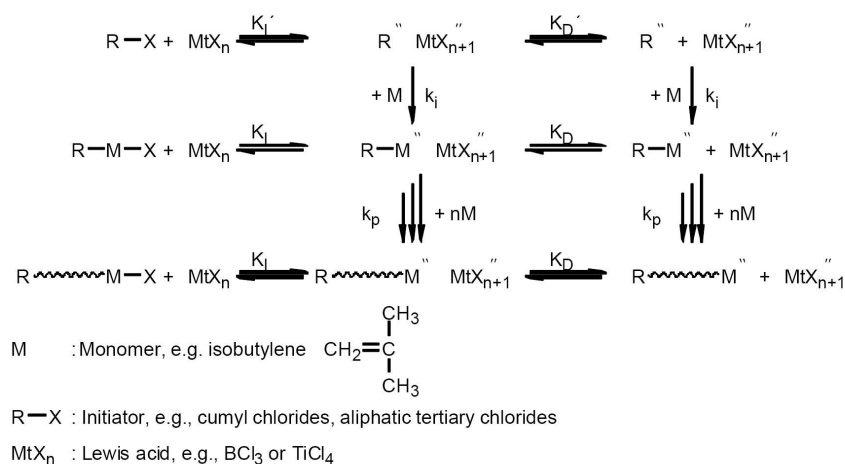


Fig. 1.1: Reactions and the respective rate constants observed in living cationic polymerizations, including initiation, propagation, dissociation and equilibrium with dormant species.

An important issue of cationic polymerization is the understanding of the way of incorporation of monomer in the growing polymer chain during propagation, assuming ideal conditions. A dynamic equilibrium between inactive (dormant) and active species (Fig 1.1) is the proposed mechanism, when the basic experimental/kinetic facts are considered [20]. This equilibrium can be influenced by cocatalyst and solvent as discussed later. If the equilibrium between the active and inactive species is neglected, this scheme also includes the "ideal" living polymerization. It is impossible to distinguish between the two ways of living polymerizations, if the rates of exchange between active and inactive species are much higher than the rate of propagation. The rate of propagation for ideal living polymerizations and polymerizations with reversible termination is expressed by the following equations:

$$R_p = k_{app}[M] = k_p[P^*][M],$$

$$\text{in "ideal" case } [P^*] = [I]_o$$

and with reversible termination:

$$P' + C \rightleftharpoons P^* \Rightarrow K_I = P^*/(P' \cdot C),$$

taking the following assumptions into account:

$$P^* \ll P', P' \approx I_o, C \approx C_o \approx [MtX_n]_o \Rightarrow K_I = P^*/(I_o \cdot C_o),$$

$$[P^*] \approx K_I[MtX_n]_o[I]_o \text{ (neglecting dissociation of ion pairs),}$$

where  $[P^*]$  is the concentration of living chain ends,  $[P']$  the concentration of dormant chain ends,  $[I]_o$  the initial initiator concentration,  $[C]_o = [MtX_n]_o$  the initial catalyst concentration, and  $K_I$  the equilibrium constant of ionization. As the number of polymer chains during polymerization ( $[P] = [I]_o$ ) is constant,  $DP_n$  does not depend on it. The equilibrium between inactive and active species is usually stronger shifted toward the inactive species ( $K_I \ll 1$ ). This can be stated by the fact of a chlorine end group instead of a methoxy end group when quenching a polymerization of isobutylene with methanol in the presence of electron donors [21].

Transfer can occur to monomer, to transfer agent or as a spontaneous transfer

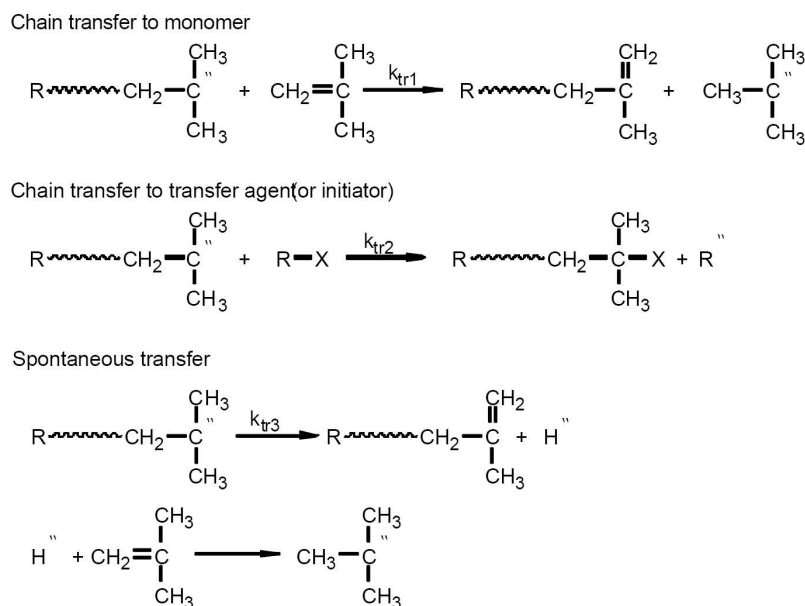


Fig. 1.2: Possible transfer reactions and rate constants observed in cationic polymerizations.

due to elimination of a proton at the chain end (Figure 1.2). In all cases the ionicity of the chain end is important. The latter two types of transfer reactions can be diminished by addition of electron donors. In the case of transfer to monomer one can distinguish between three different transfer reactions [22]. It was also shown with isobutylene that temperature has an important effect on these reactions. Also solvent and additives control the kinetics of these reactions.

Quenching of a reaction is a convenient way to introduce different functionalities onto the end of the polymer chain. For example with methanol the Lewis acid can be deactivated, leading to a chlorine end group.  $\text{Mt}(\text{OR})_n$  is a much weaker acid than  $\text{MtCl}_n$ . Therefore, after the formation of  $\text{Mt}(\text{OR})_n$  the degree of ionization of the chain end is very low, the probability of propagation also lowers toward zero. In our case, end functionalization was carried out with thiophene [7]. Martinez-Castro *et al.* reported, that a huge excess of thiophene is necessary to obtain end capped polymer with a still accessible proton in 5-position. Otherwise coupling occurs, leading to doubling of molecular weight of polymer, which cannot be further used as a macroinitiator.

An important feature of living cationic polymerization is the distance of the charge and the counterion at the reaction center both in the ion generating and propagating step. The Winstein spectrum (Figure 1.3) is frequently used to elucidate the different kinds of propagating species which can exist in such a polymerization system. One important aspect considering the equilibria is that the rates of exchange between the species have a strong effect on the MWD of the end product [23]. Concerning initiation, total control is achieved if it is performed only by the added initiator and not by moisture or impurities. If more than one type of initiator is present, Poisson MWD can not be attained, instead a broadening or even a multimodal MWD will appear. Therefore, it is important to work under extremely pure conditions. This can even be improved by additives, as discussed later. Fur-

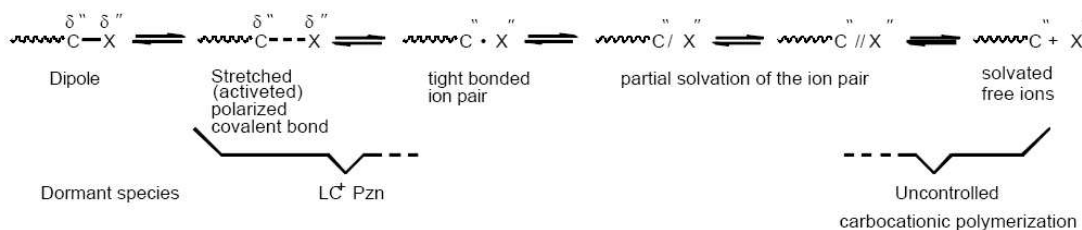


Fig. 1.3: Possible intermediate states that are important in cationic polymerizations.

thermore, initiation has to be fast, at least comparable to propagation, if narrow MWD is desired [21, 24].

### 1.1.2 Monomers

Isobutylene can only be polymerized by cationic polymerization. Besides olefins, also vinyl ethers can be used. The requirement for polymerization is to develop a carbocation which can be sufficiently stabilized. In addition to the site of polymerization, a monomer can be functionalized with certain groups [25], as it will be discussed later. Cationic ring-opening polymerization is another opportunity to polymerize monomers like THF and ethylene oxide.

Since the polymers prepared in this project are planned to be used as amphiphilic AB block copolymers, the second monomer should be hydrophilic or even ionic. This makes it impossible to obtain the block copolymer just with living cationic polymerization, as monomers like (meth)acrylates cannot be used. This is due to the ester group, as they can not stabilize a cation at the chain end. In addition, oxygen atoms of the ester group are also known to complex the Lewis acid. This will deactivate the metal compound, leading to termination. To overcome this problem, the block copolymers have to be prepared from PIB macroinitiators using anionic polymerization for the second monomer.

### 1.1.3 Initiating Systems

For a good control of the living cationic polymerization, besides the choice of the solvent (discussed later), initiator and cocatalyst are the most important part of the system. For a narrow MWD ( $PDI < 1.2$ ), the rate of initiation has to be higher than the rate of propagation. Therefore the right system has to be chosen, according to the monomer and the solvent used. In Figure 1.4 common initiators for the living cationic polymerization of isobutylene are shown.

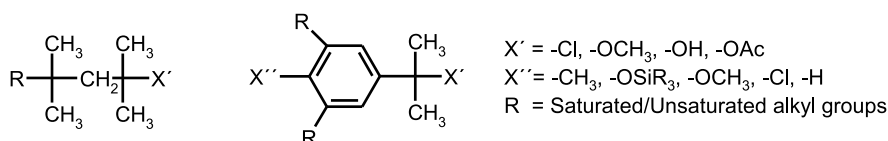


Fig. 1.4: Different initiators used for cationic polymerization of isobutylene.

In the case of the cumyl type initiators, mono-, di- and trifunctional ones are frequently used, which makes it possible to synthesize linear AB, ABA or star-shaped  $(AB)_3$  block copolymers [21]. Lewis acids as  $TiCl_4$ ,  $BCl_3$ ,  $AlCl_3$ ,  $SnCl_4$  or Zn halides are used as coiniciators [26]. The right selection of Lewis acids depends on different factors like the monomer, the  $M_n$  of the polymer and the solvent, since its acidity affects the ionization equilibrium between inactive and active species (cf. Figure 1.1). In this work  $TiCl_4$  was used as a coiniciator for the polymerization of isobutylene.

#### 1.1.4 Solvents

The choice of solvents is restricted to a few possibilities in living cationic polymerization of isobutylene. Besides the solubility of the polymer, the influence of the solvent polarity on the ionization equilibrium of the initiator and the living chain end (see Figure 1.1) and on the kinetics and the livingness of the polymerization has to be considered.  $CH_2Cl_2$  and a mixture of  $CH_2Cl_2$  : *n*-hexane (40:60 *v/v* %) are often used to obtain polymers with a narrow MWD. The main problem with  $CH_2Cl_2$  is a relatively high concentration of moisture (about  $10^{-3}$  M). This problem can be reduced with the use of a proton trap, as discussed later. As already mentioned, the resulting polymer should be soluble during polymerization to maintain a constant concentration of the propagating species. It is known, that PIBs with a  $M_n > 2500-3000 \frac{g}{mol}$  start to precipitate in pure  $CH_2Cl_2$ , followed by a loss of control of the reaction. *n*-hexane on the other hand can be used to dissolve PIB polymers with high molecular weight. In addition, *n*-hexane shifts the equilibrium between inactive and active species toward the inactive one. Therefore a strong Lewis acid like  $TiCl_4$  must be used for polymerizations in these mixtures of solvents.

Changes from a non-polar to a polar solvent or vice versa have remarkable effects on the kinetics of the living cationic polymerization due to shifts of the equilibria shown in Figure 1.1. The rate of propagation as well as the rate of initiation are both proportional to the respective ionization constant ( $R_p \propto k_p \cdot K_I$ ,  $R_i \propto k_i \cdot K'_I$ ). There are reports on experiments with vinyl ethers [27] showing that the apparent rate constant in  $CH_2Cl_2$  is 40 times higher than in  $CH_2Cl_2$ :*n*-hexane (1:9).

As mentioned above, solvents also have an effect on the MWD. A broader MWD is obtained in a non-polar solvent [28] because  $K_I$  and  $K'_I$  are influenced by the polarity to a different extent in this case. It is reported by Sawamoto *et al.* that by changing the solvent, the kinetics can be modified even with respect to reaction orders in monomer [29]. The reaction order of different vinyl ethers is of zeroth order in *n*-hexane and first order in toluene or  $CH_2Cl_2$ . This can be explained by interactions of the vinyl ether monomer and the solvent with the living chain, leading to changes in the polymerization mechanism.

#### 1.1.5 Additives

Besides electron donors for the reduction of the rate constants of propagation and transfer/termination (not used in this work), proton traps are a second type of additives added to the cationic polymerization system in order to improve the control of the polymerization. The effect is not attributed to stabilization of the propagating species as it is with electron donors but to scavenging of protons [30, 31]. Proton

traps normally are strong bases (pyridine derivatives, used in this work: 2,6-di-tert-butyl pyridine (DtBP)) which only reacts with acidic protons and not with other electrophiles. Quantitative results concerning this topic have been published [32]. The conclusion is that the alkyl groups in the 2- and 6-position have to be *t*-butyl if the rate constant of the reaction with other electrophiles shall be suppressed to an acceptable level. DtBP, a sterically hindered pyridine derivative is used in the same concentration which must be expected in regard to adventitious moisture in  $\text{CH}_2\text{Cl}_2$  ( $\approx 10^{-3}$  M).

Another way to tune the polymerization is the addition of salts. This leads to narrower MWD, but the concentration of the salt has to be kept in a certain range. Otherwise the occurrence of a bimodal MWD is reported [33]. Upon addition of salts the ionic strength of the media is changed, leading to shifts in the Winstein spectrum toward the inactive species, lowering the rate of propagation and also the rates of side-reactions [33, 34].

## 1.2 Anionic Polymerization

### 1.2.1 General Concepts of Controlled/Living Anionic Polymerization

Living anionic polymerization is known to be extremely sensitive to moisture. With real living reactions, molecular weights up to millions can be reached. The huge amount of different monomers makes it possible to apply living anionic polymerization to multiple systems, depending on the initiator, the counterion as well as solvents and additives.

In Figure 1.5 the stabilization of the occurring anion during the polymerization of an acrylic monomer is shown. The polar, electron withdrawing side-group activates the monomer. At the same time the opportunity of delocalization of the anionic charge stabilizes the carbanion due to the formation of an ester enolate. In Figure 1.5

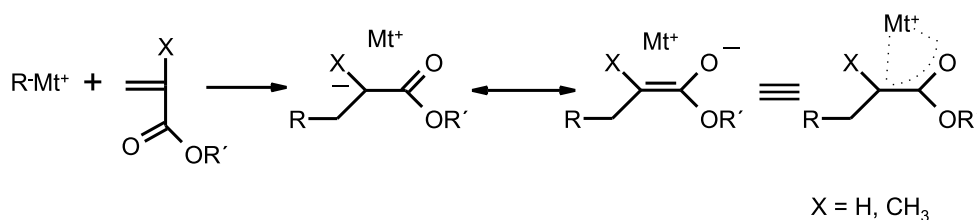


Fig. 1.5: Mesomeric structures existing in anionic polymerization of (meth)acrylates.

the two extreme cases - the enolate and the carboxylate - are shown on the right side; the real structure with delocalized  $\pi$ -electrons is in between.

As already explained during cationic polymerization (Figure 1.3), depending on the polarity of the solvent, the additives and the counterions, ion pair, solvated ion pairs, free anions, and associated ion pairs can be found. For making sure to have a real living polymerization, a fast exchange between the species in equilibrium is necessary. This should - as in cationic polymerization - be fast compared to the rate of propagation [35]. Otherwise side reactions can occur, leading to worse control of the reaction and causing a broadening of MWD. Again, equilibria may be influenced by additives (e.g. salts, and ligands) [36].

Another important point is the composition of the system used for the polymerization. Depending on the type of solvent (polar like THF, DME, THP or non-polar like toluene, benzene, hexane) and type of monomer (polar like (meth)acrylates or ethyleneoxide or non-polar like styrene or butadiene) different reaction parameters have to be set. For example the solvent has a big influence on the tacticity and the stereochemistry of the polymer [37] and therefore on its properties.

In this project polar monomers like *t*BMA and *t*BA are polymerized in THF. For such a system free anions, contact ion-pairs, and aggregates coexist [38]. The rate of propagation here is much higher for the free anions than for the other two chain ends ( $k_p^{(-)} \gg k_p^{(\pm)} \gg k_p^{agg}$ ).

### 1.2.2 Monomers

Living anionic polymerization can be used to polymerize different kinds of monomers [39]. Ranging from non-polar monomers like styrenes and conjugated dienes to polar monomers as (meth)acrylates, vinyl ketones, and vinyl pyridines numerous monomers can be polymerized. Even heterocycles like epoxides or lactams can be polymerized by ring opening polymerization [40]. The only restriction is due to acidic protons in alcohols, acids or amines as they can be abstracted by the propagating species. Therefore protected monomers bearing acetals, silyl derivatives, and *t*-butyl esters [41] are used that should be stable in alkaline solutions. The protection group is easily removable in acidic media, resulting in water soluble polymers.

In this work the hydrophilic monomers MMA and AA are of special interest since they are frequently used in the preparation of amphiphilic copolymers with PS as the hydrophobic block [42, 43]. The resulting PIB-based block copolymers are also expected to be soluble in water. During polymerization of these monomers, one has to be aware of the possible complications, i.e. the presence of termination. Therefore, careful selection of conditions is necessary in order to have a polymerization which proceeds in a controlled manner.

Gerner *et al.* report that especially in the case of (meth)acrylates, potential termination reactions exist depending on the chosen conditions [44]. The problem of a nucleophilic attack at the carbonyl group on the monomer or the polymer chain can be reduced selecting the right initiators. An attack by the living chain end, has been proved not to be important [38]. The amount of backbiting reactions can be influenced by increasing the size of counterion, choosing the adequate polarity of the solvent, monomer concentration, and lowering the reaction temperature.

### 1.2.3 Initiators

As already mentioned, initiation should be fast and efficient. The reactivity of an initiator depends on the nucleophilicity of the anion, which roughly correlates with the  $pK_A$  value of the non-metallated compound. In Figure 1.6 some initiators are shown starting with BuLi which is the most nucleophilic one and some counterions where  $\text{Li}^+$  is the smallest and most strongly bound one.

The initiators used in the former work of Feldthusen *et al.* are synthesized by reactions of alkali metal-based initiators with a precursor, obtained from cationic polymerization (Figure 1.7). They reported on endcapping of PIB with diphenylethylene (DPE), shown in Figure 1.7. This offered a nice way of almost quantitative yield

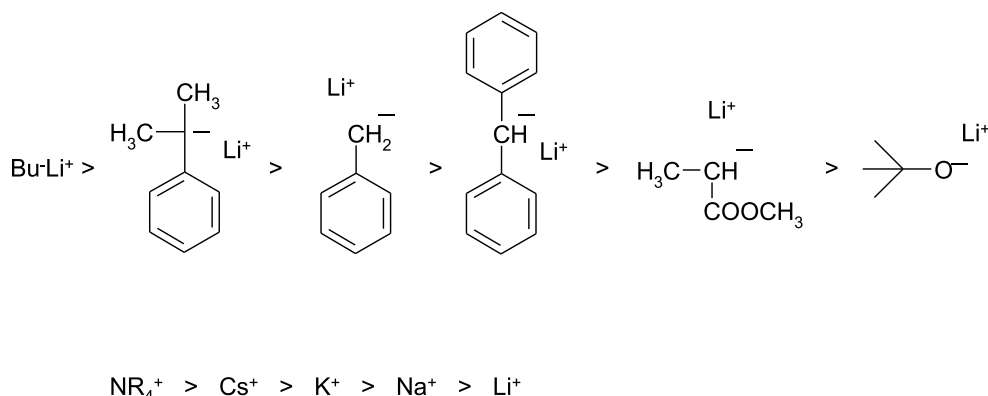


Fig. 1.6: Initiators used in living anionic polymerizations, decreasing nucleophilicity (from left to right, top) and counterions with decreasing size (from left to right, bottom).

of the precursor from the macroinitiator. The endcapped PIB was activated with K/Na alloy or BuLi. Metalation with alkali metals, however, is inconvenient and lithiation with BuLi would be preferable. Unfortunately, lithiation of DPE endcapped PIB by alkyl lithium does not proceed quantitatively. Therefore the method following Martinez-Castro was used in this work.

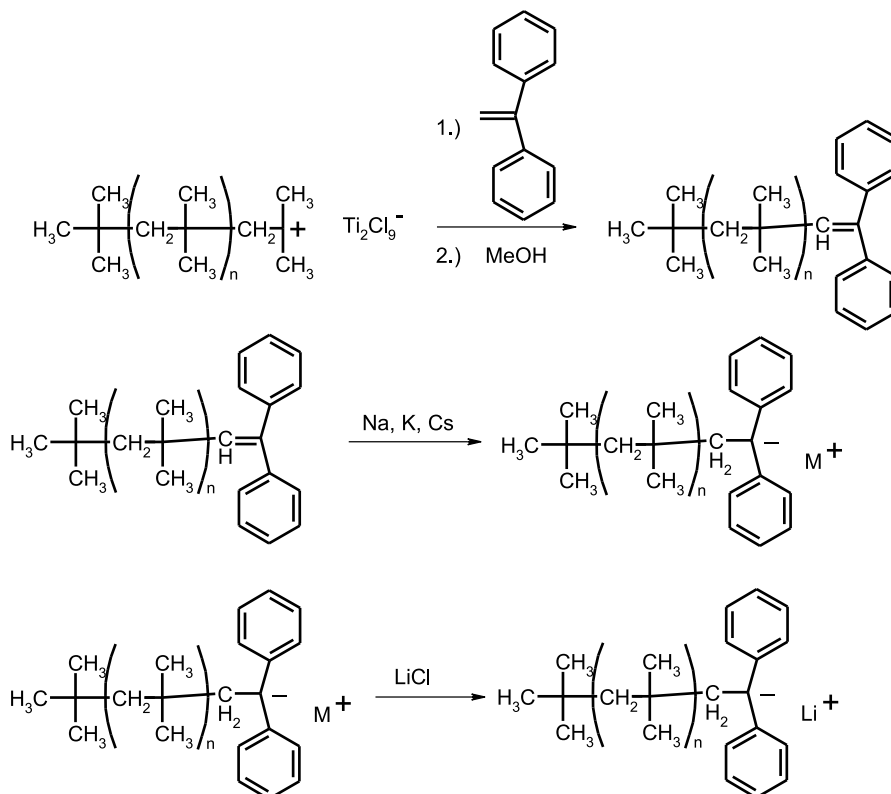


Fig. 1.7: Formation of a macroinitiator via end capping of living PIB with DPE, followed by activation in anionic polymerization with Na/K-alloy.

This method, invented by Martinez-Castro *et al.* [7], offers a smart tool to combine two different kinds of monomers that are not polymerizable with the same

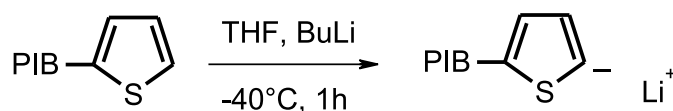


Fig. 1.8: *In-situ* preparation of the macroinitiator based on PIB-T with BuLi.

technique. The advantages of combination of living cationic and living anionic polymerization will be discussed later. According to Martinez-Castro *et al.* the cationic polymerization of IB was endcapped with thiophene (T). After purification of the PIB-T it can be reactivated with BuLi (see Figure 1.8). The resulting macroinitiator is T-stable up to 40°C. This offers a nice way to get rid of the excess of BuLi that is used for activation, as BuLi is only stable in THF at lower temperatures [45]. This only works in THF, as BuLi does not react with other solvents like toluene. After cooling down to -40° C , *t*BMA and *t*BA can be polymerized in a controlled manner.

#### 1.2.4 Additives

Additives are an important part in living anionic polymerization as they are able to shift the reactivity of the species occurring in the polymerization reaction. Known additives are LiCl, TMEDA, crown ethers, lithium alkoxides etc. [46, 47, 48, 49]. LiCl is used as additive for counterion exchange in the polymerization of *t*BA in this project [48]. The added salt affects the polymerization with different respects. Due to dissociation of associated ion pairs the exchange kinetics of the equilibrium of dormant species, aggregated with Li-counterions and the propagation species is fastened, leading to more narrow MWD. Different complexes of the living polymer chain and the counterion were reported. The 1:1 complex ( $[LiCl]/[I] \leq 1$ ) has a rate constant comparable to that of the ion pair and the 2:1 complex ( $[LiCl]/[I] > 1$ ) has a lower one. Concerning the LiCl to initiator ratio it has been shown that with  $[LiCl]/[I] > 10$  no changes, e.g. in MWD, could be detected [50]. Therefore, in this work a 10 fold excess of LiCl was used in all experiments.

#### 1.2.5 Combination of Living Cationic and Living Anionic Polymerization

Here the main aim was to study the behavior of amphiphilic block copolymers in solution. As already mentioned, the best way to polymerize IB is living cationic polymerization. As the second monomers used in this work (*t*BMA and *t*BA) are not polymerizable cationically, a second technique has to be applied. Besides anionic polymerization a number of different other polymerization techniques could have been used to obtain block copolymers. Especially Atom Transfer Radical Polymerization (ATRP) and Reversible Addition Fragmentation Chain Transfer Polymerization (RAFT) are of great interest.

The big advantage of ATRP is its tolerance (compared to anionic polymerization) to impurities like oxygen or water [51]. Compared to anionic polymerization only few purification steps like bubbling the reaction solution with N<sub>2</sub> for several minutes is enough to obtain narrow MWD and sufficiently high  $M_n$ . The problem occurring in the experiments during this work (not extended further) was the end capping in cationic polymerization with an agent capable of initiating the ATRP.

This group should have an activated Br or Cl as a functional group, needed for ATRP. During the experiments it turned out that the endcapper reacted with the Lewis acid  $\text{TiCl}_4$ , resulting in side reactions. Even protecting groups were not stable enough to survive the rather tough reaction conditions. Toman *et al.* succeeded by using  $\text{Et}_2\text{AlCl}$  instead of  $\text{TiCl}_4$  as a coinitiator [52]. With this technique they obtained even pentablock copolymers with a MWD of around 1.4.

With RAFT block copolymers can be obtained [53] as well. Especially to obtain PAA, RAFT has the advantage that acrylic acid can be used for polymerization directly without protection group. This eliminates the step of hydrolysis of the protective groups and makes sure to have only PAA as the lyophilic part of the polymer. The polymerization can be even carried out in water. The problem is, that our macroinitiator is not soluble in polar solvents. So this technique is also of limited interest for this special topic.

According to the large experience according anionic polymerization in our laboratory we decided to use anionic polymerization to synthesize the block copolymers.

### 1.3 Architectures of Copolymers

Up to now a wide variety of copolymer architectures, obtained by different polymerization techniques have been reported [54, 55]. Besides linear block copolymers, which are of main interest in this work, also brush-like [56] or star-like [7, 57] copolymers attract great interest.

The simplest architecture for block copolymers is the sequential linear polymerization of the monomers. These chains also can have different structure. Besides the AB style block copolymers also ABA type [54, 55, 58] and ABC type ones are reported. Also statistical copolymers, where the monomers are inserted randomly and gradient copolymers, where the monomers are inserted starting from almost homopolymer of the first monomer with increasing ratio of the second monomer can be obtained. For our purpose, linear AB type polymers are suited best to be compared to low molecular weight surfactants. They can be obtained by sequential addition of the monomers to a reaction, as reported by Szwarc *et al.* [58] or by combination of different polymerization techniques [59], as already discussed. The investigations in this work were made with linear AB block copolymers.

### 1.4 Solution Behavior of Amphiphilic Block Copolymers

Low molecular surfactants with an hydrophobic, aliphatic chain and a hydrophilic head group have physical and chemical behavior comparable to amphiphilic copolymers. In both cases one can distinguish between two classes: ionic and nonionic systems. In low molecular surfactant chemistry the most widely used ionic chemicals are anionic sodium dodecylsulfate (SDS) and cationic cetyl-trimethyl ammonium bromide (CTAB) (see Figure 1.9). For uncharged systems, mostly ethyleneglycol based esters like propylene glycol monostearate (see Figure 1.9) or sugar based surfactants are investigated. Also zwitterionic surfactants are reported.

In polymer chemistry also comparable structures can be synthesized. As well polyanionic and polycationic bearing blockcopolymers as neutral copolymers are reported. For the uncharged species, ethylene oxide based copolymers are the most

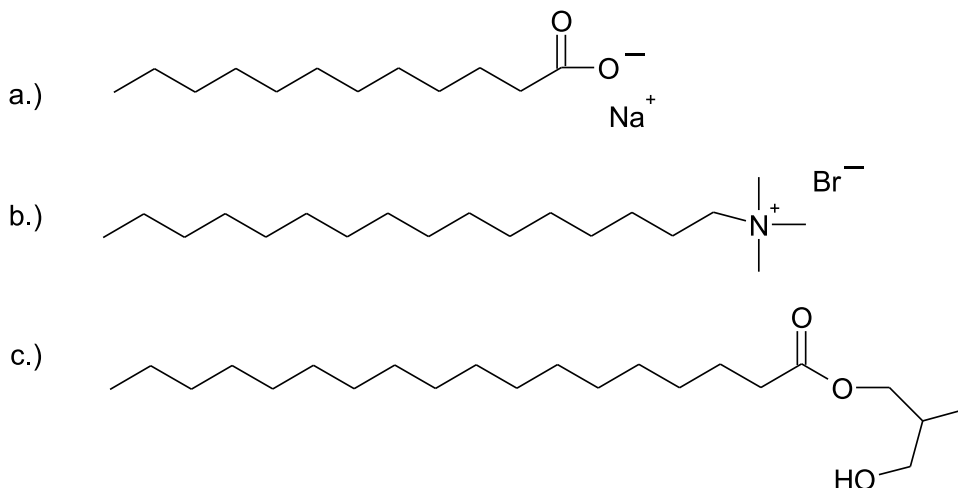


Fig. 1.9: The most important low molecular weight surfactants used are the anionic SDS (a.), the cationic CTAB (b.) and ethylene glycol esters (e.g. propylene glycol monostearate, (c.)).

important ones. Here, especially Pluronics (PEO-*b*-PPO-*b*-PEO) are important for industrial applications like defoaming during production of sugar up to lubrication in metal industry [60]. As they are easily available, they are of great interest for basic research e.g. in phase behavior of oil-water-mixtures [61] or as carriers for gold nanoparticles [62].

The charged polymeric analogues to low molecular weight surfactants are block copolymers with a hydrophobic and a polyelectrolyte block [5]. They combine the properties of electrolytes and surfactants with the structures of block copolymers. As already mentioned in the introduction, the most important fact is their ability to react on external stimuli like pH or ionic strength or even temperature. This offers a wide field of changeable parameters to influence the physico-chemical properties in aqueous solutions of the copolymers.

Polyelectrolytes can be divided up into weak and strong electrolytes. The number of charges on weak polyelectrolytes depends on pH value, i.e. the charge and even the solubility is different under acidic and basic conditions. A weak positively charged polyelectrolyte is poly(vinylpyridine) (PVP). Here the N-atom can be in position 2 and 4 of the pyridine moiety. Under acidic conditions the N-atom can be reversibly protonated [63]. To obtain a strong positive polyelectrolyte, PVP can be quaternized. This is mainly done with MeI [64] or with EtBr [8, 9].

Most important for this work are the weak negatively charged polyelectrolytes like poly(acrylic acid) and poly(methacrylic acid) (Figure 1.10). Their block copolymers were studied to a large extent by Eisenberg *et al.* [42, 43]. His group mostly focuses on block copolymers based on polystyrene (PS) as hydrophobic block. In the work presented here, we also used PAA and PMAA due to their stimuli-responsive behavior when changes in pH or ionic strength are applied. The most important strong anionic polyelectrolyte is the sodium salt of poly(styrene 4-sulfonate) (PSS). Guenoun *et al.* investigated the salt dependence of a poly(*t*-butylstyrene-*b*-sodium styrene sulfonate) (PtBS-PSSNa) [65], finding an influence of  $c_{NaCl}$  on aggregation number.

The corresponding homopolymers are water soluble, depending on the pH in

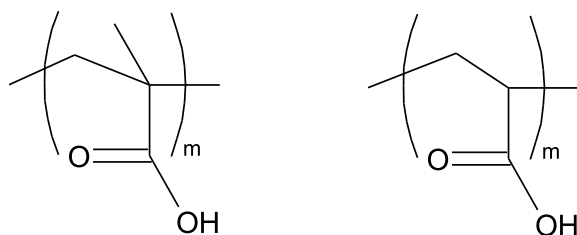


Fig. 1.10: PMAA (left) and PAA (right) are the most important negatively charged weak polyelectrolytes.

the case of weak polyelectrolytes. In combination with a hydrophobic polymer like polystyrene (PS), polybutadiene (PB) or polyisobutylene (PIB) amphiphilic polymers are obtained. They can be dissolved in water as well. In the case of PS this procedure is not straight forward. As PS has a glass transition temperature ( $T_g$ ) of about  $104^\circ\text{C}$  it is in a glassy state at RT. So the usual way to obtain aqueous solutions is to dissolve it in a common solvent for both blocks, e.g. dioxane as reported for PS-*b*-PAA [66]. Then the solution has to be dialyzed slowly against  $\text{H}_2\text{O}$ /dioxane-mixtures and finally against pure deionized water to obtain aggregates. In the case of PIB-based block copolymers it was already reported by Pergushov *et al.* that it can be directly dissolved in water due to the lower  $T_g$  of PIB of around  $-55^\circ\text{C}$ , leading to a non-glassy hydrophobic block.

Soluble amphiphilic block copolymers can form aggregates above a certain concentration. This concentration is the so called *cmc*, the critical micellar concentration. Below this concentration only single molecules or smaller aggregates exist. The *cmc* of amphiphilic block copolymers normally ranges at around  $10^{-6}$  to  $10^{-8} \frac{\text{mol}}{\text{l}}$  [9]. So even at small amounts of polymer micellar assemblies are formed. The size of these assemblies depends on the number of copolymer chains involved, the so called aggregation number  $N_{agg}$ .

Depending on the solvent [66] or on the block length ratio of the soluble and insoluble block [6] different morphologies were found. Most importantly, it was reported by Eisenberg that in PS-*b*-PAA long core-forming blocks and high water contents favor the formation of vesicles and that short core forming blocks and low water contents favor open bilayers (e.g., lamellae). In this system with increasing water content, single chains, spheres, rods, bilayers and inverted structures were obtained.

In this work the spherical micelles (Figure 1.11) formed by  $\text{PIB}_x\text{-}b\text{-PMAA}_y$ , as reported up to now, are studied. In this case the core-forming hydrophobic part is PIB. The corona consists of PMAA or PAA. At high pH values the acidic groups are totally neutralized, e.g. the polyelectrolyte has its maximum charge density. After addition of acid, at a pH of about 4 the aggregates start precipitating. This is due to the fact, that the  $\text{COO}^-$  groups are reprotonated and less hydrophilic than before. The charges in the corona are not sufficient to keep the micelle in solution.

#### 1.4.1 Characterization of Block Copolymers in Solution

Aqueous solutions of block copolymers offer a wide field of opportunities for characterization. The first step is to determine the *cmc* of the system. This can be done

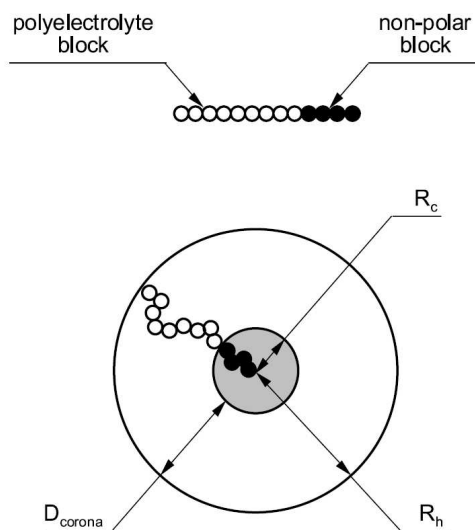


Fig. 1.11: Spherical micelles consist of an insoluble core (grey) formed by the hydrophobic block and a soluble corona (white) consisting of the polyelectrolyte block [9].

either by Fluorescence Correlation Spectroscopy (FCS, not done in this work) or by fluorescence measurement. Here a polar, slightly water soluble fluorescence dye (pyrene) is added to polymer solutions. From changes in the fluorescence spectra of the dye one can conclude the starting point of aggregation (*cmc*).

As it can be seen in Figure 1.11, different sizes of the assemblies can be investigated. The radius of the core,  $R_c$ , can be deduced from Small Angle Neutron Scattering (SANS) or Small Angle X-Ray Scattering (SAXS). From these techniques, also information about the shape of the particle, e.g. spheres, rods or vesicles, can be obtained. Another helpful scattering technique is the Dynamic Light Scattering (DLS). Via CONTIN algorithm a distribution of hydrodynamic radii,  $R_h$ , can be obtained. In the case of micelles only few, ideally one species should be found. In addition to that, from Static Light Scattering (SLS) the radius of gyration,  $R_g$ , can be measured. From the ratio  $\frac{R_g}{R_h}$  one can have a hint on the structure of the aggregates formed. The difference of  $R_h$  and  $R_c$  is a measure of the thickness of the corona. These values can be compared to the theoretical maximum extension of the polymer, the contour length,  $L_c$ , calculated from  $DP_n \cdot 2.5 \text{ \AA}$  per monomer unit.

The behavior of the corona can be investigated in terms of titrations. Here as well pH-titrations as salt dependent titrations in case of the complexes can be done. The turbidity and the pH-values as well as the activity of the  $\text{Na}^+$ -counterions can be followed during the measurements.

A direct image of the micellar assemblies in solution can be obtained from Cryogenic Transmission Electron Microscopy (cryo-TEM). During sample preparation thin films of almost monolayers of the micelles are formed. In frozen state the particles can be observed directly as they exist in solution. The sample is always influenced by the treatment before freezing in, e.g. blotting away parts of the solution, which applies shear forces to the micelles. A better way to investigate the real structure in solution would be the Freeze-Fracture technique, that is still under construction in our institute and not available yet.

### 1.4.2 Complexation of $PIB_x$ - $b$ - $PMAA_y$

After dissolving the diblock copolymer, the above described micelles are obtained. The charges in the corona of those aggregates can be used to interact with oppositely charged systems. This leads to complexes as already described by Pergushov *et al.* [8, 9]. The charge ratio of the polyanion compared to the polycation added is of interest.  $Z$  is defined as the ratio of positive and negative charges,  $\frac{[+]}{[-]}$  within the polymer chains. This ratio has to be kept below a certain threshold. This can be explained by the reduced polarity of the complex formed by the oppositely charged polymer chains. For complexation of homopolymers, it is already reported, that water-soluble complexes can be obtained by mixing weak polyelectrolytes as polyacids or their salts with polybases [11]. The driving force for this process is the release of the counterions. This results in an increase of the entropy of the system. Depending on the ratio of the species, water soluble complexes are obtained. In case of  $Z = 1$ , flocculation occurs for different systems.

To overcome the problem of precipitation it was reported on complexation of polyelectrolytes with diblock copolymers with an oppositely charged block [11]. The second block of the copolymer has to be water soluble to avoid precipitation of the complexed species. In our case, the second block is hydrophobic PIB. Hence complexation is only possible to  $Z$ -values far below 1. Pergushov *et al.* [8] reported that with the system  $PIB_x$ - $b$ - $PMAA_y$  complexed with quaternized P4VP which are also used in this work, water soluble complexes can only be obtained up to a charge ratio of 0.4. Beyond this value they observed decreasing transmittance in UV-measurements. This shows the beginning of the formation of larger aggregates that are precipitating. Thus, in this work presented here, for all complexes formed  $Z$  was between 0.1 and 0.4.

Pergushov *et al.* proposed a core-shell-corona structure for these complexes (cf. Figure 1.12, [9]). The hydrophobic PIB core is surrounded by a shell of complex

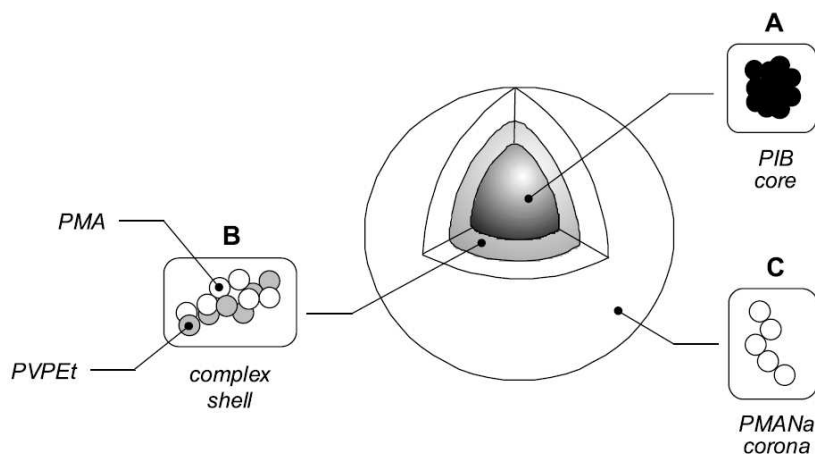


Fig. 1.12: Proposed core-shell-corona structure of a complexed micelle: the hydrophobic PIB core is surrounded by a shell of complex consisting of PMAA and P4VPQ. The non complexed polyanions remain in the corona and keep the complex in solution [9].

consisting of PMAA and P4VPQ with a ratio close to unity. The non complexed polyanions remain in the corona and keep the complex in solution. This they con-

cluded from well separated complex species, seen by means of Analytical Ultracentrifugation (AUC). Here only one kind of species can be detected after complexation. This means that the polycation is totally incorporated. Additionally the missing aggregation of particles is a hint for the existence of repulsion between the IPECs. This can only be due to residual negative charges in the corona of the aggregates and IPECs, respectively.

From the fact that no higher order aggregation can be detected, Pergushov also concluded that no crosslinking of micelles via polycation occurs. Hence the cationic polyelectrolyte has to penetrate into the corona of the micelle to escape from the vicinity of neighboring micelles. As already known from complexes consisting of oppositely charged homopolymers, the 1:1 complex is hydrophobic. This can be explained by the lack of charges of the formerly uncomplexed polyelectrolyte. Hence the complex shell is forced to minimize the interface with water. This can be achieved by penetration of the complex, e.g. the polycation, toward the hydrophobic core. Finally according to the proposition of Pergushov *et al.* the PIB core is covered by a shell consisting of the complex. The thickness of this shell is determined by the  $Z$ -value of the complex.

#### 1.4.3 Decomposition of $PIB_x$ - $b$ - $PMAA_y$ based Complexes

By changing the ionic strength of the solution, the IPEC may be influenced. Kabanov *et al.* [67] already investigated the behavior of IPECs at higher salt concentration. They observed dissociation of formed complexes of poly(acrylic acid) (PAA) with poly(ethylenimine) (PEI). In nonstoichiometric complexes they observed different regions depending on the amount of added salt. For low ionic strength they report on stable complexes. Upon addition of salt they observe increasing turbidity of their complex solutions. Kabanov explains it with the formation of loops of the excess components due to shrinkage of the complex particle. At a certain point the complexes can undergo disproportionation into stoichiometric and nonstoichiometric complexes. The stoichiometric complex particles precipitate. With increasing salt content the complex starts to dissociate. This can be stated by means of AUC. Above a salt concentration of 2 M only separated polyelectrolytes can be detected.

In our work the behavior of complexed micelles is investigated. The system slightly differs from the system of Kabanov. In their work they just investigated nonstoichiometric complexes of homopolymers. In this thesis the influence of ionic strength on complexes of  $PIB_x$ - $b$ - $PMAA_y$  with P4VPQ are investigated. The dissociation of the complexes was followed by means of turbidity measurements, cryo-TEM, SANS and AUC.

## 2. AIM AND STRATEGY

In this work the amphiphilic block copolymer  $\text{PIB}_x\text{-}b\text{-PMAA}_y$  with a large variety of block lengths of both PIB and PMAA are investigated. The  $\overline{DP}_n$  for the hydrophobic PIB was set in the range of 25 to 75, whereas the  $\overline{DP}_n$  for PMAA blocks was set from 170 up to 1600. The investigations were extended to  $\text{PIB}_x\text{-}b\text{-PAA}_y$ , obtained via a similar synthetic route. The polymers were synthesized by a combination of living cationic polymerization and living anionic polymerization to obtain  $\text{PIB}_x\text{-}b\text{-PMAA}_y$  and  $\text{PIB}_x\text{-}b\text{-PtBA}_y$ . After hydrolysis of the Pt-BMA and Pt-BA blocks with HCl in dioxane a water-soluble diblock copolymer was obtained.

In the frame of this work, special interest was set on the behavior of the micellar aggregates formed in alkaline solutions with respect to the influence of both the block length of PIB and PMAA chains as well as the block length ratio. The response of PMAA and PAA blocks on external stimuli like pH or ionic strength (addition of salt), resulting in changes of  $R_c$ ,  $R_h$  or of  $N_{agg}$ , are investigated. Therefore a wide variety of techniques, including SANS, SLS, DLS, turbidity and potentiometric titrations and cryo-TEM were used. Especially the dynamic behavior in terms of changes in the  $\overline{N}_{agg}$  upon external stimuli was investigated and compared to systems already reported in literature. The results obtained for  $\text{PIB}_x\text{-}b\text{-PMAA}_y$  were finally compared to investigations made with  $\text{PIB}_x\text{-}b\text{-PAA}_y$ .

The negative charges in the corona of the micellar assemblies offer the opportunity of complexing the  $\text{COO}^-$  with oppositely charged polyelectrolytes. In our case quaternized P4VP was used to form water soluble complexes. The IPECs formed were investigated by means of SANS, DLS, turbidity and potentiometric titrations, AUC and cryo-TEM with respect to their behavior depending on the different block lengths of both, PIB and PMAA, blocks. The influence of the amount of polycation as well as the dynamic behavior of the IPECs is reported. Finally the influence of changes in ionic strength on the IPECs and the process of dissociation of the complex is investigated.

The investigations were extended to a new diblock copolymer,  $\text{PIB}_x\text{-}b\text{-PAA}_y$ . For this polymer, we were especially interested in the dynamic behavior with respect to the influence of point of time of addition of salt, as in a former work of Colombani *et al.* an unattended behavior of the PAA block containing copolymer, in their case  $\text{PnBA}_x\text{-}b\text{-PAA}_y$ , was observed. In our work, the copolymer was investigated by means of SANS, cryo-TEM and DLS.

By combining different characterization techniques we obtained a deeper insight in the effect of external stimuli on the block copolymers synthesized. The results are compared with similar investigations for diblock copolymers with PS as the hydrophobic block, thus providing a frozen system at RT.

### 3. OVERVIEW OF THE THESIS

This thesis consists of ten chapters including two publications and one Chapter which are presented in Chapters 5 to 7.

Polyisobutylene-*block*-poly(methacrylic acid) (PIB<sub>*x*</sub>-*b*-PMAA<sub>*y*</sub>) diblock copolymers with different block length ratios were synthesized and characterized in Chapter 5. The micellar solutions were investigated by means of potentiometric titrations, cryogenic transmission electron microscopy (cryo-TEM), dynamic light scattering (DLS), static light scattering (SLS) and small angle neutron scattering (SANS) to reveal their stimuli responsive behavior upon changes of pH and ionic strength as well as their dynamic behavior with regard to changes in aggregation number ( $\overline{N_{agg}}$ ) of the micellar assemblies.

The micellar aggregates investigated in Chapter 5 were used to form water-soluble Interpolyelectrolyte Complexes (IPECs) with quaternized poly(4-vinyl pyridine) (P4VPQ) as polycation. In Chapter 6 the influence of amount of polycation as well as the behavior of the PIB<sub>*x*</sub>-*b*-PMAA<sub>*y*</sub> micelles is investigated by means of cryo-TEM, DLS and SANS. Especially the process of formation and dissociation upon increasing the ionic strength of the micellar solution is reported.

In Chapter 7, a diblock copolymer comparable to the PIB<sub>*x*</sub>-*b*-PMAA<sub>*y*</sub> reported, was investigated. The Polyisobutylene-*block*-poly(acrylic acid) (PIB<sub>*x*</sub>-*b*-PAA<sub>*y*</sub>) synthesized showed different behavior compared to the methacrylate. Especially the influence of the point of time of addition of NaCl on the formation of assemblies was investigated by means of cryo-TEM, DLS and SANS.

In the following, a summary of the main results is presented.

#### 3.1 Polyisobutylene-*block*-poly(methacrylic acid) Diblock Copolymers: Self-Assembly in Aqueous Media

Different amphiphilic diblock copolymers, PIB<sub>*x*</sub>-*b*-PtBMA<sub>*y*</sub>, were synthesized via combination of cationic polymerization of isobutylene (IB), resulting in a macroinitiator, and anionic polymerization of *t*BMA as described elsewhere [7]. The special interest in this work was to obtain diblock copolymers with variations of both block lengths, for polyisobutylene (PIB) in the range of 25 to 75 and for poly(*t*-butyl acrylate) (PtBMA) in the range of 170 to 1600. The synthesis resulted in well defined polymers with narrow  $\overline{DP}_n$  of 1.03 to 1.2.

The critical micellar concentration (*cmc*) of the hydrolyzed PIB<sub>*x*</sub>-*b*-PMAA<sub>*y*</sub> copolymers was found to depend mainly on the hydrophobic part of the copolymer. From cryo-TEM images, well defined spherical micelles with a PIB core and PMAA

corona were found for all investigated polymers at  $c_{CsCl} = 0.1$  M (cf. Figure 3.1).

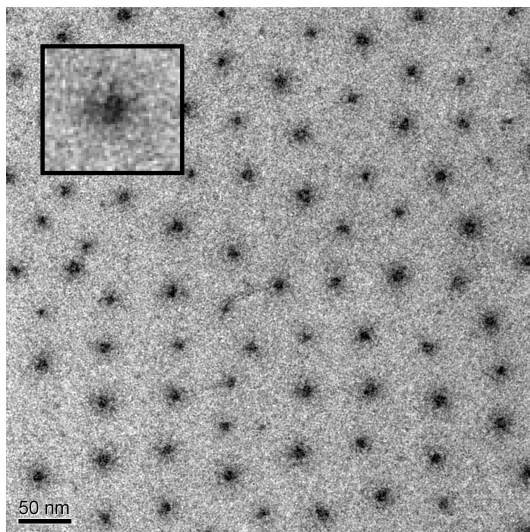


Fig. 3.1: Cryo-TEM image of aqueous solution of  $PIB_{30}\text{-}b\text{-}PMAA_{170}$  with  $0.1$  M  $CsCl$ ,  $0.01$  M  $TRIS$ ,  $c_{pol} = 0.5$  wt%.

Potentiometric measurements of the micellar solutions revealed a behavior that coincides with theoretical predictions. For the measured polymer solutions, the apparent  $pK_a$  depends on the ionic strength of the solution.

By means of DLS, the responsiveness of the micelles on external stimuli was investigated. The increase in  $R_h$  of the diffusive species with increasing pH (cf. Figure 3.2) can be explained by an increasing repulsion of the negatively charged

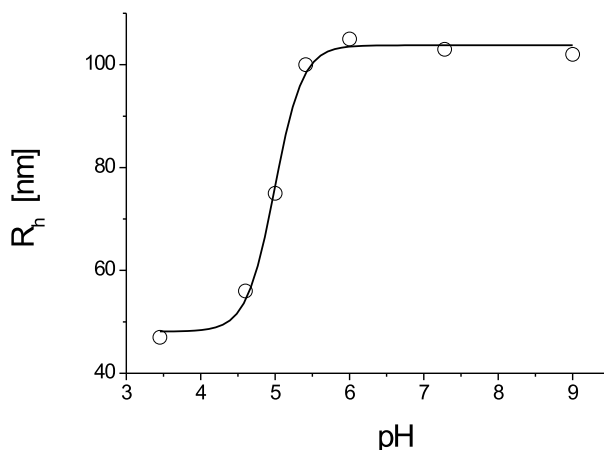


Fig. 3.2: The  $pH$ -dependence of  $R_h$  for the  $PIB_{75}\text{-}b\text{-}PMAA_{1600}$  micelles,  $c_{NaCl} = 0.1$  M,  $\Theta = 90^\circ$ .

PMAA blocks. This causes more pronounced stretching of the PMAA chains and therefore an increasing size of the micellar assembly. This phenomenon can be counterbalanced by rising the ionic strength of the micellar solution. Thus, the size of the micelles decreases, as the PMAA blocks can arrange in a much denser way due to the screening effect of the salt.

The size of the aggregates is also affected by changes of  $\overline{N_{agg}}$  upon changes of pH or ionic strength. SLS measurements reveal that especially for the diblock copolymers PIB<sub>75</sub>-*b*-PMAA<sub>1600</sub> and PIB<sub>30</sub>-*b*-PMAA<sub>190</sub>  $\overline{N_{agg}}$  increases with salt concentration according to theoretical predictions. Furthermore a strong influence of the hydrophilic PMAA block on  $\overline{N_{agg}}$  can be stated. Already small changes of  $\overline{DP_n}$  of PMAA of 170 to 190 results in a decrease of  $\overline{N_{agg}}$ . This can be explained by the interfacial area occupied by a single hydrophilic block. The higher the  $\overline{DP_n}$  of a PMAA chain is, the more space is needed to allow free rotation within the micellar corona and the more space is occupied at the core-corona interface.

The evaluation of SANS data strongly suggests that the PIB<sub>*x*</sub>-*b*-PMAA<sub>*y*</sub> system behaves dynamic, i.e. also the core of the micelle reacts on external stimuli upon changes in  $\overline{N_{agg}}$  (cf. Figure 3.3). By means of SANS, samples that were directly

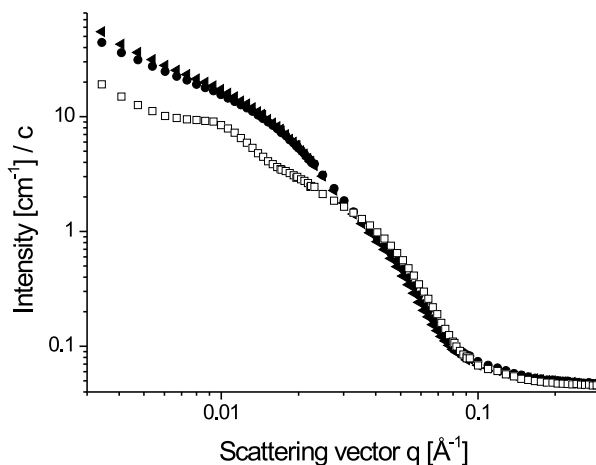


Fig. 3.3: Scattering curves obtained from SANS of micellar solutions of PIB<sub>30</sub>-*b*-PMAA<sub>190</sub> with 0.1 M NaCl prepared at pH 9 ( $\square$ ), prepared at pH 5.2 ( $\blacksquare$ ) and prepared at pH = 12 and brought to pH = 5 ( $\bullet$ ).

prepared at pH 5.2 were compared to samples prepared at pH 12 and afterward brought to pH 5.2. On the one hand a clear change of the shape of the scattering curves of the PIB<sub>*x*</sub>-*b*-PMAA<sub>*y*</sub> samples at pH 12 and 5.2 can be seen. On the other hand, the samples for pH 5.2 prepared in different routes almost superimpose perfectly. Also from quantitative evaluation of the scattering curves by applying a core-corona model with stiff protruding hydrophilic chains a change of core size can be obtained. This is a clear hint on rearrangement of the micellar core upon changes of the pH value.

Changes in ionic strength also lead to a change in core size, as seen from SANS evaluation. Nevertheless the influence of salt on the core size seems to be less pronounced compared to pH changes.

The block length influence on the  $\overline{N_{agg}}$  is seen by SANS as well. Here, with increasing hydrophilic block length, the  $\overline{N_{agg}}$  is decreasing due to the interfacial area occupied by the PMAA chains. For the PIB block length the dependence of the  $\overline{N_{agg}}$  is inverse. Here, for higher  $\overline{DP_n}$  of the hydrophobic block the  $\overline{N_{agg}}$  also rises. This can be explained by the surface-volume ratio of spheres that is the better, the larger the radius of the micelle is. This leads to an optimization in core-corona

- and therewith water - interface upon increasing the  $R_c$  of the micellar assembly.

Finally a good understanding of the influence of block lengths and block length ratios of the  $\text{PIB}_x\text{-}b\text{-PMAA}_y$  system is obtained. Furthermore the investigation strongly suggest that the micelles formed by  $\text{PIB}_x\text{-}b\text{-PMAA}_y$  are dynamic, i.e. they react on external stimuli by changes in the  $\overline{N_{agg}}$ .

### 3.2 Water-Soluble Interpolyelectrolyte Complexes of Polyisobutylene-block-Poly(methacrylic acid) Micelles: Formation and Properties

Amphiphilic diblock copolymers synthesized and well characterized in Chapter 5 were used to form water-soluble IPECs. Therefore,  $\text{PIB}_x\text{-}b\text{-PMAA}_y$  copolymers with a wide range of block length of both, the hydrophobic PIB with  $\overline{DP_n}$  of 20 to 75 and hydrophilic PMAA with  $\overline{DP_n}$  from 100 to 2600 were used for complexation with P4VPQ. Up to  $Z = \frac{[+]}{[-]} = 0.4$  the IPECs remain water-soluble. Beyond this threshold, depending on the block length ratio, precipitation of the complexes is stated. By means of turbidimetric titration, the complexation process was followed. Upon addition of the polycation to the micellar solution a pronounced decrease in transmission can be stated. While stirring the solution, the transmission of the solution containing the  $\text{PIB}_x\text{-}b\text{-PMAA}_y$  micelles and the P4VPQ increases again. This can be explained by a two step process of formation of the IPEC (cf. Figure 3.4). The kinetically driven part is the formation of large aggregates of micelles that are

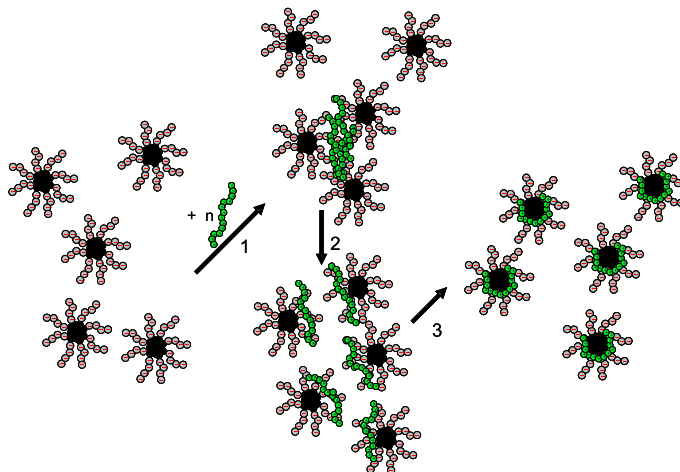


Fig. 3.4: *Proposed mechanism of formation of IPECs of spherical negatively charged polyelectrolyte micelles with cationic polyelectrolyte: After an addition of the cationic polyelectrolyte to the solution of micelles, cationic macromolecules interact with the micellar coronas, resulting in formation of large aggregates (kinetic regime). The large aggregates disappear with time due to polyion exchange reactions (thermodynamic regime). Hence, distribution of the cationic polyelectrolyte among the micelles is obtained. Due to the polycation penetrating deeply into the micellar corona, finally a core-shell-corona structure [8] is formed.*

complexed. This can be seen by an increase in turbidity, which is a clear hint on the formation of larger assemblies. The nature of the assemblies is not clear yet. Both,

interlinked micelles complexed with a polycation and assemblies formed due to hydrophobic interactions between complexed coronas can be possible explanations. In the second step, the thermodynamically driven rearrangement of the complexes is the driving force for equilibration of the large assemblies in favor of single complexed micelles. The hydrophobic complex tries to minimize the interface to water by penetration of the polycation into the corona, finally resulting in a shell of complex around the PIB core and a corona of residual uncomplexed PMAA (cf. Figure 3.5).

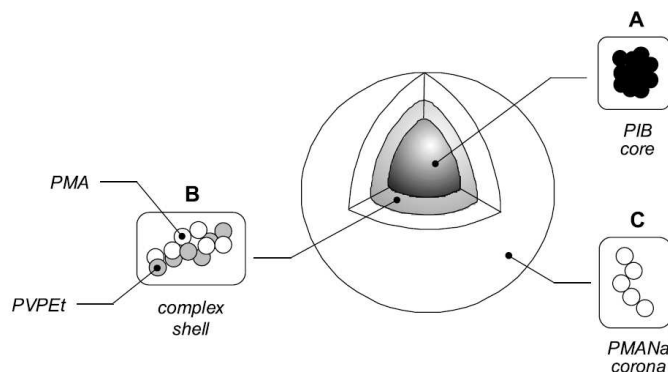


Fig. 3.5: Spherical complex micelles consist of an insoluble PIB core (grey) formed by the hydrophobic block, a insoluble shell of complex wrapped around the core and a soluble corona (white) consisting of the polyelectrolyte block [9].

From cryo-TEM images (cf. Figure 3.6) this structure can not be clearly seen.

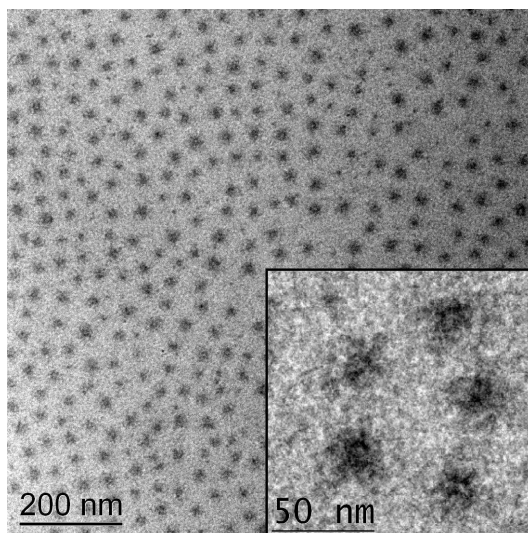


Fig. 3.6: Cryo-TEM image of complex of  $P_4VPQ$  with  $PIB_{30}-b-PMACs_{170}$  at  $Z = 0.4$ ,  $c_{CsCl} = 0.1M$ ,  $CsOH$ ,  $\alpha = 1$ .

This is due to the electron scattering contrast between the complex and the background, consisting of PMAA, salt and water. Compared to images from pure micellar solutions, slight differences in the scattering behavior of the micellar assemblies can be stated.

A pronounced decrease in  $R_h$  of the micelles and the complex of about 20 % can be seen by means of DLS for all  $PIB_x-b-PMAA_y$  copolymers investigated (cf.

Figure 3.7). As about 40 % of the negative charges of the PMAA blocks in the

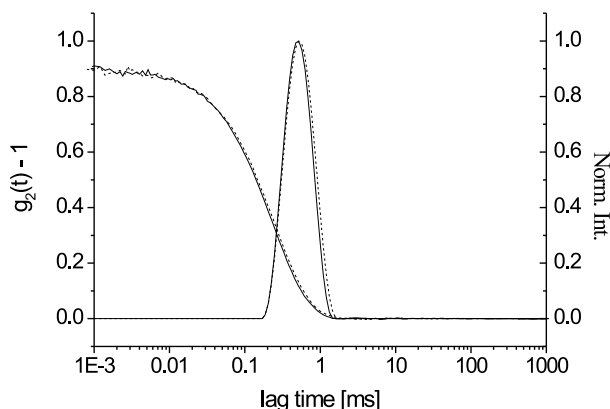


Fig. 3.7: Intensity autocorrelation function and CONTIN-plot of micellar solution (dashed) and IPEC with P4VPQ at  $Z = 0.4$  (solid) of PIB<sub>75</sub>-b-PMAA<sub>615</sub>,  $c_{TRIS} = 0.01M$ ,  $\alpha = 1$  with  $c_{NaCl} = 0.1 M$ ,  $\Theta = 90^\circ$ .

corona of the micelle are complexed, they are assumed to be collapsed on the PIB core. Thus, they contribute less to the "stretching out" and therefore to the  $R_h$  of the micelle. From SANS measurements of micellar and complex solutions, a linear increase of the scattering intensity with increasing  $Z$  can be seen.

In the second part of this chapter, the dissociation phenomenon of the complexes on increasing the ionic strength is investigated. In Figure 3.8 the dissociation of

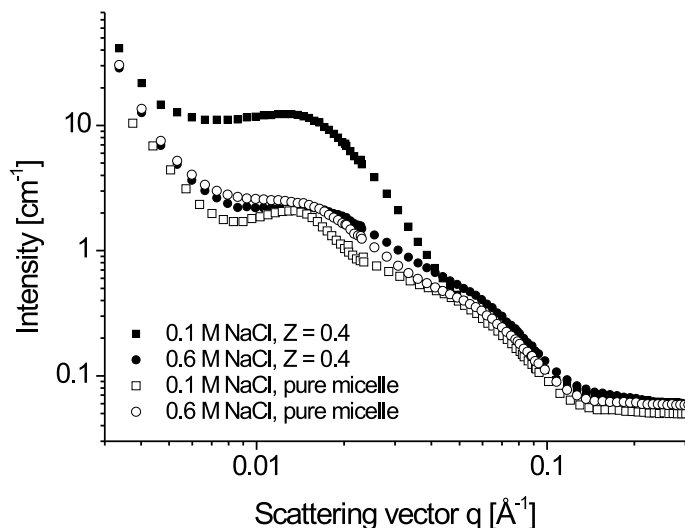


Fig. 3.8: Dissociation of complex formed by PIB<sub>20</sub>-b-PMAA<sub>100</sub> with P4VPQ,  $Z = 0.4$ ,  $c_{TRIS} = 0.01 M$ . The SANS scattering curves represent (from top to bottom, full symbols)  $c_{NaCl} = 0.1 M$  and  $0.6 M$ . The open symbols represent (from top to bottom) the scattering curve obtained by a micellar solution of PIB<sub>20</sub>-b-PMAA<sub>100</sub>,  $c_{NaCl} = 0.1 M$  and  $0.6 M$ ,  $c_{TRIS} = 0.01 M$ .

a complex formed by PIB<sub>20</sub>-b-PMAA<sub>100</sub> and P4VPQ upon a change of  $c_{NaCl}$  from 0.1 M to 0.6 M is shown. The decrease of the overall scattering intensity can be explained by a release of the polycation from the PIB<sub>20</sub>-b-PMAA<sub>100</sub> micelle. This

is also stated by AUC measurements. There, besides the micelles, a second species can be detected, which can be attributed to free P4VPQ.

The dissociation process of the complexes formed by different  $\text{PIB}_x\text{-}b\text{-PMAA}_y$  with P4VPQ can be followed by potentiometric titration with a  $\text{Na}^+$  selective electrode (cf. Figure 3.9). Compared to a NaCl containing background solution, a

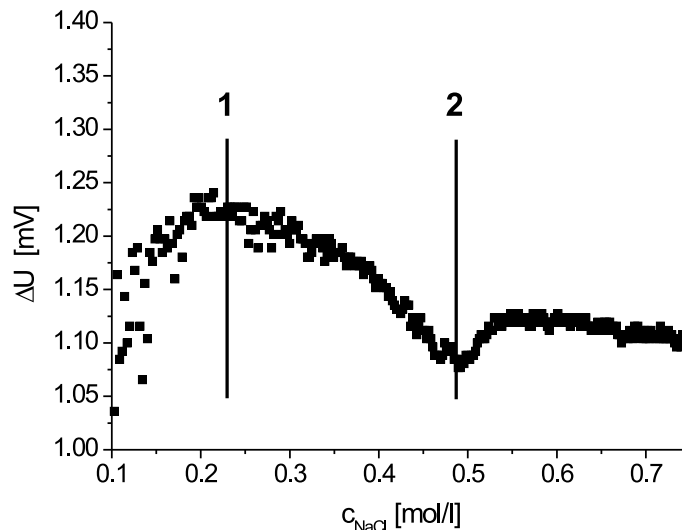


Fig. 3.9: Difference of potentiometric titration curves with sodium-selective electrode. A relative maximum (1) and a minimum (2) of the difference is observed.

different behavior of the complex can be observed. Starting from a maximum in difference, the activity decreases continuously compared to the background. The explanation is the Manning condensation of  $\text{Na}^+$  counterions to the PMAA chains in the corona of the micelle. They stepwise replace the polycation of the complex, causing the dissociation of the complex. This results in a decreased activity of the micellar solution, as the  $\text{Na}^+$  ions cannot contribute to the activity any more. After the complete dissociation of the complex, the activity reaches a plateau value. Hence it can be concluded, that the change in activity of the solution upon increasing the ionic strength of the solution is the same as in the case of the background solution.

Comparing different methods, a starting point of dissociation of the complex can be seen at  $c_{\text{NaCl}}$  of about 0.2 to 0.3 M. The end point of this process is reached at  $c_{\text{NaCl}}$  around 0.5 M. This can be seen for all  $\text{PIB}_x\text{-}b\text{-PMAA}_y$  polymers investigated in this work.

### 3.3 Aqueous Solutions of Polyisobutylene-block-Poly(acrylic acid) Diblock Copolymers: Path Dependent Formation of Non-Equilibrium Assemblies

A novel polymer, polyisobutylene-*block*-poly(acrylic acid) (PIB-*b*-PAA) was synthesized via combination of cationic polymerization of IB and anionic polymerization of *tert*-butyl acrylate. Hydrolysis resulted in a water-soluble diblock copolymer. Samples with different point of time of addition of salt were prepared, i.e. salt was added before or after dissolution of the polymer.

Cryo-TEM images of samples with CsCl as salt (cf. Figure 3.10) show spherical micelles with low polydispersity. This coincides with the observations made

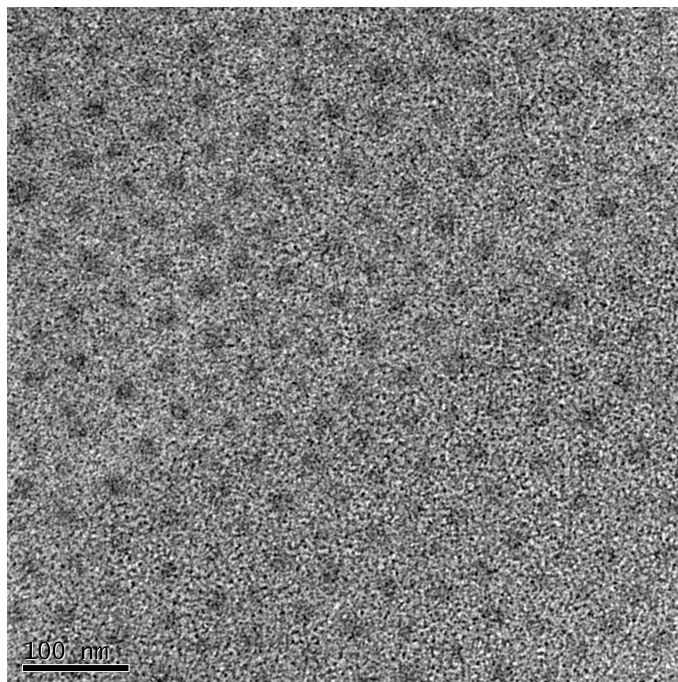


Fig. 3.10: Cryo-TEM image of  $PIB_{30}$ - $b$ - $PAA_{430}$ ,  $c_{Pol.} = 0.5$  wt-%,  $\alpha = 1$ ,  $c_{CsCl} = 0.1$  M,  $c_{TRIS} = 0.01$  M. Here, salt was added after total dissolution of the polymer (PD).

for copolymers with poly(methacrylic acid) as the hydrophilic block of the diblock

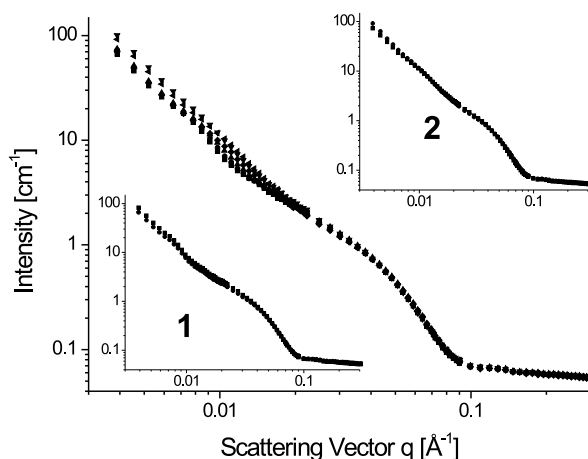


Fig. 3.11: SANS curves obtained from  $D_2O$  solutions (PD method) of  $PIB_{30}$ - $b$ - $PAA_{430}$  with different salt concentrations ranging from 0.1 M NaCl to 1.0 M NaCl (bottom to top). Insets: SANS curves from  $D_2O$  solutions of  $PIB_{30}$ - $b$ - $PAA_{430}$  at  $c_{NaCl} = 0.1$  M (1) and  $c_{NaCl} = 1.0$  M (2) prepared with PD (■) and BD (●) method,  $c_{POL.} = 1$  wt-%.

copolymer. The same can be stated for cryo-TEM images for samples with NaCl

prepared according to the PD method. Here, also homogeneous spheres are obtained.

By means of SANS (cf. Figure 3.11) no big influence of the point of time of addition of salt to the samples in D<sub>2</sub>O can be observed. Even the amount of salt added seems to play a minor role. It is striking that the core size of the particles seem not to be influenced at all as the scattering curves for all samples almost superimpose.

An unexpected effect of point of the time of addition of salt is most pronounced for samples prepared in H<sub>2</sub>O with NaCl as salt. Here for samples, when salt was added before dissociation of the polymer, a nonequilibrium state can be observed, resulting in precipitation of nonspherical aggregates as seen from cryo-TEM images. For samples, where salt was added after dissociation of the polymer, according to DLS the assemblies are smaller and do not precipitate. This is a hint on more equilibrated structures.

Comparing the DLS results from D<sub>2</sub>O and H<sub>2</sub>O samples it is evident, that the solvent has an influence as well. for the D<sub>2</sub>O samples, the assemblies are smaller in size and the difference between samples, where salt was added before and after dissolution of the polymer, is much less pronounced. The same can be stated for the influence of the counterion, as assemblies obtained from samples prepared with Cs<sup>+</sup>-salts are much more regularly shaped and smaller than Na<sup>+</sup> ion based solutions. Up to now no clear explanation for this phenomenon is obtained. Further investigations are necessary. Comparison to micelles formed by Poly(*n*-butyl acrylate)-*block*-poly(acrylic acid) (P*n*BA-*b*-PAA) indicates a non-equilibrium behavior of our system.

### 3.4 Individual Contributions to Joint Publications

The results presented in this thesis were obtained in collaboration with others, and submitted to publication as indicated below. In the following, the contributions of my coauthors to the different publications are specified.

#### Chapter 5

This work was submitted to *Langmuir* under the title "Polyisobutylene-*block*-poly(methacrylic acid) diblock Copolymers: Self-Assembly in Aqueous Media" by Markus Burkhardt, Nemesio Martinez-Castro, Sandrine Tea, Markus Drechsler, Ivan Babin, Ivan Grishagin, Ralf Schweins, Dmitry V. Pergushov, Michael Gradzielski, Alexander B. Zezin, Axel H.E. Müller. The synthesis of the block copolymer was performed by me as reported in the introduction. Together with the local contact Ralf Schweins I performed the SANS measurements at the Institut Max von Laue-Paul Langevin (ILL, Grenoble, France). The radialization of the raw data and the fits of the experimental data were performed by me with the help of Prof. Dr. Michael Gradzielski. Nemesio Martinez-Castro introduced me into the synthesis of the diblock copolymers. Ivan Babin and Ivan Grishagin carried out the *cmc* measurements at Moscow State University and some DLS measurements during their internship in Bayreuth in August 2005. Markus Drechsler performed the cryo-TEM measurements. During her internship from April to June 2004, Sandrine Tea contributed with the synthesis of two diblock copolymers and investigations by means of DLS. SLS measurements, the residual DLS measurements and the potentiometric

titrations were performed by me. Alexander Zezin and Dmitry V. Pergushov participated in discussions of the results.

### Chapter 6

This work was submitted to *Langmuir* under the title "Water-Soluble Interpolyelectrolyte Complexes of Polyisobutylene-*block*-Poly(methacrylic acid) Micelles: Formation and Properties" by Markus Burkhardt, Markus Ruppel, Markus Drechsler, Ralf Schweins, Dmitry V. Pergushov, Michael Gradzielski, Alexander B. Zezin, Axel H.E. Müller. The synthesis of the block copolymer was performed by me as reported in the introduction and in Chapter 5. Together with the local contact Ralf Schweins I performed the SANS measurements at the Institut Max von Laue- Paul Langevin (ILL, Grenoble, France). The radialization of the raw data and the fits of the experimental data were performed by me with the help of Prof. Dr. Michael Gradzielski. Markus Ruppel introduced me into the use of the titration apparatus and helped me in interpreting the results obtained by the sodium selective electrode. The AUC measurements were performed by Dmitry Pergushov at Moscow State University. Markus Drechsler performed the cryo-TEM measurements. The DLS measurements and the potentiometric titrations were performed by me. Alexander Zezin and Dmitry V. Pergushov participated in discussions of the results.

### Chapter 7

This work is to be submitted to *Macromolecular Rapid Communications* under the title "Aqueous Solutions of Polyisobutylene-*block*-Poly(acrylic acid) Diblock Copolymers: Path Dependent Formation of Non-Equilibrium Assemblies" by Markus Burkhardt, Roland Walker, Markus Drechsler, Ralf Schweins, Dmitry Pergushov, Alexander B. Zezin, Michael Gradzielski, Axel H.E. Müller. The synthesis of the block copolymer was done by Roland Walker and me as reported in the introduction. Roland Walker also contributed to this work by carrying out some DLS measurements. Together with the local contact Ralf Schweins I performed the SANS measurements at the Institut Max von Laue - Paul Langevin (ILL, Grenoble, France). The radialization of the raw data were performed by me with the help of Michael Gradzielski. Markus Drechsler conducted the cryo-TEM images. The residual DLS measurements and experiments with deuterated samples were performed by me. Alexander Zezin and Dmitry V. Pergushov participated in discussions of the results.

## 4. EXPERIMENTAL PART AND METHODS

### 4.1 Materials

#### 4.1.1 Cationic Polymerization

**Monomer:** Pure isobutylene (IB) was donated by BASF. For purification, it was passed through a drying column, "Labclear filter" (Aldrich) containing  $\text{CaSO}_4$  and #13 molecular sieves.

**Solvents:**  $\text{CH}_2\text{Cl}_2$  and *n*-hexane were dried over  $\text{CaH}_2$  and distilled right before use.

**Initiator:** TMPCl was synthesized from the corresponding olefin compounds 2,4,4-trimethyl-1-pentene (Fluka, 98%) by hydrochlorination with  $\text{HCl}_{(g)}$  at 0° C for 6 h. Right before use, it was distilled under vacuum.

**Coinitiator:**  $\text{TiCl}_4$  (Aldrich, 99.9%) was used as received.

**Additive:** DtBP (Aldrich, 97%) was used as received.

**Gas:** In order to purify/dry the nitrogen (99.9993% Riessner, Lichtenfels), it was passed through a drying column, "Labclear filter" (Aldrich) containing  $\text{CaSO}_4$  and #13 molecular sieves.

**Quenching agents:** Thiophene (Aldrich, 99+%) was purified by fractionated distillation. Methanol (Fluka, p.a.) was bubbled with nitrogen at least for 10 minutes before being added to the polymerization.

#### 4.1.2 Anionic Polymerization

**Monomers:** *t*BMA and *t*BA (BASF) were distilled over  $\text{CaH}_2$ . Both monomers were degassed by three freeze-thaw-cycles using high vacuum technique. Before condensing them into a bulb equipped with Rotaflo they were titrated with  $\text{AlEt}_3$  until a yellow color appeared.

**Solvent:** THF was refluxed for 3 days over  $\text{CaH}_2$ , followed by refluxing for 3 days over K/Na-alloy, all under nitrogen atmosphere. The solvent was directly entered into the reactor by pipelines, evacuated and stored under nitrogen.

**Macroinitiator:** The precursor for the macroinitiator was received from synthesis of PIB in living cationic polymerization. The treatment of the precursor is explained in experimental section (see below).

**Metals/alloys:** From potassium (Merck, > 98% in paraffin oil) and sodium (Merck, > 99% in paraffin oil) (3:1-5:1) the hydroxide surface was removed and subsequently they were melted in vacuo resulting in an alloy.

**Additives:**  $\text{LiCl}$  (Merck, > 99%) was dried for 48 hours at 200° C under high vacuum and stored under nitrogen. *n*-BuLi (Aldrich, 1.6 M in *n*-hexane), and *sec*-BuLi (Aldrich, 1.4 M in cyclohexane/hexane 92:8) were used as received.

**Gas:** Nitrogen (99.9993% and 99.9995%, Riessner, Lichtenfels) used at the vacuum-

line was purified/dried by passing it through an oxisorb filter (Messer Griesheim) containing chromium(II) oxide, and three flasks containing toluene, K/Na alloy, and a small amount of benzophenone.

#### 4.1.3 Preparation of Solutions

**Solvents:** Millipore (Milli-Q) water was freshly taken from the *Millipore+* apparatus, equipped with filtration packs *QPAK2E* (0.5  $\mu\text{m}$  prefilter, macroporous activated carbon, high purity mixed bed ion exchange resin, Organex polisher). The resistance of the water always was around 18.2 M $\Omega$  to make sure that all ions were removed. D<sub>2</sub>O (Deutero, 99.9%) was used as received.

**Additives:** NaCl (Riedel de Haën, p.a. grade), CsCl monohydrate (Fluka,  $\geq 95\%$ ), CsOH (Acros, p.a. grade), NaOH platelets (Merck, p.a. grade) and TRIS ( $\alpha, \alpha, \alpha$ -tris-(hydroxymethyl)methylamin; Aldrich, 99.9+%) were used as received. DCl and NaOD solutions (Deutero) were diluted with D<sub>2</sub>O to obtain the wanted pD-value.

**Polycation:** Poly-(4-N-vinylpyridine) (Aldrich) and EtBr (Merck,  $\geq 99\%$ ) were used without further purification.

## 4.2 Cationic Polymerization

Living cationic polymerization was carried out in a simple hood-setup avoiding the use of glove boxes and vacuum-lines. Before starting with the polymerization, a 500 ml three-necked flask equipped with a septum, a magnetic stirrer, and a nitrogen inlet (Figure 4.1) was evacuated twice for 20 minutes and flushed with nitrogen. The whole apparatus was connected to a burette for condensing the IB. Then a mixture of CH<sub>2</sub>Cl<sub>2</sub>/*n*-hexane 40:60 (*v/v*%, 120 ml/180 ml) was added under N<sub>2</sub> counterflow and cooled down to  $-78^\circ\text{C}$ . 0.355 ml (0.127 g, 0.67 mmol) of DtBP were added via septum and stirred for 10 min. 15 ml (10.57 g, 0.188 mol) of IB was condensed into the burette. Then, 0.6 ml (0.525 g, 3.53 mmol) of TMPCl was transferred into the reactor via needle and stirred for 5 min. After that, 1.5 ml (2.68 g, 0.014 mol) of TiCl<sub>4</sub> was added and stirred for further 10 min, the condensed IB was added into the reactor. After 1 h 28.3 ml (29.74 g, 0.353 mol) of thiophene (T) was added into the reactor. The occurrence of a reaction could be seen by a change of color from yellowish to slightly orange/red color. After 1.5 h, 30 ml (23.55 g, 0.75 mol) of prechilled methanol was added to the polymerization reaction in order to quench the polymer, seen by a change of color from slightly orange to colorless.

The PIB-T was washed with H<sub>2</sub>O and NaCO<sub>3</sub> solution until neutral pH was obtained. The solution was filtered to remove precipitates coming from neutralization reactions. The organic phase was dried with MgSO<sub>4</sub> or Na<sub>2</sub>SO<sub>4</sub> and filtered. The solvent was removed with a rotary evaporator. The excess of thiophene was removed by repeated precipitation of the PIB-T into MeOH.

## 4.3 Anionic Polymerization

All the chemicals used in living anionic polymerization were dried carefully in order to obtain livingness of polymerization. High vacuum technique was used to be sure that no oxygen disturbs the polymerization process.

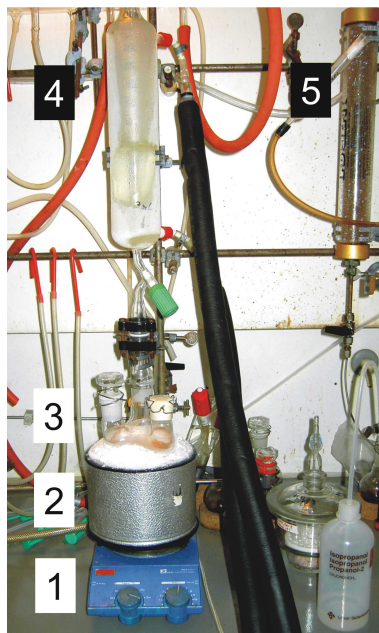


Fig. 4.1: Typical setup for cationic polymerization of PIB used in this work. A three-necked bulb (3) with connection to the condenser for IB (4), a septum and a glass plug was cooled to  $-78^{\circ}\text{C}$  with  $\text{CO}_2$ -ice (2) and stirred (1). The IB was purified with a column as described above (5) before condensing the desired amount of monomer.

The precursor for the macroinitiator (PIB-T) was dried and degassed for 24 h under high vacuum as described elsewhere [7]. It was weighed in an ampule and dried THF (see above) was condensed onto the PIB-T. The solution containing the macroinitiator was inserted via a transfer needle into a 1 l stirred glass reactor (Büchi) with a thermostatted cooling jacket, steel capillary connections to introduce gases and solvents and devices to measure temperature and pressure. THF was entered directly from distiles via pipelines. In case of *t*BA also LiCl solution was added into the reactor via transfer needle. The LiCl solution was prepared as described in literature, weighing a desired amount of LiCl into a flask equipped with a Rotaflo. The LiCl was heated up to  $300^{\circ}\text{C}$  under vacuum for 3 days to remove water. Then dried THF, prepared as described above, was condensed onto the LiCl to obtain a stock solution with  $c_{\text{LiCl}} = 16\text{ mM/l}$ . After the reactor was cooled down to  $-40^{\circ}\text{C}$  an 1.3-fold excess of *n*-BuLi was added and reacted for 1.5 h. Then the reaction was heated up to  $+40^{\circ}\text{C}$  in order to destroy unreacted BuLi for 1 h and then stored at RT over night.

After cooling down to  $-40^{\circ}\text{C}$  again, the wanted amount of monomer (*t*BMA, *t*BA) was entered from ampules via transfer needles. After the reaction was finished, 20 ml of prechilled methanol were added to quench the reaction. The solution was concentrated by evaporating solvent before precipitating the polymer into MeOH (*t*BMA) or MeOH/water (50/50%) (*t*BA).

#### 4.4 Synthesis of Polycation

Poly(N-ethyl-4-vinylpyridinium bromide) (P4VPQ) used in this work was synthesized by an exhaustive quaternization of poly(4-vinylpyridine) with weight-average

molar mass  $M_w = 60\,000$  g/mol (Aldrich,  $DP_w = 600$ ) and  $M_w = 50\,000$  g/mol (Polysciences Inc.,  $DP_w = 500$ ) with a tenfold excess of ethyl bromide (EtBr) in methanol at  $60^\circ\text{C}$  under reflux. The obtained polymer was precipitated into diethyl ether to remove unreacted polymer. P4VPQ was dried under vacuum at  $30^\circ\text{C}$  over night to remove residual solvent and EtBr. As determined by  $^1\text{H-NMR}$  spectroscopy, the molar fraction of quaternized pyridine units in the resulting polymer was close to 0.9, corresponding to about 540 and 450 charged monomer units per polymer chain, respectively.

#### 4.5 Hydrolysis of $\text{PIB}_x\text{-}b\text{-PtBMA}_y$ and $\text{PIB}_x\text{-}b\text{-PtBA}_y$

The hydrolysis of  $\text{PIB}_x\text{-}b\text{-PtBMA}_y$  and  $\text{PIB}_x\text{-}b\text{-PtBA}_y$  copolymers to obtain water-soluble  $\text{PIB}_x\text{-}b\text{-PMAA}_y$  and  $\text{PIB}_x\text{-}b\text{-PAA}_y$ , respectively, was carried out in dioxane under reflux ( $80^\circ\text{C}$ ). A 1.5-fold excess of HCl with respect to the *t*-Bu protection groups of the polyacids was added to a 10 wt-%-solution of the polymer and refluxed for 24 h. After concentrating by removing part of the solvent, the solution was precipitated into  $\text{Et}_2\text{O}$  and stirred over night (PIB with  $M_n < 10,000$  is soluble in  $\text{Et}_2\text{O}$ ) [69]. The solution was centrifuged, the supernatant solution containing unreacted PIB was removed. The polymer was dried in a vacuum oven at RT over night.

#### 4.6 Preparation of Micelles and Complexes

To prepare a stock solution of the copolymer,  $\text{PIB}_x\text{-}b\text{-PMAA}_y$ , NaCl (Merck) and TRIS buffer (2-amino-2-(hydroxymethyl)-1,3-propanediol, Fluka) were dissolved in NaOH-solution at RT under continuous stirring for at least 24 h. The amount of NaOH was calculated according to the number of COOH-groups of the weighed polymer. The solutions containing NaCl all showed low viscosity and were transparent. Solutions without added NaCl showed higher viscosity.

The polycation solution was prepared by dissolving the P4VPQ in Milli-Q water with the same ionic strength as the copolymer solution. Complexes were formed by slow addition of polycation to a micellar solution of the copolymer with the desired amount of NaCl and TRIS. The polycation was added under vigorous stirring. Turbid solutions were stirred until they were transparent again before further addition of polycation. No macroscopic precipitation was observed during the preparation of the complexes. Before measurements were carried out, the solutions were equilibrated by stirring for 24 h at room temperature.

#### 4.7 Light Scattering

Light can interact with particles in different ways, namely be transmitted, scattered or absorbed. This can be combined in

$$I_o = I_s + I_{tr} + I_{abs}, \quad (4.1)$$

where  $I_s$  is the intensity of the scattered light,  $I_{tr}$  the transmitted intensity and  $I_{abs}$  the absorbed intensity of an incident intensity  $I_o$ . If absorption can be neglected,

the scattering is the process that is used in Static Light Scattering (SLS) and Dynamic Light Scattering (DLS) to deduce measures like hydrodynamic radius  $R_h$  via diffusion coefficients  $D$  (DLS) or radius of gyration  $R_g$ , molecular weight  $M_w$  or the second virial coefficient  $A_2$ , giving information about the interactions of the polymer with the solvent or other polymer molecules. In DLS the fluctuations of intensity are recorded, being a measure of the diffusion of the particles through the scattering volume. In contrast to that, in SLS the total scattering intensity of a species is measured at different concentrations and angles, leading to a ZIMM- or Berry-plot, where the slopes and the intercept allow to calculate the wanted parameters.

In all scattering experiments one has to make sure to avoid contamination with dust. As scattering power depends on the 6<sup>th</sup> power of radius, those particles would lead to totally wrong results. Therefore all solutions have to be filtered carefully prior to the measurements.

A typical setup for light scattering experiments is shown in Figure 4.2. Polarized

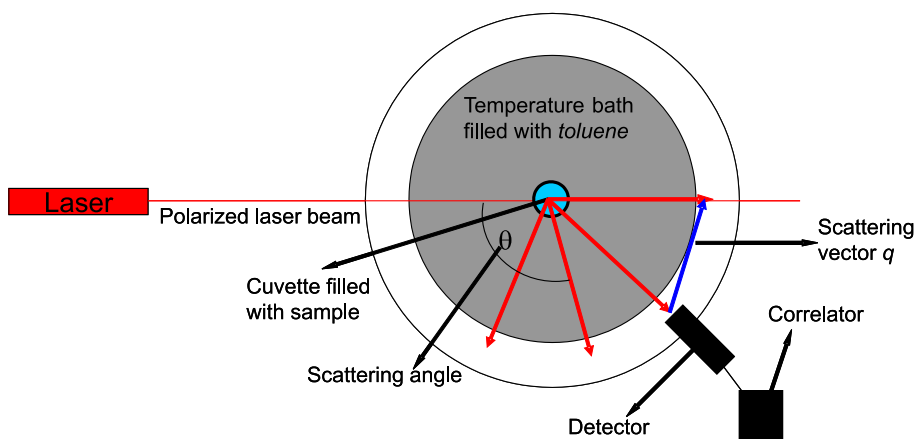


Fig. 4.2: A typical setup for light scattering experiment consists of a laser, a scattering sample, a movable photon detector and a photon correlator (DLS).

laser light is scattered by a sample placed in a toluene refractive index matching bath. The scattered light can be detected by a photon multiplier at different angles. A photon correlator enables DLS measurements.

#### 4.7.1 Static Light Scattering (SLS)[70, 71]

In light scattering different phenomena have to be taken into account. In the case of polymer solutions, Rayleigh and Debye scattering play the most important role. In case of scattering particles with  $d < \frac{\lambda}{20}$  Rayleigh scattering of an isolated scatterer occurs. Here the following equations are applied:

$$\frac{Kc}{R_{\Theta}} = \frac{1}{M_w} + 2A_2c, \quad (4.2)$$

$$\text{with } K = \frac{4\pi^2 n^2 (dn/dc)^2}{\lambda^4 N_A}, R_{\Theta} = \frac{I_s}{I_o} \frac{r^2}{1 + \cos^2 \Theta} \quad (4.3)$$

where  $K$  is the optical constant of the apparatus,  $R_{\Theta}$  is the Rayleigh ratio and is defined as the relative scattering intensity measured at an angle  $\Theta$  and a distance  $r$  from the scattering center,  $c$  is the polymer concentration,  $M_w$  is the weight-average

molecular weight,  $A_2$  is the second virial coefficient of the osmotic pressure,  $n$  is the refractive index of the solvent and  $I_s$  is the scattering intensity, depending on  $\Theta$  and  $r$ .

It is necessary to use polarized light to obtain an angular independent scattering. Today's lasers emit polarized light, so no further polarization is necessary. This polarization leads to a constant  $R_\Theta$  for small particles, as  $(1 + \cos^2\Theta) = 2$ . From SLS of small particles,  $M_w$  and  $A_2$  can be obtained from extrapolation to zero concentration, implying measurements of several concentrations.

As soon as the diameter of a scattering particle exceeds  $\frac{\lambda}{20}$  (Debye scattering), the requirement of isolated, non interacting scattering centers is not valid any more. In the case of larger particles like polymers and aggregates intramolecular interferences between scattering centers of the same chain become important. Here the scattering intensity is angular dependent, and from the angular dependence the size of the molecule can be derived. The equation developed to cover the Debye scattering, the so called Zimm-equation,

$$\frac{Kc}{R_\Theta} = \left( \frac{1}{M_w} + 2A_2c \right) \left( 1 + \frac{q^2}{3} \langle r_g^2 \rangle_z \right) \quad (4.4)$$

contains the scattering vector  $q = \frac{4\pi n}{\lambda} \sin \frac{\Theta}{2}$ . The second bracket is the form factor  $P_\Theta$ , allowing to deduce  $\langle r_g^2 \rangle_z$ , the  $z$ -average mean-square radius of gyration.

After measuring the angular dependence of different concentrations of a sample, a Zimm-plot, shown in Figure 4.3, can be used to obtain the results described above.

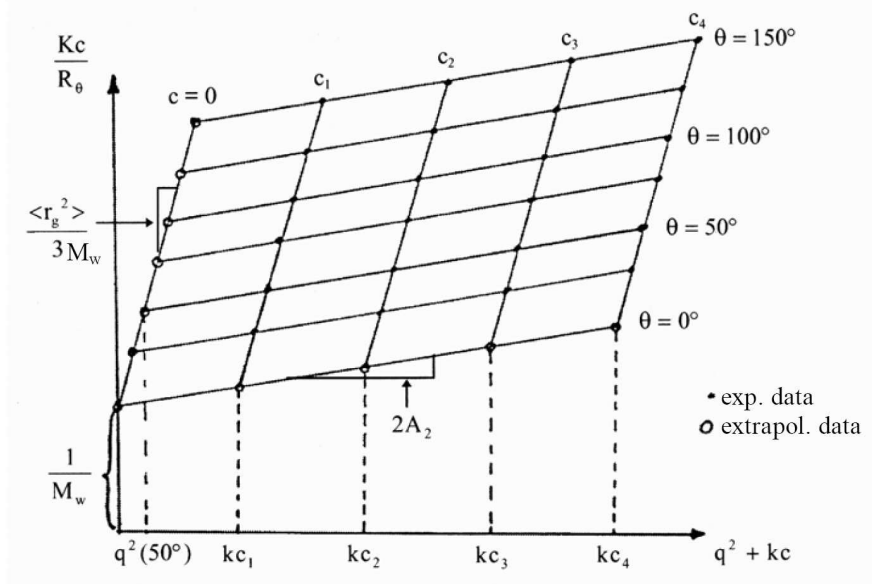


Fig. 4.3: From a Zimm plot, the  $M_w$ ,  $r_{g,z}$  and  $A_2$  of a system can be obtained by extrapolation to zero concentration and angle.

From Zimm equation, the molecular parameters can be determined via the fol-

lowing extrapolations:

$$\begin{aligned}
 (1) c \rightarrow 0, \Theta \rightarrow 0 : \frac{Kc}{R_\Theta} &= \frac{1}{M_w} \\
 (2) c \rightarrow 0 : \frac{Kc}{R_\Theta} &= \frac{1}{M_w} \left( 1 + \frac{q^2}{3} \langle r_g^2 \rangle_z \right) \\
 (3) \Theta \rightarrow 0 : \frac{Kc}{R_\Theta} &= \frac{1}{M_w} + 2A_2c.
 \end{aligned} \tag{4.5}$$

In the case of larger aggregates, sometimes the dependence of  $Kc/R_\Theta$  on  $q^2$  is moderately curved. This causes the extrapolation to be less accurate. Berry [72] proposed plotting the square root of  $Kc/R_\Theta$  against  $q$  and  $c$ , respectively, because these plots show less curvature. As a reason for this it was presumed that the contribution of the third virial coefficient  $A_3$  becomes significant, and that  $A_3 \propto A_2^2$ . Thus at zero angle

$$\left( \frac{c}{R_\Theta} \right)_{\Theta \rightarrow 0}^{\frac{1}{2}} = \left( \frac{1}{\overline{M_w}K} \right)^{\frac{1}{2}} (1 + \overline{M_w}A_2c) \tag{4.6}$$

and at zero concentration

$$\left( \frac{c}{R_\Theta} \right)_{c \rightarrow 0}^{\frac{1}{2}} = \left( \frac{1}{\overline{M_w}K} \right)^{\frac{1}{2}} \left[ 1 - \frac{8\pi^2}{3\lambda^2} \langle r_g^2 \rangle_z \sin^2\left(\frac{\Theta}{2}\right) \right]. \tag{4.7}$$

Hence, from Table 4.1 the coefficients are shown, used for evaluation of the equation obtained from linear regression, resulting in

$$y = a + bx + cx^2 \dots \tag{4.8}$$

of the measured data according to Zimm and Berry.

	$\overline{M_w}$	$\langle r \rangle^2$	$A_2$
Zimm	$\frac{1}{a}$	$\frac{3 \cdot b}{a}$	$\frac{b}{2}$
Berry	$\left(\frac{1}{a}\right)^2$	$\frac{6 \cdot b}{a}$	$b \cdot a$

Tab. 4.1: Coefficients from linear regression used for evaluation of the light scattering data according to Zimm and Berry.

In the present studies, stock solutions of  $\text{PIB}_x\text{-}b\text{-PMAA}_y$  were prepared. Dialysis for at least two days against an aqueous solution with the same ionic strength was used to obtain solvent for diluting the samples to prepare different concentrations as well as for the determination of the  $\frac{dn}{dc}$  (see below). SLS measurements were carried out on a Sofica goniometer with He-Ne laser ( $\lambda = 632.8 \text{ nm}$ ) at RT. Prior the measurements, sample solutions were filtered through Millipore nylon filters of pore size  $0.45 \text{ }\mu\text{m}$ .

### 4.7.2 Refractive Index Increment $dn/dc$

For SLS measurements the refractive index increment,  $\frac{dn}{dc}$ , which represents the scattering contrast of the solution compared to the particles, has to be measured. The slope of a plot of refractive indices  $n$  of solutions with different polymer concentrations against  $c$  can be obtained by linear fitting. A Diffraction Refractometer DnDC2010/620 (PSS) was used to measure the refractive index increment,  $\frac{dn}{dc}$ , of the polymer solution at  $\lambda = 620$  nm.

### 4.7.3 Dynamic Light Scattering (DLS)

Brownian motions of molecules are the base of DLS. Movements of polymers cause fluctuations in detected scattering intensity. Dissolved molecules move in all directions with the same probability and they have a continuous rate distribution. The Doppler effect explains the changes in frequency of scattered light seen by the detector. Compared with the incident light  $I_o$  a broadening of the spectrum is observed. Thus, scattering is always quasielastic and not, as assumed, elastic.

The resulting fluctuations of the scattered light with time are measured normally according to the Homodyne method, i.e. the scattered light is directed to the photon detector. The output signal of the detector is proportional to the intensity of light  $I(t)$  and proportional to the mean square of the electric field  $|E(t)|^2$ . The output signal of the detector is auto-correlated with time according to the following equation [73, 74]:

$$g_2(t) = \frac{\langle I(0) \cdot I(t) \rangle}{\langle I(0) \rangle^2} \quad (4.9)$$

with  $g_2(t)$  as the normalized intensity autocorrelation function. The field autocorrelation function,  $g_1(t)$ , describes the fluctuations of the electric field of the scattered light. It can be obtained from  $g_2(t)$  using the Siegert relation [75]:

$$g_1(t) = \frac{\langle E(0) \cdot E(t) \rangle}{\langle E(0) \rangle^2} = \sqrt{\frac{g_2(t) - A}{B}} \quad (4.10)$$

with  $A, B$  normally being unity.  $A$  is determined by an experimental baseline, and  $B$  is a coherence factor accounting for deviation from ideal correlation.

In the case of monodisperse hard spheres,  $g_1(t)$  can be described by an exponential function:

$$g_1(t) = e^{-\Gamma \cdot t}. \quad (4.11)$$

The decay rate  $\Gamma$  is directly connected with the translational diffusion coefficient  $D$  of the species via  $\Gamma = Dq^2$ . The Stokes-Einstein equation [73, 76]

$$R_h = \frac{k_B T}{6\pi\eta D} \quad (4.12)$$

connects the diffusion of a species with their hydrodynamic radius  $R_h$ , taking the viscosity  $\eta$  of the solvent into account, with the Boltzmann constant  $k_B$  and  $T$  the temperature in K.

For a system of polydisperse spheres, the following equation holds:

$$g_1(q, t) = \sum_j a_j(q) e^{-\Gamma_j t} \quad (4.13)$$

with  $a_j(q)$  the relative amplitudes

$$a_j(q, ) = \frac{c_j M_j P_j(q)}{\sum_j c_j M_j P_j(q)} \quad (4.14)$$

with  $M_j$  the molecular weight and  $P_j$  the form factor of the particle  $j$ . With spheres larger than  $\frac{\lambda}{20}$  and  $P_j(q) < 1$  one can observe an angular dependence of  $g_1(t)$ .

Changes from hard spheres to polymer molecules in solution involve rotational diffusion and internal modes in addition to translational diffusion. Rotational diffusion is of particular importance in rod-like molecules, whereas internal modes are significant in large coil-like molecules [76]. From a mathematical point of view, these factors involve additional additive and multiplicative terms. The terms can be eliminated by angle dependent measurements as the amplitudes approach zero for  $q^2 > 0$  [73]. The determination of the mean diffusion coefficient and standard deviation for polydisperse systems is best accomplished by the CONTIN method [77, 78]. The function  $g_1(t)$  is described by a continuous distribution:

$$g_1(q, t) = \int_{\Gamma_{min}}^{\Gamma_{max}} G(\Gamma) e^{-\Gamma \cdot t} d\Gamma \quad (4.15)$$

with  $G(\Gamma)$  describing the fluctuation rate distribution function. This equation can be inverted by a Laplace transformation. This inversion is problematic as there is basically an unlimited number of solutions that describe the data within experimental error. In order to minimize these solutions, the CONTIN analysis uses the following regularization:

$$R_n(G(\Gamma)) = \int_{\Gamma_{min}}^{\Gamma_{max}} \left( \frac{\delta^n G(\Gamma)}{\delta \Gamma^n} \right) d\Gamma \quad (4.16)$$

where  $n$  is the order of regularization. Regularization of 0th order represents minimization of the integration area of function  $G(\Gamma)$ ; regularization of 2nd order corresponds to smoothing of function  $G(\Gamma)$ . The original CONTIN routine calculates a rate distribution ( $\log(\Gamma)$  scale), whereas the CONTIN routine of the ALV software calculates a time distribution ( $\log(t)$  scale) that is proportional to the distribution of hydrodynamic radius. The ALV software also enables a direct fit of  $g_2(t) - 1$  via a special algorithm. This usually yields a smoother distribution function with less artifacts as compared to  $g_1(t)$

$$g_2(t) - 1 = \left( \int_{t_{min}}^{t_{max}} e^{-t} G(t) dt \right)^2. \quad (4.17)$$

Care must be exerted on interpreting results so as to avoid artifacts, especially in the case of a low signal-to-noise ratio, an inappropriate baseline or inappropriate choice of  $\Gamma_{max}$  and  $\Gamma_{min}$ . Thus, the signal-to-noise ratio should always be high. For evaluation of the results, it should be considered that two different distributions can only be distinguished with the CONTIN program if the respective hydrodynamic radii differ from each other by a factor of at least two. The radii or rather diffusion coefficients obtained by the CONTIN method are  $z$ -average values. In order to eliminate the influence of form factors for large molecules, the  $D$  and  $R_h$  values, respectively, measured at different angles have to be extrapolated to  $q^2 > 0$ .

The DLS measurements were carried out in sealed cylindrical scattering cells ( $d = 10$  mm) at five scattering angles  $30^\circ$ ,  $60^\circ$ ,  $90^\circ$ ,  $120^\circ$  and  $150^\circ$  with the use of an ALV DLS/SLS-SP 5022F equipment consisting of an ALV-SP 125 laser goniometer, an ALV 5000/E correlator, and a HeNe laser with the wavelength ( $\lambda = 632.8$  nm) for  $3 \times 100 - 300$  s. The CONTIN algorithm was applied to analyze the obtained correlation functions. Hydrodynamic radii were calculated according to the Stokes-Einstein equation.

#### 4.8 Small Angle Neutron Scattering (SANS)

Small Angle Neutron Scattering (SANS) [79, 80, 71] is one of the most important techniques to investigate the structure of polymers in solution and in bulk. The technique is based on the fact that neutrons interact with matter. According to *deBroglie* each moving particle can be considered as a wave with a certain wavelength  $\lambda$  (particle-wave dualism). This can be expressed by

$$\lambda = \frac{h}{m \cdot v} \quad (4.18)$$

with  $m$  and  $v$  representing the mass and the velocity of the particle. Thus, effects occurring in SANS can be treated in the same way as effects in X-Ray or light scattering. Due to different wavelengths of these techniques different dimensions can be investigated (see Table 4.2).

Radiation	Wavelength [Å]	Resolution [Å]
X-Rays	1 - 4	$0.5 \cdot 10^2 - 5 \cdot 10^2$
Neutrons	1 - 20	$0.5 \cdot 10^3 - 2 \cdot 10^3$
Light	$4 \cdot 10^3 - 6 \cdot 10^3$	$\sim 10^3 - 10^5$

Tab. 4.2: Due to different wavelengths of the radiation different dimensions are accessible with LS, SANS and SAXS/WAXS.

In SANS the differential scattering cross section  $\frac{d\Sigma}{d\Omega}$  is the value comparable to the Rayleigh ratio  $R_\Theta$  from SLS. It is a measure of the number of neutrons scattered per time and space compared to the intensity  $I_o$  of the incident beam. After normalization with the scattering volume  $V$  a differential scattering cross section independent of the setup is obtained:

$$\frac{d\Sigma}{d\Omega} = \frac{A \cdot I(q)}{V \cdot I_o} \quad (4.19)$$

with  $A$  being the area of the sample scattering and  $I_o$ , the number of neutrons per time. The scattering vector  $q$  is defined as

$$q = \frac{4\pi}{\lambda} \cdot \sin\left(\frac{\Theta}{2}\right) \quad (4.20)$$

with  $\lambda$  being the wavelength and  $\Theta$  the scattering angle.

In SANS the contrast of the sample compared to the background (solvent, sample cell, detector dark count) comes from differences in scattering length density  $\bar{\rho}$  of different species in the sample, comparable to the  $\frac{dn}{dc}$  value in SLS. When neutrons are scattered by an atom, the scattering length  $b_i$  is a measure of the scattering power of each sort of atoms. The overall scattering length density  $\bar{\rho}$  can be calculated as

$$\bar{\rho} = \frac{1}{V} \sum b_i. \quad (4.21)$$

The contrast between sample and background is proportional to the square of the difference in their scattering length density. The differential scattering length density can be calculated as

$$\frac{d\Sigma}{d\Omega} = {}^1N \cdot (\bar{\rho} - \rho_s)^2 \cdot \langle V^2 \cdot P(q) \cdot S(q) \rangle \quad (4.22)$$

with particle density  ${}^1N$ , solvent scattering length density  $\rho_s$ , particle volume  $V$ , form factor  $P(q)$  and structure factor  $S(q)$ . This is only valid for coherent scattering. As there is always a certain amount of neutrons scattered incoherently, the scattering intensity contains an isotropic background that has to be subtracted from the measured intensity. The intensity coming from incoherent scattering  $I_{incoh}$  can be obtained from the slope of the plot of  $I \cdot q^4$  versus  $q^4$ , according to

$$\lim_{q \rightarrow \infty} I(q) \cdot q^4 = A \cdot \frac{S}{V} + I_{incoh} \cdot q^4 \quad (4.23)$$

Evaluations of double logarithmic plots of scattering intensity  $I(q)$  against  $q$  can be used for fitting the curves according to theory of particles with different shapes. Besides rods, vesicles and spheres many other form factors have already been published in literature. In our case, the form factors for spherical particles containing a core-shell or core-shell-corona structure are of interest. In case of the core-shell

model with constant scattering length densities  $\rho_c$  (core) and  $\rho_0$  (solvent) it was assumed that the scattering length density of the shell ( $\rho_s$ ) decreases with [9]:

$$\rho_s = \rho_1 \left( \frac{r}{R_c} \right)^{-a}, R_c < r < R_m \quad (4.24)$$

with  $R_m$  being the maximum radius of the aggregate and  $a = 2$  (stiff chains) describing the radial scattering length density profile in the micellar corona as shown in Figure 4.4. For  $D_2O$   $\rho_o = 63.6 \cdot 10^9 \text{ cm}^{-2}$  was used. For PIB (core) a den-

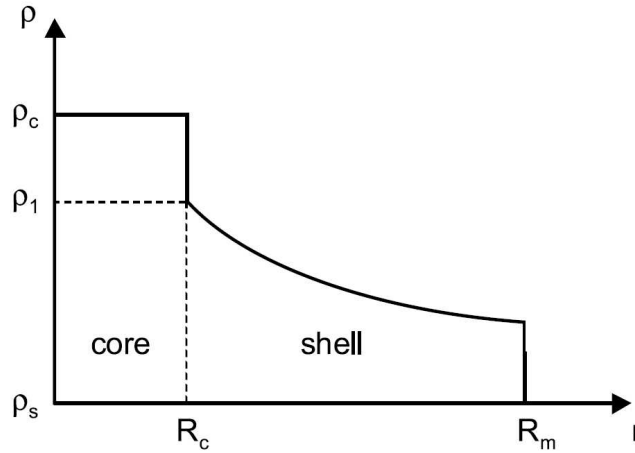


Fig. 4.4: Scattering length densities assumed for a simple core-shell model. A constant core scattering density is followed by an exponential decrease of the scattering density of the surrounding shell.

sity of  $0.918 \frac{g}{\text{cm}^3}$  was assumed, leading to  $\rho_c = -3.3 \cdot 10^9 \text{ cm}^{-2}$ . The value of  $\rho_s$  was evaluated under the assumption that the micellar corona is filled with  $D_2O$  ( $\rho_{D_2O} = 1.105 \text{ g/cm}^3$ ) and PMAA (with partial molar volumes of the monomer unit of 59.3 and 39.6  $\text{cm}^3/\text{mol}$  for protonated and ionized forms, respectively [82, 83]).

The resulting scattering intensity then can be expressed as

$$I(q) = {}^1 N \int_0^{\text{inf}} dR_c f(R_c) P(q, R_c, a, R_m) S(q) \quad (4.25)$$

with the form factor  $P(q)$ , the structure factor  $S(q)$ , the number density of particles  ${}^1 N$  and the distribution function of core radii with Schulz distribution [84]. The form factor can be written as [85, 86]:

$$\begin{aligned} \frac{P(q)}{P(0)} = & \left\{ \left[ \frac{1}{3} {}_0F_1 \left( \frac{3}{2}; -\frac{q^2 R_c^2}{4} \right) - \frac{\rho_1}{\rho_c(3-a)} {}_1F_2 \left( \frac{3-a}{2}, \frac{3}{2}, \frac{5-a}{2}, \frac{q^2 R_c^2}{4} \right) + \right. \right. \\ & \left. \left. + \left( \frac{R_c}{R_m} \right)^{a-3} \frac{\rho_1}{\rho_c(3-a)} \times {}_1F_2 \left( \frac{3-a}{2}, \frac{3}{2}, \frac{5-a}{2}, \frac{q^2 R_c^2}{4} \right) \right] / \right. \\ & \left. / \left[ \frac{1}{3} + \frac{\rho_1}{\rho_c(3-a)} \left( \left( \frac{R_c}{R_m} \right)^{a-3} - 1 \right) \right] \right\}^2 \end{aligned} \quad (4.26)$$

with  ${}_0F_1(q, R_c)$  and  ${}_1F_2(q, R_c, a)$  representing hypergeometric functions. To describe  $S(q)$  a random-phase approximation for charged spherical particles interacting through a screened Coulomb potential was applied [87].

The core radius obtained from the fitting of the SANS curves allows to calculate the aggregation number  $N_{agg}$ :

$$N_{agg} = \frac{4}{3}\pi R_c^3 \frac{\rho_{PIB}}{M_{PIB}N_A} \quad (4.27)$$

with Avogadro number  $N_A$  and the bulk density and molecular weight  $\rho_{PIB}$  and  $M_{PIB}$  respectively.

The measurements in this work were performed at D11 and D22 at the *Institut Laue-Langevin* (ILL) at Grenoble (F). The advantage of especially D11 is the wide range of detector distances (1.1 m up to 40.5 m) accessing even the low  $q$ -region. In Grenoble also the neutron flux is high compared to other neutron sources in Europe, resulting in a better signal to noise ratio of the measurements.

A typical setup for SANS is shown in Figure 4.5 [88]. For the samples, 2 mm

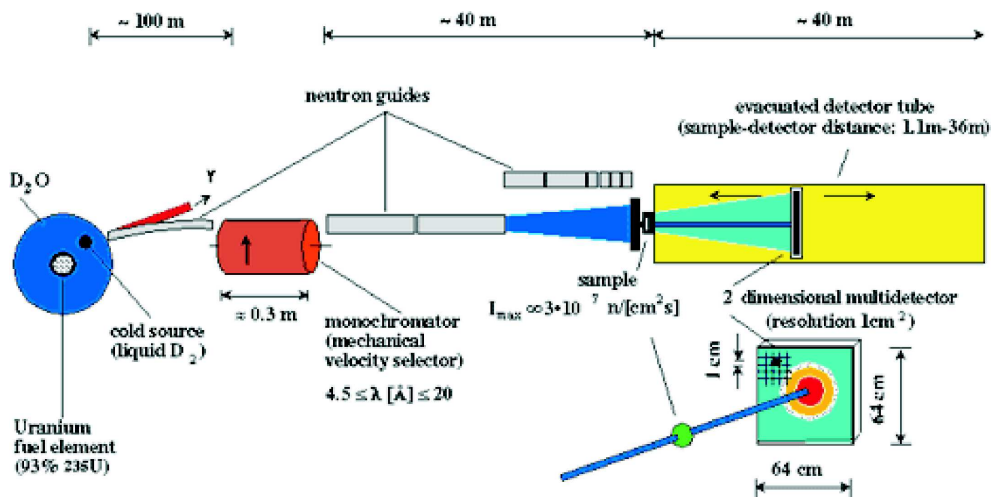


Fig. 4.5: Setup of a SANS experiment including neutron source, sample and detector system [88].

Hellma quartz cells were used. Wavelengths  $\lambda$  of  $6\text{\AA}$  and  $8\text{\AA}$  were selected.

The measurements were made with sample-to-detector distances of 1.1, 4, and 16 m, accessing a total range of  $q = 0.003 - 0.33 \text{\AA}^{-1}$ . In some cases, measurements with detector distance of 36 m were made. The detector sensitivity and the intensity of the primary beam were calibrated with a 1 mm reference water sample. The obtained data were radially averaged, corrected for the detector background, the detector dead time, and the scattering from an empty cell. Then they were converted into absolute units by a comparison with the scattering from water according to standard routines supplied by the ILL [81], using GRASP software.

### 4.9 Potentiometric Titration

Titration measurements of micellar solutions and complexes were carried out in aqueous solutions of the polymers with the METROHM Titrand 809. For pH-dependent measurements, the "Unitrode with Pt 1000" or the "Auqatrode Plus with Pt 1000" was used. The  $\text{Na}^+$ -ion activity was followed by the "Polymer membrane electrode Na". Measurements of the turbidity of the solutions were carried out using a "Spectrode 523nm". For complexation, a calculated amount of the P4VPQ was added to a solution containing micelles with maximum dosing rate ( $6.66 \frac{\text{ml}}{\text{min}}$  for 2 ml device,  $66.66 \frac{\text{ml}}{\text{min}}$  for 20 ml device). The turbidity was monitored until a plateau was reached. Then further polycation was added, trying to obtain complexes with higher  $Z$ -value.

### 4.10 Fluorescence Measurements

The critical micellar concentration ( $cmc$ ) was determined by Fluorescence Spectroscopy. The emission spectra of a fluorophore like pyrene depend on the polarity of the surrounding media [89, 90]. Added to an aqueous solution of amphiphilic molecules below  $cmc$ , the intensity ratio of the band  $I_1$  and  $I_3$  in fluorescence spectra can be calculated. Due to the polar surrounding, the ratio should be around 1.8. With increasing polymer concentration, aggregation of the hydrophobic parts occurs and the  $cmc$  is reached. Beyond the  $cmc$ , the pyrene molecules can dissolve in the hydrophobic cores of the aggregates, changing the polarity of the surrounding media. This also has an influence in the  $\frac{I_1}{I_3}$ -ratio, dropping down to around 1.2.

The samples for fluorescence measurements were prepared according to a procedure similar to that described elsewhere [91, 92]. Pyrene (Aldrich) was dissolved in acetone. Some drops were entered into dark vials via a Hamilton microsyringe. The acetone was evaporated slowly. Then the polymer solution was added. The samples were stirred at  $40 - 50^\circ \text{C}$  for 48 h to allow equilibration. The pyrene concentration was kept at  $5 \cdot 10^{-7} \frac{\text{mol}}{\text{l}}$ . This is only slightly lower than the saturation concentration of fluorescent dye in water at  $T = 22^\circ \text{C}$ .

Steady-state fluorescence spectra of the air-equilibrated samples were recorded with a Hitachi F-4000 fluorescence spectrophotometer (right angle geometry,  $1 \text{ cm} \times 1 \text{ cm}$  quartz cell). The widths of slits were chosen to be 3 and 1.5 nm for excitation and emission, respectively.

### 4.11 *UV-Vis-Spectroscopy*

Measurements of absorption are based on the Bouguer-Lambert-Beers law. The absorption is defined as [93]

$$A_{\tilde{\nu}} = \lg \left( \frac{I_0}{I} \right)_{\tilde{\nu}} = \lg \left( \frac{100}{T(\%)} \right)_{\tilde{\nu}} = \varepsilon_{\tilde{\nu}} \cdot c \cdot d \quad (4.28)$$

with the incoming intensity  $I_0$ , transmitted intensity  $I$ , the molar extinction coefficient  $\varepsilon_{\tilde{\nu}}$  the concentration of the sample  $c$  and the thickness of the sample  $d$ .

Measurements were made on a Perkin-Elmer Lambda15 UV/vis spectrophotometer in the wavelength range from 210 to 900 nm. Measurements were carried out in solution. The spectrum from a quartz cuvette (10 mm, 110 QS Suprasil, HELLMMA) containing pure solvent was subtracted from sample spectra.

### 4.12 *Cryogenic Transmission Electron Microscopy (Cryo-TEM)[94]*

For Cryo-TEM studies, a drop of the sample was put on an untreated bare copper transmission electron microscopy (TEM) grid (600 mesh, Science Services, München, Germany), where most of the liquid was removed with blotting paper, leaving a thin film stretched over the grid holes. The specimens were instantly shock frozen by rapid immersion into liquid ethane and cooled to approximately 90 K by liquid nitrogen in a temperature controlled freezing unit (Zeiss Cryobox, Zeiss NTS GmbH, Oberkochen, Germany). The temperature was monitored and kept constant in the chamber during all of the sample preparation steps. After freezing the specimens, the remaining ethane was removed using blotting paper. The specimen was inserted into a cryo-transfer holder (CT3500, Gatan, München, Germany) and transferred to a Zeiss EM922 EF-TEM instrument. Examinations were carried out at temperatures around 90 K. The transmission electron microscope was operated at an acceleration voltage of 200 kV. Zero-loss filtered images ( $\Delta E = 0$  eV) were taken under reduced dose conditions (100 - 1000 e/nm<sup>2</sup>). All images were registered digitally by a bottom mounted CCD camera system (Ultrascan 1000, Gatan) combined and processed with a digital imaging processing system (Gatan Digital Micrograph 3.9 for GMS 1.4). To improve the contrast, the samples were dissolved using CsOH and CsCl to achieve the desired  $\alpha$  and ionic strength.

## BIBLIOGRAPHY

- [1] E.S. Gil, S.M. Hudson; *Prog. Polym. Sci.*, **2004**, *29*, 1173;
- [2] A. Blom, C. Drummond, E.J. Wanless, P. Richetti, G.G. Warr; *Langmuir*, **2005**, *21*, 2779;
- [3] P. Rigler, W. Meier; *J. Am. Chem. Soc.*, **2006**, *128*, 367;
- [4] T. Dwars, E. Paetzold, G. Oehme; *Angew. Chem. Int. Ed.*, **2005**, *44*, 7174;
- [5] S. Förster, V. Abetz, A.H.E. Müller; *Adv. Polym. Sci.*, **2004**, *166*, 173;
- [6] H. Shen, A. Eisenberg; *Macromolecules*, **2000**, *33*, 2561;
- [7] N. Martinez-Castro, M.G. Lanzendörfer, A.H.E. Müller, J.C. Cho, M.H. Acar, R. Faust; *Macromolecules*, **2003**, *36*, 6985;
- [8] D.V. Pergushov, E.V. Remizova, J. Feldthusen, A.B. Zezin, A.H.E. Müller, and V.A. Kabanov; *J. Phys. Chem. B*, **2003**, *107*, 8093;
- [9] D.V. Pergushov, E.V. Remizova, J. Feldthusen, M. Gradzielski, P. Lindner, A.B. Zezin, A.H.E. Müller, and V.A. Kabanov; *Polymer*, **2004**, *45*, 367;
- [10] H. Schuch, J. Klingler, P. Rossmanith, T. Frechen, M. Gerst, J. Feldthusen, A.H.E. Müller; *Macromolecules*, **2000**, *33*, 1734;
- [11] A.F. Thünemann, M. Müller, H. Dautzenberg, J.-F. Joanny, H. Löwen; *Adv. Pol. Sci.*, **2004**, *166*, 113;
- [12] V.G. Babak, E.A. Merkovich, J. Desbrieres, M. Rinaudo; *Pol. Bull.*, **2000**, *45*, 77;
- [13] R. Konradi, J. Rühle; *Macromolecules*, **2005**, *38*, 6140;
- [14] T. Matsudo, K. Ogawa, E. Kokufuta; *Biomacromolecules*, **2003**, *4*, 1794;
- [15] I. Gossel, L. Shu, A.D. Schluter, J.P. Rabe; *J. Am. Chem. Soc.*, **2002**, *124*, 6860;
- [16] T. Sonoda, T. Niidome, Y. Katayama; *Recent Research Developments in Bioconjugate Chemistry*, **2005**, *2*, 145;
- [17] J.F. Quinn, J.C.C. Yeo, F. Caruso; *Macromolecules*, **2004**, *37*, 6537;

- 
- [18] B. Qi, X. Tong, Y. Zhao; *Macromolecules*, **2006**, *17*, 5714;
- [19] O. Colombani, M. Ruppel, M. Burkhardt, M. Drechsler, M. Schumacher, M. Gradzielski, R. Schweins, A.H.E. Müller; *Macromolecules*, **2007**, *40*, 4351;
- [20] B. Ivan; *Makromol. Chem., Macromol. Symp.*; **67**, 311; **1993**;
- [21] J. P. Kennedy, B. Ivan; *Designed Polymers by Carbocationic Macromolecular Engineering: Theory and Practice*; Hanser Publishers: Munich; **1992**;
- [22] P. Sigwalt; *Makromol. Chem., Macromol. Symp.*; **47**, 1791; **1991**;
- [23] K. Matyjaszewski, C. H. Lin; *Makromol. Chem., Macromol. Symp.*; **47**, 211; **1991**;
- [24] B. Ivan, J. P. Kennedy; *Macromolecules*; **28**, 2880; **1990**;
- [25] I. Majoros, J. P. Kennedy, T. Kelen, T. M. Marsalko; *Polym. Bull.*; **31**, 255; **1993**;
- [26] K. Matyjaszewski; *Cationic Polymerizations: Mechanisms, Synthesis, and Applications*; Marcel Dekker Inc.: New York / Basel / Hong Kong; **1996**;
- [27] O. Nuyken, H. Kroener, H. Aechtner; *Makromol. Chem., Macromol. Symp.*; **32**, 181; **1990**;
- [28] M. Zsuga, J. P. Kennedy, T. Kelen; *Makromol. Chem., Macromol. Symp.*; **32**, 145; **1990**;
- [29] M. Sawamoto, T. Higashimura; *Makromol. Chem., Macromol. Symp.*; **32**, 131; **1990**;
- [30] R. Faust, B. Ivan, J. P. Kennedy; *J. Macromol. Sci., Chem.*; **A28**, 1; **1991**;
- [31] R. Faust, B. Ivan, J. P. Kennedy; *Polym. Prepr.*; **31**, 466; **1990**;
- [32] A. Dembinski, Y. Yagci, W. Schnabel; *Polym. Commun.*; **34**, 3738; **1993**;
- [33] T. Kelen, M. Zsuga, L. Balogh, I. Majoros, G. Deak; *Makromol. Chem., Macromol. Symp.*; **67**, 325; **1993**;
- [34] T. Pernecker, J. P. Kennedy; *Polym. Bull.*; **26**, 305; **1991**;
- [35] G.V. Schulz; *Adv. in Chem. Sci.*; **128**, 1; **1973**;
- [36] R. Fayt, R. Forte, R. Jacobs, R. Jerome, T. Ouhadi, P. Teyssie, S.K. Varshney; *Macromolecules*; **20**, 1442; **1987**;
- [37] K. Hatada, T. Kitayama, K. Ute; *Progr. Polym. Sci.*; **13**, 189; **1988**;

- 
- [38] A.H.E. Müller; *Carbanionic Polymerization: Kinetics and Thermodynamics*; Comprehensive Polymer Science, G. Allen and J. C. Bevington, Eds., Pergamon: Oxford; **1988**;
- [39] H.L. Hsieh, R.P. Quirk; *Anionic Polymerization: Principles and Practical Applications*; Marcel Dekker, Inc.: New York / Basel / Hong Kong; **1996**;
- [40] N. Martinez-Castro; *New block copolymers of Isobutylene by combination of cationic and anionic polymerization*; Dissertation, **2004**;
- [41] S.K. Varshney, C. Jacobs, J.P. Hautekeer, P. Bayard, R. Jerome, R. Fayt, P. Teyssie; *Macromolecules*; **24**, 4997; **1991**;
- [42] X.F. Zhong, S.K. Varsheny, A. Eisenberg; *Macromolecules*; **25**, 7160; **1992**;
- [43] X.Y. Liu, J. Wu, J.-S. Kim, A. Eisenberg; *Langmuir*; **22**, 419; **2006**;
- [44] F.J. Gerner, H. Höcker, A.H.E. Müller, G.V. Schulz; *Eur. Polym. J.*; **20**, 349; **1984**;
- [45] M.E. Jung, R.B. Blum; *Tetrah. Lett.*; **43**, 3791; **1977**;
- [46] S. Antoun, J. S. Wang, R. Jerome, P. Teyssie; *Polymer*; **37**, 5755; **1996**;
- [47] J. S. Wang, R. Jerome, R. Warin, H. Zhang, P. Teyssie; *Macromolecules*; **27**, 3376; **1994**;
- [48] X.F. Zhong, S.K. Varshney, A. Eisenberg; *Macromolecules*; **25**, 7160; **1992**;
- [49] X. Andre, M. Zhang, A.H.E. Müller; *Macromol. Rapid Commun.*; **26**, 558; **2005**;
- [50] D. Kunkel; *Dissertation*; Mainz; **1992**;
- [51] K. Matyjaszewski, J. Xia; *Chem. Rev.*; **101**, 2921; **2001**;
- [52] L. Toman, M. Janata, J. Spevacek, P. Vlcek, P. Latalova, A. Sikora, B. Masar; *J. Pol. Sci. A*; **43**, 3823; **2005**;
- [53] Y. Inoue, J. Watanabe, M. Takai, S.I. Yusa, K. Ishihara; *J. Pol. Sci. A*; **43**, 6073; **2005**;
- [54] N. Hadjichristidis, M. Pitsikalis, H. Iatrou; *Adv. Polym. Sci.*; Springer-Verlag: Berlin, Heidelberg, **189**, 1; **2005**;
- [55] N. Hadjichristidis, S. Pispas; *Adv. Polym. Sci.*; Springer-Verlag: Berlin, Heidelberg, **200**, 37; **2006**;

- 
- [56] M. Zhang, A.H.E. Müller; *J. Pol. Sci.: Part A*; **43**, 3461; **2005**;
- [57] M.H. Stenzel-Rosenbaum, T.P. Davis, V. Chen, A.G. Fane, Anthony; *Macromolecules*; **34**, 5433; **2001**;
- [58] M. Szwarc, F. Leavitt; *J. Am. Chem. Soc.*; **78**, 2656; **1956**;
- [59] Y. Yagci, M.A. Tasdelen; *Prog. Polym. Sci.*; **31**, 1133; **2006**;
- [60] BASF; [http://worldaccount.basf.com/wa/EU~de\\_DE/Catalog/Chemicals/pi/BASF/Subbrand/pluronic\\_pe](http://worldaccount.basf.com/wa/EU~de_DE/Catalog/Chemicals/pi/BASF/Subbrand/pluronic_pe); **2006-10-16**;
- [61] P. Alexandridis, U. Olsson, B. Lindman; *J. Phys. Chem.*; **100**, 280; **1996**;
- [62] K.H. Bae, S.H. Choi, S.Y. Park, Y. Lee, T.G. Park; *Langmuir*; **22**, 6380; **2006**;
- [63] U. Borchert, U. Lipprandt, M. Bilanz, A. Kimpfler, A. Rank, R. Peschka-Süss, R. Schubert, P. Lindner, S. Förster; *Langmuir*; **22**, 5843; **2006**;
- [64] M. Biesalski, J. Rühle; *Macromolecules*; **37**, 2196; **2004**;
- [65] P. Guenoun, H.T. Davis, M. Tirrell, J.W. Mays; *Macromolecules*; **29**, 3965; **1996**;
- [66] S.E. Burke, A. Eisenberg; *Langmuir*; **17**, 6705; **2001**;
- [67] A.B. Zezin, V.A. Kabanov; *Pure appl. Chem*; **56**, 343; **1984**;
- [68] K.N. Bakeev, V.A. Izumrudov, V.A. Kabanov; *Doklad. Akad. Nauk. SSSR*; **299**, 1405; **1988**;
- [69] J. Feldthusen; *Synthesis of Tailored Polymer Structures by the Combination of Cationic and Anionic Polymerizations*; Thesis; **1998**;
- [70] W. Brown; *Light Scattering: Principles and Development*; Clarendon Press: Oxford; **1996**;
- [71] P. Lindner, T. Zemb; *Neutrons, X-rays and light: Scattering Methods Applied to Soft Condensed Matter*; Elsevier: Amsterdam; **2002**;
- [72] G.G. Berry; *J. Chem. Phys.*; **44**, 4550; **1966**;
- [73] B.J. Berne, R. Pecora; *Dynamic Light Scattering*; John Wiley & Sons: New York; **1976**;
- [74] K.S. Schmitz; *An Introduction to Dynamic Light Scattering by Macromolecules*; Academic Press, Inc.: San Diego; **1990**;
- [75] A.J.F. Siegert; *MIT Rad. Lab. Report*; 465; **1943**;

- 
- [76] W. Burchard, W. Richterling; *Progr. Colloid Polym. Sci.*; **80**, 151; **1989**;
- [77] S.W. Provencher; *Makromol. Chem.*; **180**, 201; **1979**;
- [78] S.W. Provencher; *Computer Phys. Commun.*; **27**, 229; **1982**;
- [79] S.H. Chen; *Ann. Rev. Phys. Chem.*; **37**, 351; **1986**;
- [80] J.S. Higgins, H.C. Benoit; *Polymers and Neutron Scattering*; Clarendon Press: Oxford; **1996**;
- [81] GRAS<sub>ans</sub>P; Charles Dewhurst; email: dewhurst@ill.eu; Institut Laue Langevin, Grenoble, France;
- [82] C. Tondre, R. Zana; *J. Phys. Chem*; **70**, 3451; **1972**;
- [83] A. Ikegami; *Biopolymers*; **6**, 431; **1968**;
- [84] G.V. Schulz; *Z. Phys. Chem. B*; **43**, 25; **1939**;
- [85] S. Förster, C. Burger; *Macromolecules*; **31**, 879; **1998**;
- [86] S. Förster, N. Hermsdorf, C. Böttcher, P. Lindner; *Macromolecules*; **35**, 4096; **2002**;
- [87] L. Baba-Ahmed, M. Benmouna, M.J. Grimson; *Phys. Chem. Liq.*; **16**, 235; **1987**;
- [88] <http://www.ill.eu/YellowBook/D11/>; **2006-10-20**;
- [89] K. Kalyanasundaram, J.K. Thomas; *J. Am. Chem. Soc.*; **99**, 2039; **1977**;
- [90] D.C. Dong, M.A. Winnik; *Photochem. Photobiol.*; **35**, 17; **1982**;
- [91] M. Wilhelm, C.L. Zhao, Y. Wang, R. Xu, M.A. Winnik, J.L. Mura, G. Riess, M.D. Croucher; *Macromolecules*; **24**, 1033; **1991**;
- [92] I. Astafieva, X.F. Zhong, A. Eisenberg; *Macromolecules*; **26**, 7339; **1993**;
- [93] H.H. Perkampus; *UV-VIS-Spektroskopie und ihre Anwendungen*; Springer-Verlag: Berlin; **1986**;
- [94] M. Adrian, J. Dubochet, J. Lepault, A.W. McDowell; *Nature*; **32**, 308; **1984**;

## 5. PIB<sub>X</sub>-B-PMAA<sub>Y</sub> DIBLOCK COPOLYMERS: SELF-ASSEMBLY IN AQUEOUS MEDIA

### **Polyisobutylene-*block*-poly(methacrylic acid) Diblock Copolymers: Self-Assembly in Aqueous Media**

Markus Burkhardt<sup>1</sup>, Nemesio Martinez-Castro<sup>1</sup>, Sandrine Tea<sup>1</sup>, Markus Drechsler<sup>1</sup>,  
Ivan Babin<sup>2</sup>, Ivan Grishagin<sup>2</sup>, Ralf Schweins<sup>3</sup>, Dmitry V. Pergushov<sup>2</sup>, Michael Gradzielski<sup>4</sup>,  
Alexander B. Zezin<sup>2</sup>, Axel H.E. Müller<sup>1\*</sup>

<sup>1</sup>*Makromolekulare Chemie II, Universität Bayreuth, D-95440 Bayreuth, Germany;*

<sup>2</sup>*Department of Polymer Science, School of Chemistry, Moscow State University,  
119992 Moscow, Russia;*

<sup>3</sup>*Institut Laue-Langevin, 38042 Grenoble Cedex 9, France;*

<sup>4</sup>*Stranski Laboratorium für Physikalische und Theoretische Chemie, Institut für  
Chemie, Technische Universität Berlin, D-10623 Berlin, Germany;*

\* e-mail: axel.mueller@uni-bayreuth.de

Markus Burkhardt: markus.burkhardt@uni-bayreuth.de;

Nemesio Martinez-Castro: nemesiomc@yahoo.com;

Sandrine Tea: sandrine.tea@uni-bayreuth.de;

Markus Drechsler: markus.drechsler@uni-bayreuth.de;

Ivan Babin: babin\_ia@mail.ru;

Ivan Grshagin: engewo@yahoo.com;

Ralf Schweins: schweins@ill.eu;

Dmitry V. Pergushov: pergush@genebee.msu.su;

Michael Gradzielski: michael.gradzielski@tu-berlin.de;

Alexander B. Zezin: zezin@genebee.msu.su;

## Abstract

Amphiphilic diblock copolymers, polyisobutylene-*block*-poly(methacrylic acid) (PIB<sub>x</sub>-*b*-PMAA<sub>y</sub>) with various lengths of non-polar ( $X = 25 - 75$ ) and polyelectrolyte ( $Y = 170 - 2600$ ) blocks spontaneously dissolve in aqueous media at  $\text{pH} > 4$ , generating macromolecular assemblies, the aggregation number of which depends on external stimuli (pH, ionic strength). The spherical micellar morphology with a compact core formed by the PIB blocks and a swollen corona built up from the PMAA blocks was deduced by cryogenic transmission electron microscopy. The micelles were further characterized by means of dynamic and static light scattering as well as small angle neutron scattering. The critical micellization concentration, estimated by means of fluorescence spectroscopy with the use of pyrene as a polarity probe, is decisively determined by the length of the PIB block and insensitive to changes in the length of PMAA block.

**Keywords:** *micelles, amphiphilic block copolymers, polyelectrolytes, SLS, DLS, SANS*

### 5.1 Introduction

Amphiphilic block copolymers are of great interest in various research fields. Due to the large variety of different monomers for both blocks, the desired properties like responsiveness to changes in pH, temperature or ionic strength can be easily obtained [1]. Nowadays various controlled polymerization techniques, e.g. radical, anionic, cationic are used to design polymers. Also combinations of them aiming at di-, tri- or even multi-block copolymers can be utilized to tailor different properties. Industry is interested in amphiphilic block copolymers due to their use as lubricants [2], e.g. for oil drilling, as well as in pharmaceuticals or as carriers for drugs [3]. Additionally, the use as micro- or nanocontainers for reactions similar to surfactant systems [4] has been reported very frequently. Especially polymers based on weak acids such as poly(acrylic acid) (PAA) or poly(methacrylic acid) (PMAA) have attracted considerable attention due to the ability of the system to strongly change upon variations in pH and ionic strength of the solution [5].

Therefore it is interesting to have an insight into the effect of block lengths of stimuli-responsive block copolymers on properties and structure of their assemblies in aqueous solutions. Several reports describing micellization of block copolymers with hydrophobic polystyrene (PS) block and properties of the resulting micelles have been published, as they can be easily obtained by sequential anionic polymerization. In pure aqueous solutions these polymers appear to exist in a non-dynamic or "frozen" state [6], as the glass transition temperature of PS is  $T_g = 104^\circ\text{C}$ . These "frozen" assemblies recover their dynamic behavior in water-dioxane and water-DMF mixtures. A possibility to use pure water instead of solvent mixtures is a

considerable advantage of block copolymers containing hydrophobic blocks with a  $T_g$  below room temperature (RT).

Recently, Colombani *et al.* [7] reported on poly(*n*-butylacrylate)-*block*-poly(acrylic acid) (PnBA-*b*-PAA) diblock copolymers synthesized via ATRP. They found spherical micelles in aqueous solutions, each micelle consisting of a core formed PnBA blocks and a corona formed by PAA blocks. In their work the dependence of the size of the micellar assemblies containing a core that is assumed to be above  $T_g$  at RT on external stimuli like changes in pH and ionic strength is investigated in detail.

In this paper we have used polyisobutylene (PIB) synthesized via cationic polymerization and end-capped with thiophene via quenching the polymerization with thiophene [8]. The PIB macroinitiator was used to initiate anionic polymerization of *t*-butyl methacrylate (*t*BMA). After hydrolysis of the *t*-butyl groups resulting in methacrylic acid moieties, the PIB<sub>*x*</sub>-*b*-PMAA<sub>*y*</sub> block copolymer was dissolved in aqueous media. Above the cmc the formed assemblies were characterized by means of DLS, SLS, SANS and cryo-TEM. In this paper properties of assemblies formed by PIB<sub>*x*</sub>-*b*-PMAA<sub>*y*</sub> of different block length ratios are reported. We investigated a range of block lengths for PIB ( $\overline{DP}_n = 25$  to 75) as well as for PMAA ( $\overline{DP}_n = 170$  to 2600) to have a meaningful overview of the influence of hydrophilic and hydrophobic block on the properties of the assemblies formed in water. Furthermore we compared our results to those obtained from similar block copolymers studied by us in earlier publications by Pergushov *et al.* [9, 10] and Schuch *et al.* [11]. Pergushov *et al.* reported on PIB<sub>*x*</sub>-*b*-PMAA<sub>*y*</sub> micelles with relatively short PIB block with  $\overline{DP}_n$  of 20. These spherical micelles have relatively low *cmc* of approximately  $10^{-6}$  mol/l. From SANS measurements Pergushov *et al.* evaluated a relatively small core of the micelle of 3 to 4 nm formed by the hydrophobic PIB blocks, surrounded by a PMAA shell. Schuch *et al.* also studied PIB-*b*-PMAA with longer PIB blocks of  $\overline{DP}_n$  70 and 134, concentrating on block length ratios of PIB/PMAA in the range of unity. From freeze-fracture TEM, also spherical micelles and aggregates of micelles were concluded. From DLS, Schuch *et al.* reported on rather narrow, in some cases bimodal distributions for the block copolymer micelles, also found by means of analytical ultra-centrifugation (AUC).

In this paper we report on PIB<sub>*x*</sub>-*b*-PMAA<sub>*y*</sub> block copolymers synthesized with an easier, new method [8] with block lengths chosen in the intermediate range. The influence of ionic strength and pH on the formed micellar assemblies, i.e. size and aggregation number of the copolymer micelles is shown for different copolymers to achieve a systematic understanding of the system. Especially, the dynamics (responsive behavior) of the system with a hydrophobic core above  $T_g$  are investigated by means of SANS.

## 5.2 Experimental Part

### 5.2.1 Materials

Polyisobutylene-*block*-poly(*tert*-butyl methacrylate) diblock copolymers were synthesized via combination of living cationic and anionic polymerizations as described elsewhere [8]. Size exclusion chromatography (SEC) was used to determine the molecular weight distributions of the PIB precursor (measured separately) and PIB<sub>*x*</sub>-*b*-PtBMA<sub>*y*</sub> using PIB and PtBMA standards. For the diblock copolymer, a weighted average of the homopolymer calibration curves was used. SEC was performed using PSS SDV-gel columns (5 μm, 60 cm, 1 x linear (10<sup>2</sup> – 10<sup>5</sup> Å), 1 x 100 Å) with THF as eluent at a flow rate of 1.0 ml/min at room temperature using UV (λ = 230 and 260 nm) and RI detection. The values of degree of polymerization,  $\overline{DP}_n$ , for PIB and PtBMA blocks are shown in the supporting informations. The polydispersity indices of PIB<sub>*x*</sub>-*b*-PtBMA<sub>*y*</sub> were in the range of 1.03 to 1.12. After hydrolysis of the block copolymer with hydrochloric acid in dioxane at 80 °C for 24 hours polyisobutylene-*block*-poly(methacrylic acid) (PIB<sub>*x*</sub>-*b*-PMAA<sub>*y*</sub>) copolymer was obtained.

*Sample Preparation:* To prepare a stock solution of the copolymer, PIB<sub>*x*</sub>-*b*-PMAA<sub>*y*</sub>, NaCl (MERCK) and TRIS buffer (2-amino-2-(hydroxymethyl)-1,3-propanediol, FLUKA; not used for potentiometric titrations) were dissolved in solution of NaOH at RT under continuous stirring for at least 24 h. The amount of NaOH was calculated according to the number of COOH-groups of the weighed polymer. The solutions containing added NaCl all showed low viscosity and were transparent. Solutions without added NaCl showed high viscosity.

### 5.2.2 Methods

#### *Fluorescence Spectroscopy*

The critical micellar concentrations (*cmc*) of PIB<sub>*x*</sub>-*b*-PMAA<sub>*y*</sub> were determined by means of steady state Fluorescence Spectroscopy. The samples for fluorescence measurements were prepared according to a procedure similar to that described elsewhere [12, 13, 14]. Certain aliquots of a solution of pyrene (Aldrich) in acetone were carefully dropped into empty dark vials by a Hamilton microsyringe, and afterward acetone was evaporated by gentle heating. Then the sample solutions were added. To equilibrate pyrene, the samples were kept at 40 - 50 °C for 2 days under intensive stirring. The final concentration of the fluorescent probe in the prepared samples was kept constant at 5·10<sup>-7</sup>M, that is, only slightly below the saturation concentration of pyrene in water at 22 °C. Steady-state fluorescence spectra of the air-equilibrated samples were recorded with a Thermo Spectronic Aminco Bowman Series 2 model EA-358 (USA) fluorescence spectrophotometer (right angle geometry,

1 cm x 1 cm quartz cell). The widths of slits were chosen to be 3 and 1.5 nm for excitation and emission, respectively. For emission spectra the excitation wavelength  $\lambda = 333$  nm. For excitation spectra, the emission wavelength was 383 nm.

#### *Potentiometric Titration*

The measurements were carried out for aqueous solutions ( $c_{Pol.} \approx 0.05$  wt-%) of PIB<sub>x</sub>-b-PMAA<sub>y</sub> with the METROHM Titrando 809. For pH-dependent measurements, the "Unitrode with Pt 1000" or the "Auqatrode Plus with Pt 1000" was used. Measurements of the turbidity of the solutions were carried out using a "Spectrode 523nm". The solutions were prepared as described above.

#### *Cryogenic Transmission Electron Microscopy (Cryo-TEM) [17]*

For Cryo-TEM studies, a drop of the sample ( $c = 0.5$  wt-%) was placed on an untreated bare copper TEM grid (600 mesh, Science Services, München, Germany), where most of the liquid was removed with blotting paper, leaving a thin film stretched over the grid holes. The specimens were shock frozen by rapid immersion into liquid ethane and cooled to approximately 90 K by liquid nitrogen in a temperature controlled freezing unit (Zeiss Cryobox, Zeiss NTS GmbH, Oberkochen, Germany). The temperature was monitored and kept constant in the chamber during all steps of the sample preparation. After freezing the specimens, the remaining ethane was removed using blotting paper. The specimen was inserted into a cryo-transfer holder (CT3500, Gatan, München, Germany) and transferred to a Zeiss EM922 EF-TEM instrument. Examinations were carried out at temperatures around 90 K. The transmission electron microscope was operated at an acceleration voltage of 200 kV. Zero-loss filtered images ( $\Delta E = 0$  eV) were taken under reduced dose conditions (100 - 1000 e/nm<sup>2</sup>). All images were registered digitally by a bottom mounted CCD camera system (Ultrascan 1000, Gatan) combined and processed with a digital imaging processing system (Gatan Digital Micrograph 3.9 for GMS 1.4). The samples were dissolved using CsOH (Fluka) and CsCl (Acros).

#### *Dynamic Light Scattering (DLS)*

Sample solutions for DLS experiments were obtained by an isoionic 50-fold dilution of the sample solutions prepared for the SANS measurements (1 wt-%) (see Section 2.2.6) with corresponding aqueous solutions of NaCl. The prepared sample solutions were thoroughly filtered by passing at least three times through a Nylon filter (13-HV, Millipore) with a pore size of 0.45  $\mu\text{m}$ . In addition, samples were also prepared as described above with an amount of the copolymer in the range of 0.02 wt-%. The DLS measurements were carried out in sealed cylindrical scattering cells ( $d = 10$  mm) at five scattering angles 30, 60, 90, 120 and 150° with the use of an

ALV DLS/SLS-SP 5022F instrument consisting of an ALV-SP 125 laser goniometer, an ALV 5000/E correlator, and a He-Ne laser with the wavelength  $\lambda = 632.8$  nm. The CONTIN algorithm was applied to analyze the obtained correlation functions. For selected samples with monomodal distribution, cumulant analysis was applied. Apparent hydrodynamic radii,  $R_h$ , were calculated according to the Stokes-Einstein equation.

#### *Static Light Scattering (SLS)*

For SLS, stock solutions of PIB<sub>x</sub>-b-PMAA<sub>y</sub> were prepared in the concentration range between 0.02 and 0.2 wt-%. Dialysis for at least two days against an aqueous solution with the same ionic strength and pH was used to obtain the solvent for diluting the samples and as a reference for  $dn/dc$ . SLS measurements were carried out on a Sofica goniometer with He-Ne laser ( $\lambda = 632.8$  nm) at RT. Prior to the measurements, sample solutions were filtered through Nylon filters (13-HV Millipore) with pore size of 0.45  $\mu\text{m}$ . A Berry plot was used to evaluate the data. A Differential Refractometer DnDC2010/620 (PSS) was used to measure the refractive index increment,  $dn/dc$ , of the copolymer solution at  $\lambda = 620$  nm.

#### *Small-Angle Neutron Scattering (SANS) [18, 19]*

Sample solutions for SANS experiments were prepared by dissolving PIB<sub>x</sub>-b-PMAA<sub>y</sub> in D<sub>2</sub>O (Aldrich), containing a desired amount of NaOH (Riedel-de Haën), at RT under continuous stirring overnight. The final concentration of the copolymers in the sample solutions was ca. 0.9 - 1 wt-%. In all cases, the prepared solutions were homogeneous and transparent. The sample solutions were put into quartz cells with 2 mm path length (Hellma). The degree of neutralization,  $\alpha$ , of the PMAA blocks of the copolymers was controlled by the amount of NaOH. The ionic strength of the sample solutions was adjusted by adding NaCl (Merck). The SANS measurements were performed using the instruments D11 of the Institute Max von Laue-Paul Langevin (ILL, Grenoble, France) with neutron wavelength  $\lambda = 6$  Å. Sample-to-detector distances of 1.1, 4, and 16 m were employed. With these configurations a total range of the magnitude of the scattering vector,  $q = 0.003 - 0.35$  Å<sup>-1</sup> was covered. The detector sensitivity and the intensity of the primary beam were calibrated by a comparison with the scattering from a 1 mm reference sample of water. The obtained data were radially averaged and corrected for the detector background, the detector dead time, and the scattering from an empty cell. They then were converted into absolute units by a comparison with the scattering from water according to standard routines supplied by the ILL [20] using GRASP software. It should be noted that the SANS curves presented in this paper still contain the incoherent background scattering of solvent and sample.

### 5.3 Results and Discussion

#### 5.3.1 Determination of *cmc*

The *cmc* values of the PIB<sub>*x*</sub>-b-PMAA<sub>*y*</sub> in aqueous solutions were determined using pyrene as a polarity probe, analogously to measurements carried out previously to determine *cmc* of both ionic and non-ionic amphiphilic block copolymers [12, 13, 14]. The emission spectra of pyrene strongly depend on the polarity of the surrounding media [15, 16]

There is a pronounced change of the ratio  $I_1/I_3$  ( $I_1$  is an intensity of vibronic band in emission spectrum of pyrene at 372 nm,  $I_3$  is an intensity of vibronic band at 383 nm) from approximately 1.8 in water to values around 1 in non-polar micellar phase. Hence a decrease of  $I_1/I_3$  with copolymer concentration strongly suggests that the *cmc* has been reached.

Transfer of pyrene from polar to non-polar microenvironment is also accompanied by a shift of the (0,0) band from 333 to 338.5 nm in the excitation spectra of this fluorophore. As shown by Wilhelm et al. [12], the concentration dependence of the  $I_{333}/I_{338}$  ratios obtained from pyrene excitation spectra is more sensitive to a real onset of micellization than  $I_1/I_3$  ratios.

The samples were prepared as described in the experimental section. The measurements were made for different block copolymers (cf. Figure 5.1, Table 5.1) and compared to results from literature [9, 10, 11, 13].

<i>Polymer</i>	<i>cmc</i> ( $\frac{I_1}{I_3}$ ) $10^6 \frac{mol}{l}$	<i>cmc</i> ( $\frac{I_{333}}{I_{338}}$ ) $10^6 \frac{mol}{l}$
PIB <sub>75</sub> -b-PMAA <sub>190</sub>	0.5	0.4
PIB <sub>75</sub> -b-PMAA <sub>1600</sub>	0.4	0.3
PIB <sub>25</sub> -b-PMAA <sub>2600</sub>	1.5	0.8
*PIB <sub>20</sub> -b-PMAA <sub>100</sub>	≈ 2	-
*PIB <sub>20</sub> -b-PMAA <sub>280</sub>	≈ 2	-
*PIB <sub>20</sub> -b-PMAA <sub>425</sub>	≈ 2	-

Tab. 5.1: The *cmc* values obtained from emission and excitation spectra of pyrene in aqueous solutions of PIB<sub>*x*</sub>-b-PMAA<sub>*y*</sub>; \* taken from [9, 10];

The dependence of the  $I_1/I_3$  ratio obtained from emission spectra of pyrene in aqueous solutions on PIB<sub>75</sub>-b-PMAA<sub>1600</sub> and the intensity ratio  $I_{333}/I_{338}$  from excitation spectra are shown in Figure 5.1 as functions of the copolymer concentration. Up to a certain concentration, the values remain almost constant. Above this concentration, the values decrease significantly with increasing copolymer concentration, the diblock copolymer concentrations corresponding to the onsets of these

decreases obtained from emission and excitation spectra appear to be rather close each other (Figure 5.1, Table 5.1). Such changes, as was already pointed out above, can be associated with solubilization of the fluorophore by the cores of the micelles that form. The said onsets can be correspondingly considered as an estimate of the cmc.

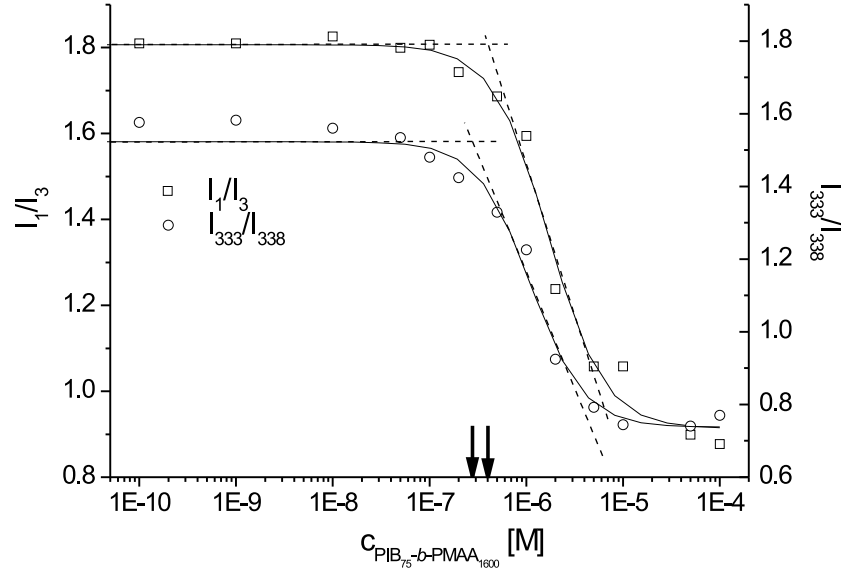


Fig. 5.1: The ratio  $I_1 : I_3$  ( $\square$ ) from emission spectra and  $I_{333} : I_{338}$  ( $\circ$ ) from excitation spectra of pyrene in aqueous solutions of  $PIB_{75}-b-PMAA_{1600}$  versus polymer concentration at  $pH = 9$ ,  $c_{NaCl} = 0.1$  M,  $c_{TRIS} = 0.01$ ,  $T = 25$  °C.

As it can be seen from Table 5.1, the two copolymers containing the longest PIB block ( $\overline{DP}_n = 75$ ) show approximately the same cmc of  $5 \cdot 10^{-7}$  mol/l. The cmc of these copolymers is lower by a factor of 2 to 3 than that of  $PIB_{25}-b-PMAA_{2600}$ , which is approximately  $1 - 1.5 \cdot 10^{-6}$  mol/l. This suggests that the length of the hydrophobic block governs the micellization process, a result typical for surfactants [22]. But in contrast to low molecular surfactants, this influence is not that pronounced. A comparison with the cmcs of  $PIB_{20}-b-PMAA_y$  with  $y = 100, 280$  and  $425$  shows that the corresponding value of  $2 \cdot 10^{-6}$  mol/l [9] matches the cmc obtained from our experiments. The obtained results evidence that the length of the hydrophilic block plays a minor role in micellization of  $PIB_x-b-PMAA_y$ . Indeed, for the measurements with our samples a change of the length of the PMAA block for a factor of 4 and even 8 does not change the cmc.

The results obtained in this work are in good agreement with the theoretical predictions by Borisov *et al.* [23] for equilibrium star-like micelles of ionic amphiphilic diblock copolymers at high ionic strength, which is fulfilled for the samples at  $c_{NaCl} = 0.1$  M. At lower salt concentrations, the cmc is explained to increase with increasing  $N_A$ . The measurements were carried out at 0.1 M NaCl as the salt concentration for all measurements described in this paper was at least 0.1 M.

Schuch *et al.* also investigated self-assembly of PIB<sub>x</sub>-b-PMAA<sub>y</sub> with the different ratios of block length  $x:y = 70:52, 70:70, 134:145$  and  $134:228$  [11], having *cmc*s below 0.3 mg/l ( $< 10^{-8}$  M). In this work, the micellization of the polymers with the longer PIB block was investigated by means of fluorescence correlation spectroscopy (FCS). The samples did not show a pronounced difference in the onset of micellization, even when the PIB block length was changed by a factor of approximately 2. Compared to our results, the *cmc* values differ slightly. This might be attributed to the different method used by Schuch *et al.*

Astafieva *et al.* also report a significant decrease of the *cmc* of PS-*b*-PAA copolymers with increasing block length of the non-polar block [13]. In their work, they used copolymers with a PS block of a  $DP_n$  ranging from 6 to 110 units. They report on *cmc*s of approximately  $5 \cdot 10^{-7}$  to  $10^{-6}$  mol/l for the copolymers with PS block lengths of 23 to 28 down to values of  $10^{-7}$  for long PS blocks up to 86. Especially, the copolymers with the shorter PS blocks up to a length of 30 units show drastic changes in *cmc*, whereas the changes reported for the copolymers with the longer PS blocks are not so pronounced. The variation of the length of the PAA block of the PS<sub>x</sub>-*b*-PAA<sub>y</sub> polymers does not influence the onset of micellization. It has to be pointed out that the PS-containing micelles were prepared via dissolution of the polymer in pure water at 100° C. The obtained micelles after being brought back to RT are reported to be non-dynamic due to the "frozen" state of the core of the micelle.

### 5.3.2 Potentiometric Titration

Titrations of micellar solutions give an insight into the degree of dissociation,  $\alpha$ , of the ionic block of the diblock copolymer. In Figure 5.2, the curves obtained by means of titration of aqueous solutions of the PIB<sub>75</sub>-*b*-PMAA<sub>1600</sub> at different starting salt concentrations  $c_{NaCl} = 0.05$  M, 0.5M and 1.0 M with 0.1 M HCl are shown.

The influence of salt on the neutralization of the copolymers is quite pronounced (cf. Table 5.2). With the same degree of neutralization,  $\alpha$ , of the samples with 0.05 M and 1.0 M NaCl, a shift of the apparent  $pK_a$  (= pH at  $\alpha = 0.5$ ) of almost one unit is measured. This phenomenon can be explained by the screening effect of added salt. Guo *et. al* [24] described the difference in concentration of salt within the corona of a spherical brush and in solution. They describe a partial replacement of the protons by counterions in the micellar corona, leading to lower pH with increasing salt concentration. According to Borisov *et al.* [23] for star-like equilibrium micelles with coronae formed by weak polyelectrolytes at low salt concentration, the average degree of dissociation of the polyelectrolyte blocks decreases with increasing number of arms and increases with increasing number of monomer units per arm. They explain it with an excess negative electrostatic potential in the micellar corona. This results in a higher pH value in the coronae of such micelles compared to that

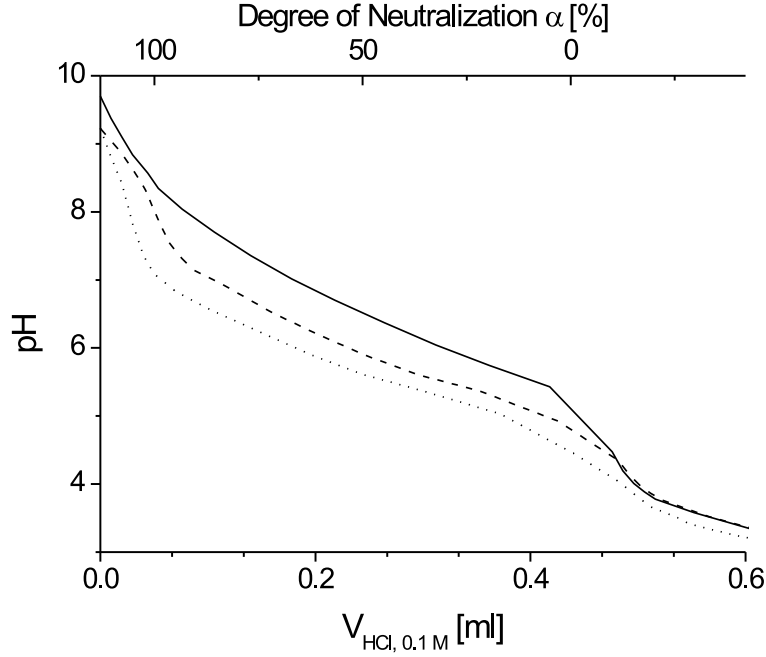


Fig. 5.2: Potentiometric titration curves of micellar solutions of  $PIB_{75}-b-PMAA_{1600}$  at  $c_{NaCl}$  of 0.05 M (solid), 0.5 M (dashed) and 1.0 M (dotted) with 0.1 M HCl,  $V_{start} = 50$  ml.

Copolymer	$c_{NaCl}$ $\frac{mol}{l}$	$pK_a$
$PIB_{75}-b-PMAA_{1600}$	0.05	6.5
$PIB_{75}-b-PMAA_{1600}$	0.5	5.90
$PIB_{75}-b-PMAA_{1600}$	1.0	5.62
$PIB_{30}-b-PMAA_{170}$	0.1	6.6
$PIB_{25}-b-PMAA_{350}$	0.1	6.46
$PIB_{75}-b-PMAA_{615}$	0.1	6.29

Tab. 5.2: Apparent  $pK_a$  values obtained by means of potentiometric titration of micellar solution of  $PIB_{75}-b-PMAA_{1600}$  at different salt concentrations.

of the surrounding solution. This effect is more pronounced, the larger the number of arms of the micelle is.

With increasing ionic strength, according to Borisov, the added salt screens the electrostatic interactions in the corona. Thus, for a given number of arms the degree of dissociation increases upon addition of salt. In this case,  $\alpha$  can be represented by the following equation:

$$\alpha = \frac{10^{pH-pK}}{1 + 10^{pH-pK}} \quad (5.1)$$

with  $pK$  being the  $pK$  value of MAA. Comparable theoretical titration curves are

discussed by Wolterink *et al.* [25].

Plamper *et al.* [26] investigated the ionization behavior of star-shaped poly(acrylic acid) (PAA) with defined arm numbers. The measurements show that with increasing number of arms, the titration curves shift to higher pH values and thus to higher apparent values of  $pK_a$ . Thus, we have two countervailing effects. As the overall apparent  $pK_a$  decreases with increasing ionic strength, the screening effect seems to dominate the ionization behavior of the  $PIB_x$ - $b$ - $PMAA_y$  micelles.

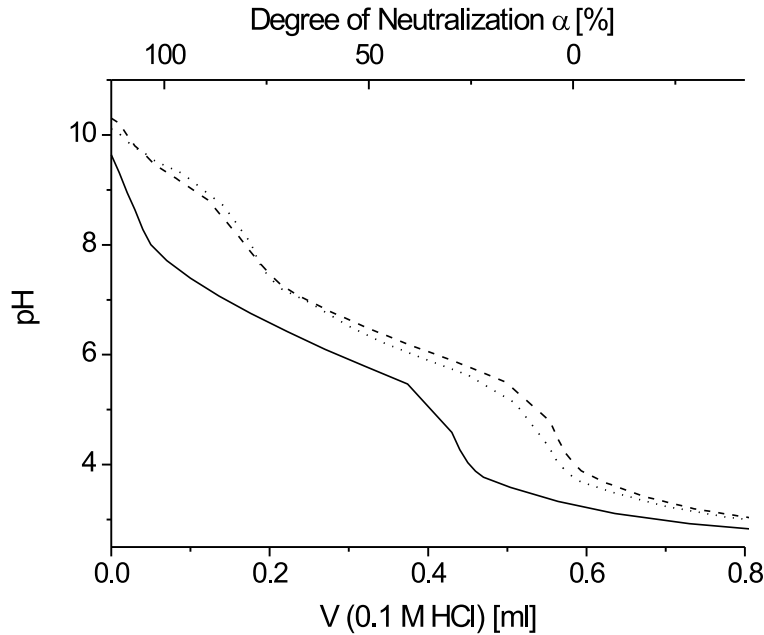


Fig. 5.3: Potentiometric titration of micellar solutions of  $PIB_{30}$ - $b$ - $PMAA_{170}$  (solid),  $PIB_{25}$ - $b$ - $PMAA_{350}$  (dashed) and  $PIB_{75}$ - $b$ - $PMAA_{615}$  (dotted) at  $c_{NaCl}$  of 0.1 M with 0.1 M HCl,  $V_{start} = 50$  ml.

Comparing the titration curves of different  $PIB_x$ - $b$ - $PMAA_y$  shown in Figure 5.3, almost no difference between the curves of  $PIB_{25}$ - $b$ - $PMAA_{350}$  (dashed) and  $PIB_{75}$ - $b$ - $PMAA_{615}$  (dotted) can be observed. As also described by Plamper *et al.*, the length of the arms has an effect on the apparent  $pK_a$  of the star-like assemblies as well. In our work, the influence cannot be clearly seen, most probably because the number of arms is not constant (see below). Thus, the influence of the number and length of arms on the apparent  $pK_a$  of PMAA blocks in the micelle appear to compensate each other.

For the shorter  $PIB_{30}$ - $b$ - $PMAA_{170}$  (Figure 5.3, solid), turbidity increased during the titration, clearly indicating aggregation of the micelles. This is also the reason for the difference of the titration curve compared to the measurements of the copolymers with longer PMAA blocks. Increasing turbidity suggests increasing particle mass and/or size. Therefore COOH-groups can probably be trapped in the formed agglomerates and cannot be detected by the pH-sensitive electrode. Hence, only the

added HCl influences the pH value, which in this case decreases faster compared to the other solutions of  $PIB_x$ - $b$ - $PMAA_y$ . Another reason for the occurrence of the larger aggregates can be the rearrangement of the copolymer micelles followed by changes in their aggregation numbers. This will be discussed further in the section 5.3.6. During aggregation protons can be expelled, leading to a lower pH compared to other block copolymer solutions.

### 5.3.3 Cryo-TEM

In addition to the scattering techniques, cryo-TEM can be used to show the corresponding shape of the nanoparticles in solution [17]. In our case samples with  $c_{polymer} = 0.5$  wt-% and salt concentrations of 0.1 M CsCl were examined and showed existence of spherical species (cf. Figure 5.4). We have used CsCl and CsOH to have  $Cs^+$  ions in solution which, being counterions to carboxylate moieties, were thought to enhance contrast of PMAA coronae of the  $PIB$ - $b$ - $PMAA$  micelles, making them visible. The darker spots in the centers of the micelles are reasonably considered as

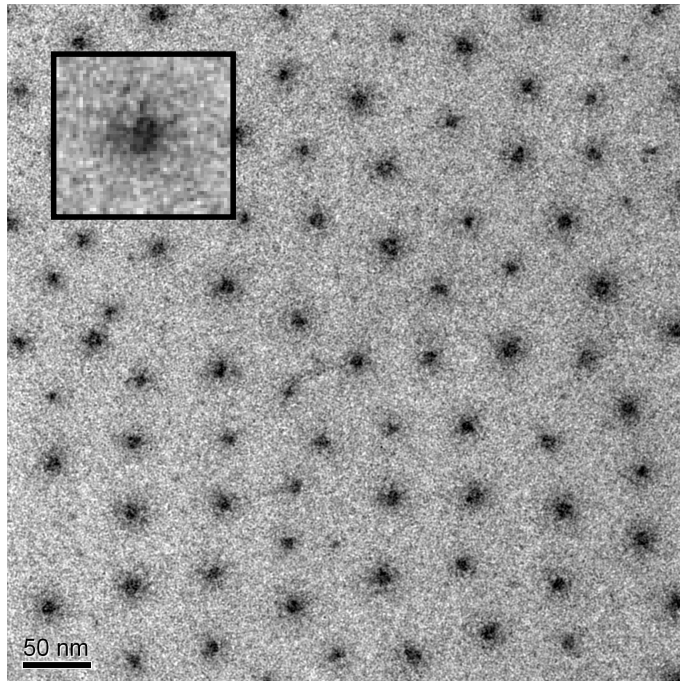


Fig. 5.4: Cryo-TEM image of aqueous solution of  $PIB_{30}$ - $b$ - $PMAC_{s170}$  with 0.1 M CsCl, 0.01 M TRIS,  $c_{pol} = 0.5$  wt-%. Side length of inset: 50 nm.

the  $PIB$  cores. Each core is surrounded by a slightly brighter shell associated with partially collapsed micellar corona [27]. The corona is formed by  $PMACs$  blocks protruding into the solvent. The darkness of the  $PIB$  core arises from the higher electron density of the collapsed  $PIB$  core compared to swollen  $PMACs$  corona surrounding the core, resulting in more pronounced scattering of electrons. The corona

cannot be totally seen as the PMACs protrudes into the solvent. As the density in the corona of the star-like micelles decreases with the distance from the PIB core, parts of the arms more distant from the core cannot be distinguished from the bright solvent background. Thus, also the wanted staining effect of the  $Cs^+$  as counterions is limited. As is seen, the polydispersity of the size of the micelles is relatively high.

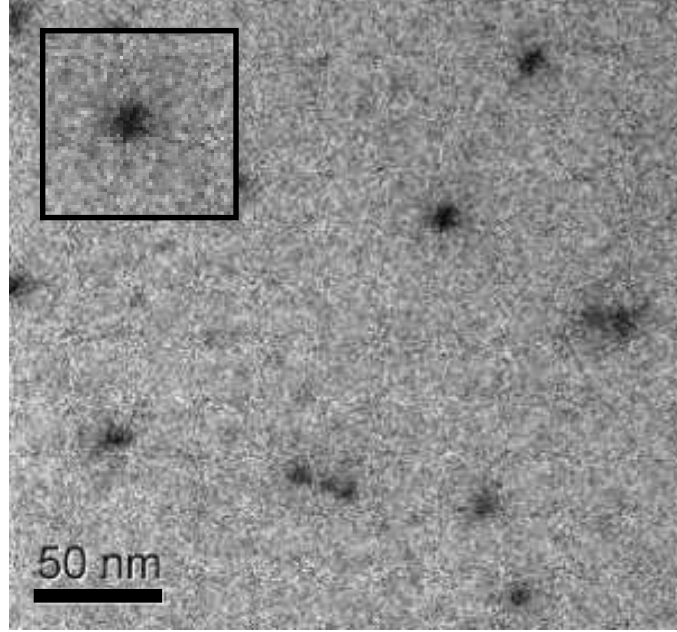


Fig. 5.5: Cryo-TEM image of aqueous solution of  $PIB_{75}-b-PMAA_{1600}$  with 0.1 M  $CsCl$ , 0.01 M TRIS,  $c_{pol} = 0.5$  wt-%. Side length of inset: 50 nm.

Compared to the copolymers with the shorter polyelectrolyte blocks, the PIB cores of the  $PIB_{75}-b-PMACs_{1600}$  micelles are highly separated. The size of the dark core for the  $PIB_{75}$  is in the same range than for the  $PIB_{30}$ . But in the latter case, no micellar corona is visible. This is due to the very long PMACs block, which, with a length of 0.25 nm per repeat unit, leads to a contour length of up to 400 nm, if totally stretched, compared to 42.5 nm in case of  $PMAA_{170}$ . The overlapping PMACs arms result in the darker background. As the concentration is relatively high, the micelles are forced to arrange in a regular array (cf. Figure 5.4). This effect is enforced by the blotting during sample preparation, which forms almost a monolayer of particles (thickness of the layer several tens of nm). SANS experiments (cf. Section 5.3.6) with higher polymer concentrations show that a highly ordered arrangement cannot be seen in untreated samples and hence is only due to the preparation for cryo-TEM. From the distance between the centers of the adjacent micelles one can estimate the average radius and volume of the micelles. The average distance, and so the diameter of a micelle, is evaluated to be  $d_{mic} = 59$  nm in the case of the  $PIB_{30}-b-PMACs_{170}$  micelles and  $d_{mic} = 113$  nm in the case of the  $PIB_{75}-b-PMACs_{1600}$  micelles respectively. That leads to a total volume of  $8.6 \cdot 10^5$  nm<sup>3</sup>

and  $6.0 \cdot 10^6 \text{ nm}^3$  per micelle, respectively. Compared to DLS results (see below), these values, however, are sufficiently underestimated due to partial overlapping of micellar coronae due to the higher concentration of  $PIB_x$ - $b$ - $PMACs_y$  used for cryo-TEM compared to DLS.

### 5.3.4 Dynamic Light Scattering

The distance between the cores of the  $PIB_x$ - $b$ - $PMAA_y$  micelles in the cryo-TEM images (Figure 5.4) can also be compared to apparent hydrodynamic radius,  $R_h$ , of such assemblies obtained by means of DLS at more diluted concentrations of  $c_{Pol.} = 0.02 \text{ wt-}\%$ . The data are collected in Table 5.3.

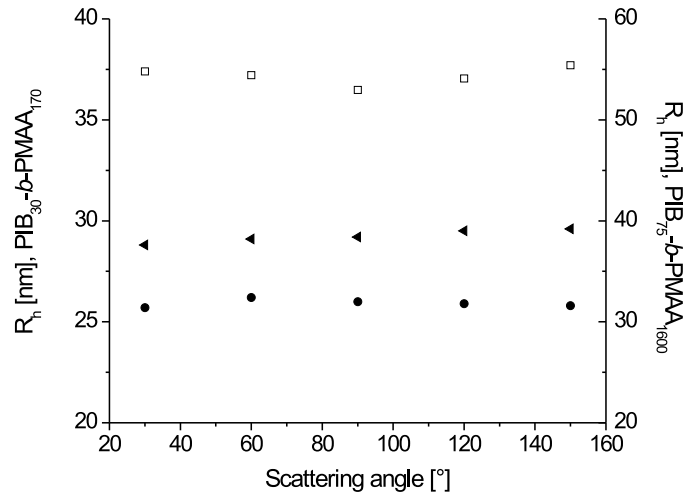


Fig. 5.6: The angular dependence of  $R_h$  obtained from DLS of  $PIB_{30}$ - $b$ - $PMAA_{170}$  micelles, at ( $\blacktriangle$ )  $c_{NaCl} = 0.1 \text{ M}$ , ( $\bullet$ )  $c_{NaCl} = 0.5 \text{ M}$ ,  $c_{TRIS} = 0.01 \text{ M}$  (pH = 9) and of  $PIB_{75}$ - $b$ - $PMAA_{1600}$  micelles at pH = 5,  $c_{NaCl} = 0.1 \text{ M}$  ( $\square$ ),  $c_{Pol.} = 0.02 \text{ wt-}\%$ .

Figure 5.6 shows the angular dependence of  $R_h$  of the  $PIB_{30}$ - $b$ - $PMAA_{170}$  at two considerably different salt concentrations at pH = 9. The absence of an angular dependence in both cases cannot be seen for all other polymers investigated in this work. Especially, the copolymers with longer PMAA blocks like  $PIB_{75}$ - $b$ - $PMAA_{615}$  show that the values of  $R_h$  decrease with increasing scattering angle. This can be attributed to the influence of the hydrodynamic form factor. CONTIN analysis revealed that mostly one type of micellar aggregates can be seen in DLS. Therefore, for selected polymers, Cumulant Analysis was applied. Therefrom PDIs of the aggregates of approximately 0.08 to 0.10 for the samples shown in Figure 5.6 were evaluated.

This can be seen at all salt concentrations used for pH-values in the range from 4 to 9, representing almost uncharged up to fully ionized PMAA block. In Figure

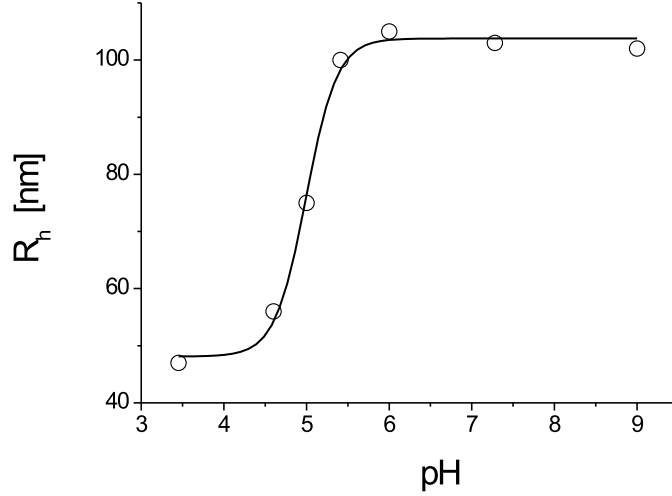


Fig. 5.7: The pH-dependence of  $R_h$  for the  $PIB_{75}$ - $b$ - $PMAA_{1600}$  micelles,  $c_{NaCl} = 0.1$  M,  $\Theta = 90^\circ$ ,  $c_{Pol.} = 0.02$  wt-%.

5.6  $PIB_{75}$ - $b$ - $PMAA_{1600}$  at  $pH = 5$  is depicted as a representative example for this behavior. The pronounced increase of the size of the  $PIB_{75}$ - $b$ - $PMAA_{1600}$  micelles observed with increasing pH in Figure 5.7 is obviously attributed to the stretching of the arms of the micelle due to increasing charge density of the PMAA block caused by ionization of the COOH-groups. The corresponding change of the average aggregation number of the micelles,  $\overline{N_{agg}}$ , as will be shown later in the SLS and SANS sections, also takes place.

In case of changing ionic strength in solutions of star-like equilibrium micelles, Borisov *et al.* [23] report on two countervailing effects. On the one hand, the  $N_{agg}$  increases upon raising salt concentration  $c_s$ , according to

$$N_{agg} \sim \frac{N_B^{10/11}}{(\alpha^4 N_A)^{3/11}} c_s^{6/11} \quad (5.2)$$

with  $N_A$  being the  $DP_n$  of the hydrophilic block and  $N_B$  being the  $DP_n$  of the hydrophobic block. On the other hand, the effect of repulsion of charges is screened by increasing the ionic strength in the system (Figure 5.8). This leads to shrinking of PMAA blocks and consequently to lower values of  $R_h$  for star-like equilibrium micelles according to

$$R_h \sim (N_A^3 \alpha)^{2/11} N_B^{2/11} c_s^{-1/11}. \quad (5.3)$$

For almost all  $PIB_x$ - $b$ - $PMAA_y$  micelles examined, the same trend is observed: the values of  $R_h$  decrease with rising salt concentration. The effect is most pronounced for the  $PIB_x$ - $b$ - $PMAA_y$  copolymers with the longer PMAA blocks (cf. Table 5.3).

Schuch *et al.* also investigated  $PIB_x$ - $b$ - $PMAA_y$  micelles [11] with a  $x:y$  block length ratio of 1:1. In that paper they report that  $R_h$  of the micelles of the copoly-

mers with  $\overline{DP}_n$  of the PMAA blocks of 50 and 70 is around 15 nm (CONTIN plot at  $\Theta = 90^\circ$ ), comparable to the contour length,  $L_c$ , of a totally stretched PMAA block. Comparing this result to our micelles with  $\overline{DP}_n$  of PMAA blocks equal to 170 and 190, the micellar radius coincides with the  $L_c$  calculated for the micelles formed by the copolymers used in this work, which are between 43 nm and 48 nm ( $R_h = 40$  nm;  $PIB_{30}$ - $b$ - $PMAA_{190}$ ,  $PIB_{31}$ - $b$ - $PMAA_{170}$ ,  $PIB_{75}$ - $b$ - $PMAA_{190}$ ), pointing to a degree of stretching of the PMAA chain of ca. 80 to 90 %.

Pergushov *et al.* also reported on solutions of  $PIB_{20}$ - $b$ - $PMAA_y$  micelles with  $y$  varying from 100 up to 425 [10]. The apparent hydrodynamic radius was determined to be approximately 20 nm for micelles formed by the shortest  $PIB_{20}$ - $b$ - $PMAA_{100}$  copolymer at concentrations of NaCl from 0.1 up to 1.0 M NaCl. The smaller size of the micellar assemblies compared to those found in this paper can be explained shorter PIB block of those copolymers. The shorter the PIB block is, the smaller is the core of the micelle and consequently the smaller is the  $\overline{N}_{agg}$  of the micellar assemblies formed. This can be stated by a comparison of the values of  $\overline{N}_{agg}$  obtained for micelles of those copolymers with the values of  $\overline{N}_{agg}$  obtained for  $PIB_x$ - $b$ - $PMAA_y$  micelles examined in this work (see section 5.3.5).

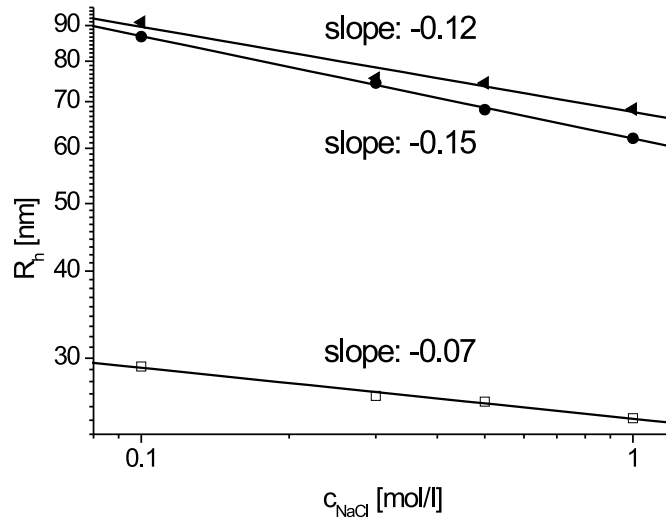


Fig. 5.8: Double-logarithmic plot of  $R_h$  of  $PIB_{30}$ - $b$ - $PMAA_{170}$  ( $\square$ ),  $PIB_{75}$ - $b$ - $PMAA_{1600}$  ( $\bullet$ ) and  $PIB_{25}$ - $b$ - $PMAA_{2600}$  ( $\blacktriangle$ ) micelles on concentration of NaCl at pH = 9,  $c_{TRIS} = 0.01M$ ,  $\Theta = 90^\circ$ .

In Figure 5.8 a double-logarithmic plot of hydrodynamic radius against salt concentration is shown. As the core size of our star-like micelles is rather small compared to the corona thickness, we can also compare it to the results shown below. It was reported that the slope of the double-logarithmic plot of corona thickness  $D_{corona}$  of equilibrium star-like micelles ( $R_{core} \ll D_{corona}$ ) against salt concentration is a

measure of the shrinkage of the corona [5]. This can also be seen from equations above.

Förster *et al.* [28] reported that at salt concentrations above 0.05 M the micelles are in the salted-brush regime, e.g. the concentration of salt in bulk solution is higher than the salt concentration within the micellar corona. In their work they obtained a  $D_{corona} \sim c^{-0.13}$  dependence for poly(ethylene)-*b*-polystyrene sulfonic acid (PEE-*b*-PSSH) micelles. Also Guenoun *et al.* [29] reported on  $c^{-0.14}$  and  $c^{-0.11}$  dependences for poly(tert-butylstyrene)<sub>x</sub>-*b*-poly(sodium styrenesulfonate)<sub>y</sub> (PtBS<sub>x</sub>-*b*-PSSNa<sub>y</sub>) micelles with  $x/y$  being 26/404 and 27/757, respectively. For the micelles of the PIB<sub>x</sub>-*b*-PMAA<sub>y</sub> copolymers examined in this work the scaling exponent values are in the same range, except of PIB<sub>30</sub>-*b*-PMAA<sub>170</sub>, as shown in Figure 5.8. For PIB<sub>25</sub>-*b*-PMAA<sub>2600</sub> a slope of -0.12 is found while for PIB<sub>75</sub>-*b*-PMAA<sub>1600</sub> it is -0.15 and therefore in nice agreement with the theoretical predictions by Borisov (cf. Equation 5.3). The distinct deviation of the scaling exponent (-0.07) for the micelles of the copolymer with the shortest PMAA block ( $\overline{DP}_n = 170$ ) from the theoretical predictions might be due to the finite size of the micellar core and a state of not perfect equilibrium.

### 5.3.5 Static Light Scattering

By means of SLS measurements molecular weights,  $\overline{M}_{w,mic}$ , of the micelles and their radii of gyration,  $R_g$ , were obtained. From  $\overline{M}_{w,mic}$  and  $\overline{M}_{w,pol}$  the average aggregation number,  $\overline{N}_{agg}$ , can be calculated (cf. Table 5.3) according to

$$\overline{N}_{agg} = \frac{M_{w,Micelle}}{M_{w,Polymer}}. \quad (5.4)$$

$PIB_x$ - $b$ - $PMAA_y$	$c_{NaCl}$ $\frac{mol}{l}$	$\overline{M}_{w,agg}$ $10^{-6} \frac{g}{mol}$	$\overline{N}_{agg}$	$R_g$ nm	$R_h$ nm	$\frac{R_g}{R_h}$	$A_2 \cdot 10^6$ $\frac{mol \cdot ml}{g^2}$
30-170	0.1	4.8	290	44	45	0.98	9.7
30-190	0.1	3.3	183	43	40	1.08	4.6
	0.3	6.3	350	57	48	1.19	1.4
	0.5	6.9	385	63	54	1.17	3.3
	0.7	11.2	620	73	65	1.12	1.1
	1.0	16.7	930	82	75	1.12	-6.1
75-190	0.1	12.8	625	38	39	0.97	8.2
75-1600	0.05	19.8	140	88	-	-	20.6
	0.1	19.3	140	110	116	0.95	19.0
	0.5	63.0	450	145	100	1.45	2.9
	1.0	93.0	660	215	98	2.19	3.2

Tab. 5.3: Results obtained by means of DLS and SLS for aqueous solutions of  $PIB_x$ - $b$ - $PMAA_y$  micelles at pH = 9,  $c_{TRIS} = 0.01M$  at RT.

Comparing the average aggregation numbers of micelles, one can see a tendency with regard to the block lengths (cf. Table 5.3). For the polymers with the shorter PIB blocks ( $PIB_{30}$ - $b$ - $PMAA_{170,190}$ ) it is evident that already a slight increase in the PMAA chain length leads to a decrease of the aggregation number, which nicely agrees with the theoretical prediction (cf. Equation 5.2). This is due to the space occupied by the PMAA arm in the corona and at the core-corona interface of the aggregate. The longer the PMAA block is, the more space is occupied in the corona. To minimize the repulsive forces, the  $\overline{N_{agg}}$  is reduced, leading to higher curvature of the hydrophobic-hydrophilic interface. This effect overcomes the high entropy loss in case of totally stretched PMAA chains. Hence, the PMAA arms are able to arrange with less energetic restrictions in the corona of the micelle and at the core-corona interface. The explanation is confirmed by the results obtained for the copolymer  $PIB_{75}$ - $b$ - $PMAA_{190}$  and  $PIB_{75}$ - $b$ - $PMAA_{1600}$ . In comparison with the copolymer  $PIB_{75}$ - $b$ - $PMAA_{190}$ , for  $PIB_{75}$ - $b$ - $PMAA_{1600}$  the  $\overline{N_{agg}}$  decreases by factor of 5, while the PMAA block length increases by roughly by a factor of 10, which coincides with the theoretical predictions (cf. Equation 5.2).

Comparing the  $\overline{N_{agg}}$  for the copolymers with different PIB block lengths, one can see, the longer the PIB block is, the higher the  $\overline{N_{agg}}$  (cf. Equation 5.2). Indeed, lengthening the PIB block forces the volume of the core to enlarge to allow incorporation of the PIB ( $N_B$ , cf. Equation 5.2). To completely cover the core-corona interface, the aggregation number should increase, as the volume of a sphere increases faster than the surface area. The increase of the aggregation number with increasing PIB block length can only be seen for two of the  $PIB_x$ - $b$ - $PMAA_y$  shown in Table 5.3. Increasing the  $\overline{DP_n}$  of PIB from 30 to 75, i.e. by a factor of 2.5, the  $\overline{N_{agg}}$  increases by a factor of 4.

In Pergushov's work the  $N_{agg}$  of  $PIB_{20}$ - $b$ - $PMAA_{100}$  diblock copolymer micelles increases with rising concentration of NaCl from  $N_{agg} = 71$  (salt free) to a maximum  $N_{agg} = 106$  (1.0 M NaCl), as determined by means of SANS. For the copolymers investigated in our work the values of  $\overline{N_{agg}}$  increase with rising salt content in much greater extent. Figure 5.9 shows a double logarithmic plot of the aggregation numbers obtained from SLS against the salt concentration. As it can be seen, the  $\overline{N_{agg}}$  increases almost linearly for all  $PIB_x$ - $b$ - $PMAA_y$ . The relative increase for all examined polymers is comparable (factor of 4 from  $c_{NaCl} = 0.1$  M to 1.0 M).

According to theoretical predictions [23] (cf. Equation 5.2), a slope of around 0.55 should be obtained. For the  $PIB_{75}$ - $b$ - $PMAA_{1600}$  and  $PIB_{30}$ - $b$ - $PMAA_{190}$ , the results obtained (values of 0.66 and 0.68) are in good agreement taking into account the accuracy of the determination of the  $\overline{N_{agg}}$ .

The  $R_g$  clearly depends on the length of the PMAA block. The values of  $R_g$  of the micelles formed by the  $PIB_x$ - $b$ - $PMAA_y$  with the shorter PMAA blocks are comparable, whereas the longer PMAA blocks result in much larger values. Additionally,

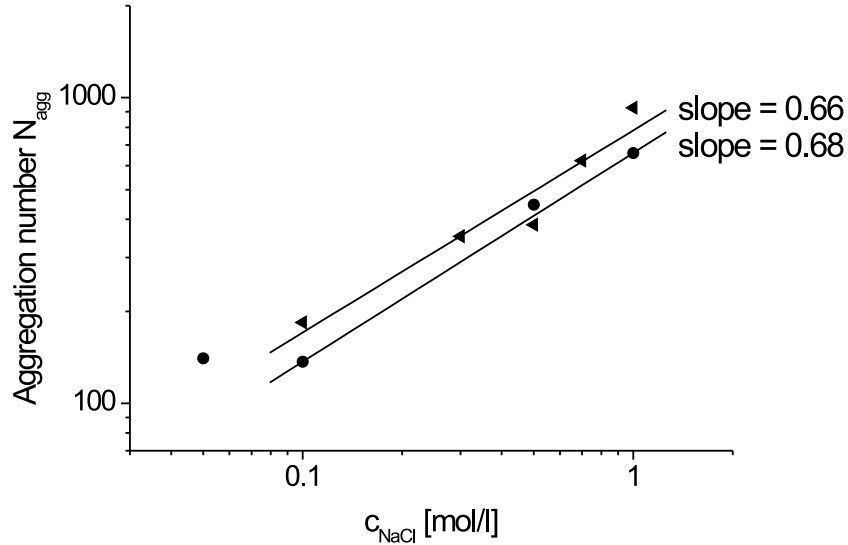


Fig. 5.9: Double logarithmic plot of  $\overline{N}_{agg}$  against concentration of NaCl for PIB<sub>75</sub>-*b*-PMAA<sub>1600</sub> (●) and PIB<sub>30</sub>-*b*-PMAA<sub>190</sub> (◄) micelles.

the ratio  $R_g/R_h$  provides an indication of the shape of the scattering particle [30]. For hard spheres the ratio is 0.775, for random coils the value is approximately 1.5. In the case of star polymers with many arms, the ratio was calculated to be approximately 1.1. As seen from Table 5.3, for the shorter PIB<sub>*x*</sub>-*b*-PMAA<sub>*y*</sub>, the ratio  $R_g/R_h$  is mostly about unity, suggesting a spherical shape of their micelles as was also seen by means of DLS and cryo-TEM. The PIB<sub>75</sub>-*b*-PMAA<sub>1600</sub> gives a  $R_g/R_h$  ratio of about 1.5 to 2.2 at  $c_{NaCl} \geq 0.5$  M. Values higher than 1.5 are typical for random coils and worm-like micelles. From cryo-TEM images it is not totally clear if the PIB<sub>75</sub>-*b*-PMAA<sub>1600</sub> micelles are of spherical shape, as due to the possible partially overlapping of the coronae formed by the long PMAA blocks only the PIB core of the micelles can be seen. The strongly overlapping PMAA chains give a large contribution to the solution state of the micelle, seen by SLS. The  $R_g/R_h$  value of 1.5, attributed to random coils, seems to fit to our micelles, taking into account that the PIB core has a size of several nm but the PMAA corona has a thickness of more than 100 nm.

The  $R_g$  and  $R_h$  values reported by Schuch *et al.* for PIB<sub>*x*</sub>-*b*-PMAA<sub>*y*</sub> micelles are comparable. This leads roughly to values of  $\frac{R_g}{R_h}$  of about 1. It is worthy to mention, that in Schuch's work, the aggregation number does not vary too much with the length of the PMAA block nor with the length of the PIB block (the variation of  $\overline{N}_{agg}$  is within  $\pm 30$ ).

Increasing the ionic strength is, as already discussed, accompanied by an increase in the value of  $\overline{N}_{agg}$ . Associated with this, the  $R_g$  and  $R_h$  are also expected to rise. On the other hand, the screening effect of the NaCl leads to a shrinkage of the micellar coronae, resulting in a decrease of size of the PIB<sub>*x*</sub>-*b*-PMAA<sub>*y*</sub> micelles.

Thus, there are two contrary salt-induced effects. The experimental results presented herein demonstrate that the block length of the PMAA block decisively determines which effect dominates. This can be stated from a comparison of the data for the PIB<sub>75</sub>-*b*-PMAA<sub>1600</sub> with those for PIB<sub>30</sub>-*b*-PMAA<sub>190</sub> (cf. Table 5.3). For the latter one, both  $R_g$  and  $R_h$  increase. For the PIB<sub>75</sub>-*b*-PMAA<sub>1600</sub>,  $R_g$  increases by a factor of 2 upon going from 0.1 M to 1.0 M NaCl, whereas  $R_h$  slightly decreases. Hence, in the case of this copolymer, the shrinkage of the micellar corona is more pronounced than the increase in size of the micelle due to the increase of  $\overline{N_{agg}}$ .

Additionally the second virial coefficient,  $A_2$ , is obtained from SLS measurements.  $A_2$  is a measure of the solvent quality and the interactions of the hydrophilic block with solvent and with polymer molecules. Values close to 0 mean almost  $\Theta$ -conditions for the copolymer. Negative values, as shown in Table 5.3, indicate aggregation of the species [31]. According to Dautzenberg *et al.* [32],  $A_2$  is proportional to

$$A_2 \sim \frac{Z^2}{n_s M^2} \sim \frac{\alpha^2}{c_s}, \quad (5.5)$$

with  $Z$ , being the number of charges,  $n_s$ , being the moles of salt, and  $M$ , being the molecular weight of the polyelectrolyte. Thus,  $A_2$  is independent of the degree of polymerization, as  $Z$  is proportional to  $M$ . The second virial coefficient decreases with decreasing  $M$  and increasing charge density  $Z$ . The same effect can be seen upon increasing ionic strength. Considering the results obtained by means of SLS at least a tendency for a decrease of  $A_2$  with increasing salt concentration for PIB<sub>30</sub>-*b*-PMAA<sub>190</sub> can be seen. The same is clearly observed for PIB<sub>75</sub>-*b*-PMAA<sub>1600</sub>. In our case, the repulsive interactions between the PMAA coronae of PIB<sub>*x*</sub>-*b*-PMAA<sub>*y*</sub> micelles significantly contribute to the value of  $A_2$ . These interactions are strongly dominated by electrostatics and therefore depend on the ionic strength and pH in the micellar solutions.

### 5.3.6 Small Angle Neutron Scattering

The obtained SANS curves were quantitatively analyzed on the basis of a core-shell model [33] with constant scattering length densities,  $\rho_c$  and  $\rho_0$ , for the core of the particle and the solvent, respectively. For all evaluations, the absolute scattering intensity was used. The scattering length density of the shell,  $\rho_s$ , was assumed to vary according to [10]:

$$\rho_s = \rho_1 \left( \frac{r}{R_c} \right)^{-a}, R_c < r < R_m \quad (5.6)$$

with  $R_c$  and  $R_m$  being the maximum radius of the core and the aggregate, respectively, and  $a = 2$  (stiff chains) describing the radial scattering length density profile in the micellar corona as shown in Figure 5.10. For D<sub>2</sub>O  $\rho_o = 63.6 \cdot 10^9 \text{ cm}^{-2}$  was

used. For the PIB (core) a density of  $0.918 \frac{g}{cm^3}$  was assumed (density of bulk PIB), leading to  $\rho_c = -3.3 \cdot 10^9 \text{ cm}^{-2}$ .

The resulting scattering intensity then can be expressed as

$$I(q) = {}^1 N \int_0^\infty dR_c f(R_c) P(q, R_c, a, R_m) S(q) \quad (5.7)$$

with the form factor  $P(q)$ , the structure factor  $S(q)$ , the number density of particles  ${}^1 N$  and the distribution function of core radii given by Schulz distribution [34]. The form factor can be written as [28, 33]:

$$\begin{aligned} \frac{P(q)}{P(0)} = & \left\{ \left[ \frac{1}{3} {}_0F_1 \left( \frac{3}{2}; -\frac{q^2 R_c^2}{4} \right) - \right. \right. \\ & - \frac{\rho_1}{\rho_c(3-a)} {}_1F_2 \left( \frac{3-a}{2}, \frac{3}{2}, \frac{5-a}{2}, \frac{q^2 R_c^2}{4} \right) + \\ & + \left. \left( \frac{R_c}{R_m} \right)^{a-3} \frac{\rho_1}{\rho_c(3-a)} \times {}_1F_2 \left( \frac{3-a}{2}, \frac{3}{2}, \frac{5-a}{2}, \frac{q^2 R_c^2}{4} \right) \right] / \\ & / \left[ \frac{1}{3} + \frac{\rho_1}{\rho_c(3-a)} \left( \left( \frac{R_c}{R_m} \right)^{a-3} - 1 \right) \right] \right\}^2 \end{aligned} \quad (5.8)$$

with  ${}_0F_1(q, R_c)$  and  ${}_1F_2(q, R_c, a)$  representing hypergeometric functions. To describe  $S(q)$ , a random-phase approximation for charged spherical particles interacting through a screened Coulomb potential was applied [35].

Since the ratio between the integrated scattering contributions from the core and the corona of the macromolecular micelles is determined by the relative lengths of hydrophobic and polyelectrolyte blocks of the copolymers used, a combination of  $\rho_1$ ,  $R_m$  and  $a$  represents only two fit parameters. It should be noted, however, that these fit parameters describing the micellar corona have only a minor effect on the resulting values of  $R_c$  which is the key parameter regarding the aggregation number as we deduce it from our analysis. Even a simple core-shell model with a constant scattering length density for the shell would yield similar values for  $R_c$ .

The aggregation number,  $\overline{N_{agg}}$ , and the area required for each ionic block to be located at the core-corona interface,  $A$ , can be calculated according to equations 5.9 and 5.10. The results are summarized in Table 5.4.

Already from qualitatively comparing the obtained SANS curves, one can obtain some information about the scattering particles. In contrast to amphiphilic block copolymers with a PS block, copolymers with PIB as hydrophobic block are expected to form dynamic micelles, which react to external stimuli like changes in pH or ionic strength, not only by a response of their polyelectrolyte shells but also via changes in core size. Changes in the core size can only be obtained by incorporation of either solvent or by a change in the aggregation number,  $\overline{N_{agg}}$ . The latter can only happen, when the core-forming block is above glass transition temperature,  $T_g$ , e.g.

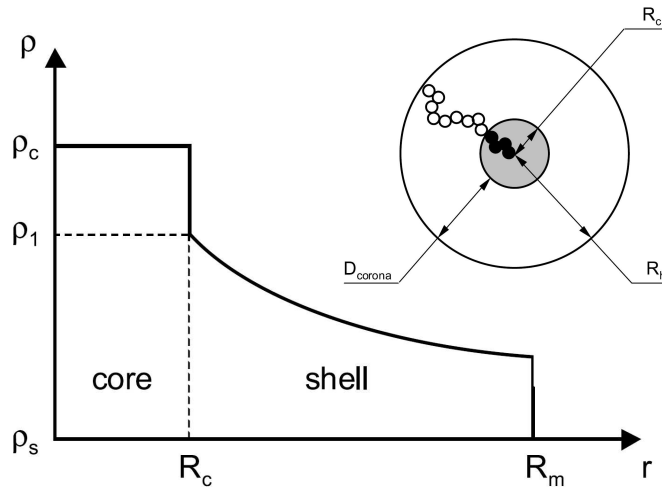


Fig. 5.10: Scattering length densities assumed for simple core-shell model. A constant core scattering length density is followed by an exponential decrease of the scattering length density of the surrounding shell. Inset: Model of a star-like macromolecular micelle in aqueous media.

segmental movements of the hydrophobic block are possible and the micelle can rearrange. The core radius,  $R_c$ , is directly obtained from fitting the SANS curves and gives the values of  $N_{agg}$  according to

$$m_{core} = \frac{4\pi}{3} \rho_{PIB} R_{core}^3 = \overline{N_{agg}} \frac{M_{PIB}}{N_A} \quad (5.9)$$

where  $M_{PIB}$  is the molecular weight of the PIB block,  $N_A$  is the Avogadro number, and  $\rho_{PIB}$  the bulk density of the PIB core (taken to be  $0.918 \text{ g/cm}^3$  according to literature).

The effects of pH and ionic strength on the values of  $R_c$  and  $\overline{N_{agg}}$  of the micelles can be reasonably explained on a basis of a simple packing model, taking into account an area,  $A$ , required for each ionic block to be located at the core-corona interface. This parameter is the equivalent of the head group area of low molecular weight surfactants. It can be calculated as

$$A = \frac{4\pi R_c^2}{N_{agg}}. \quad (5.10)$$

The obtained values of  $A$  for  $PIB_x$ - $b$ - $PMAA_y$  micelles are collected in Table 5.4.

In Figure 5.11 an example of investigations of the dynamic behavior of the system is shown. For the measurements, reference samples of the block copolymer,  $PIB_{30}$ - $b$ - $PMAA_{190}$  were prepared at pH 12 ( $\alpha = 1$ ) with  $c_{TRIS} = 0.01 \text{ M}$  ( $\square$ ). The curves are compared to curves obtained from SANS of the samples directly prepared at ca. pH 5 ( $\alpha = 0.1$ , black square) and 7 ( $\alpha = 0.65$ ). To have an insight in the responsiveness of the assemblies, we prepared samples at pH 12 and after several days of equilibration, brought to ca. pH 5 and 7, respectively, upon addition of DCl.

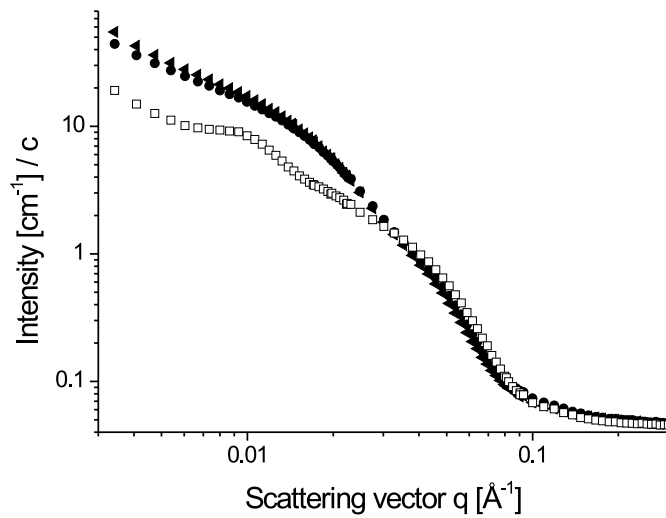


Fig. 5.11: Scattering curves obtained from SANS of micellar solutions of  $PIB_{30}-b-PMAA_{190}$  with 0.1 M NaCl prepared at pH 10 ( $\square$ ), prepared at pH 5.2 ( $\blacktriangleleft$ ) and prepared at pH = 12 and brought to pH = 5 ( $\bullet$ ).

Table 5.4 shows an overview of the obtained results. After the large jump in pH for the diblock copolymer from 10 to 5.2 a clear change in scattering behavior of the samples can be detected, the  $\overline{N_{agg}}$  changing from 85 to 165 (pH 5.2) and 149 (pH 12  $\rightarrow$  5.2), respectively. The difference between the SANS curves for the  $PIB_x-b-PMAA_y$  solutions at pH 5.2 and 12 is expectedly much larger compared to that for those at pH 7 (cf. Table 5.4).

$PIB_x$ - $b$ - $PMAA_y$ X-Y	$\alpha$	$c_{NaCl}$ [mol/l]	$R_c$ [nm]	$N_{agg}$	$A$ [nm <sup>2</sup> ]
30-190	1.0	0.1	4.0	85	2.32
	0.65	0.1	4.3	110	2.12
	0.1	0.1	4.9	165	1.85
	1 $\rightarrow$ 0.65	0.1	4.7	138	1.98
	1 $\rightarrow$ 0.1	0.1	4.8	149	1.93
75-615	1.0	0	5.1	72	4.50
	1.0	0.1	5.1	74	4.47
	1.0	0.5	5.2	77	4.41
	1.0	1.0	5.6	99	4.08
75-190	1.0	0.1	8.7	365	2.63
	0.1	0.1	12.4	1040	1.86

Tab. 5.4: The results of evaluation of the SANS curves for the solutions of  $PIB_x$ - $b$ - $PMAA_y$  micelles ( $\alpha = 1/0.65/0.1$  means  $pH = 10/7/5$ ).

The core radius of the micelle ( $R_c \sim \sqrt[3]{N_{agg}}$ ) does not change too much upon the change of pH from 12 to 7. Here the corresponding  $\overline{N_{agg}}$  are 85 (pH 10), 110 (pH 7) and 138 (pH 12  $\rightarrow$  7).

Thus, the micelles react on external stimulus of pH-changes in the size of their core. This is clear evidence for the dynamic behavior of the examined  $PIB_x$ - $b$ - $PMAA_y$  micelles.

The changes in  $\overline{N_{agg}}$  can be explained by reduction of the repulsion of the PMAA blocks in the corona of  $PIB_x$ - $b$ - $PMAA_y$  micelles as already discussed according to Equation 5.2. Due to the lower pH value the charge density of such blocks decreases, leading to weaker repulsion of the arms of the micelles. Indeed, the interfacial area occupied by one single block copolymer chain decreases with decreasing pH at the core-corona interface (cf. Table 5.4).

Concentration-dependent SANS measurements for  $PIB_{75}$ - $b$ - $PMAA_{615}$  are shown in Figure 5.12. The concentrations were set from 0.14 to 2 wt-%. Samples with  $c >$

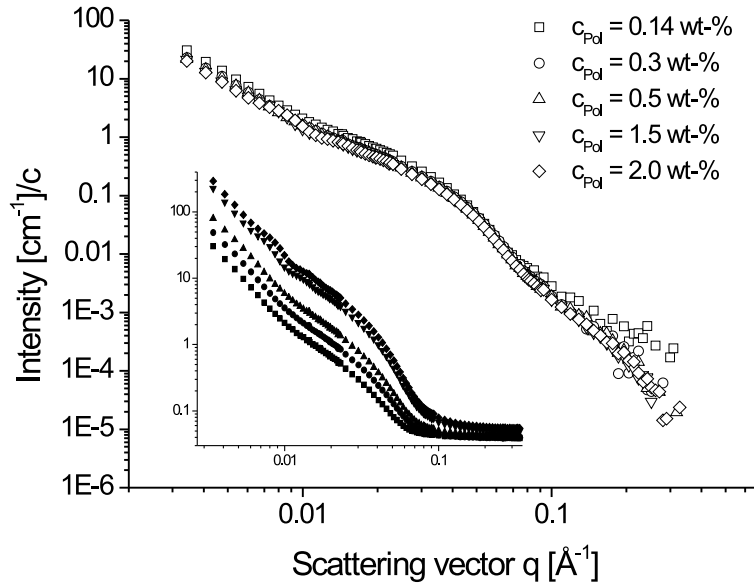


Fig. 5.12: Concentration dependence of SANS intensities for  $PIB_{75}$ - $b$ - $PMAA_{615}$  at pH = 9,  $c_{TRIS} = 0.01M$ ,  $c_{NaCl} = 0.1M$ , normalized by the concentration. In the inset the unnormalized curves are plotted.

2 wt-% could not be measured due to their high viscosity. The incoherent scattering background is subtracted and the curves are normalized by the  $PIB_x$ - $b$ - $PMAA_y$  concentration. As is seen, the shape differs only very slightly. Apparently these block copolymers are not sensitive to changes of the total concentration, a behaviour which is different to that of ionic surfactants which usually show pronounced changes of their aggregation behaviour with increasing concentration. In the inset of Figure 5.12 especially for the higher concentrations an appearance of a small correlation peak at around  $q = 0.009$  and  $0.015 \text{ \AA}^{-1}$  can be seen. This comes from the onset

of the arrangement of the micelles, leading to a correlation between the cores of the micelles. From the position of this peak at the highest concentration a distance between the cores of approximately 72 nm can be evaluated according to

$$d = \frac{2\pi}{q}. \quad (5.11)$$

Assuming that the micelles are arranged in a way that the coronae are touching, a radius of the micelles of approximately 36 nm can be calculated. Compared to results obtained for the same system by means of DLS, where an apparent  $R_h$  of 80 nm was found, one has to take into account, that for SANS measurements the concentration is up to 2 wt-%, whereas for DLS measurements the samples were diluted for 50 times. Obviously for low copolymer concentrations (DLS) the micelles are well separated and the corona can extend in an undisturbed way, whereas at high copolymer concentrations (SANS) the coronae are already overlapping. This can also be seen in cryo-TEM, where the samples were also prepared at a concentration of around 0.5 wt-%. The coincidence of the  $c$ -normalized curves also indicates that the size and the shape of the  $PIB_x-b-PMAA_y$  micelles does not depend on the concentration of the diblock copolymer in solution.

The effect of the degree of neutralization,  $\alpha$ , on the  $PIB_x-b-PMAA_y$  micelles is shown in Figure 5.13. A clear dependence of the absolute scattering intensity on  $\alpha$

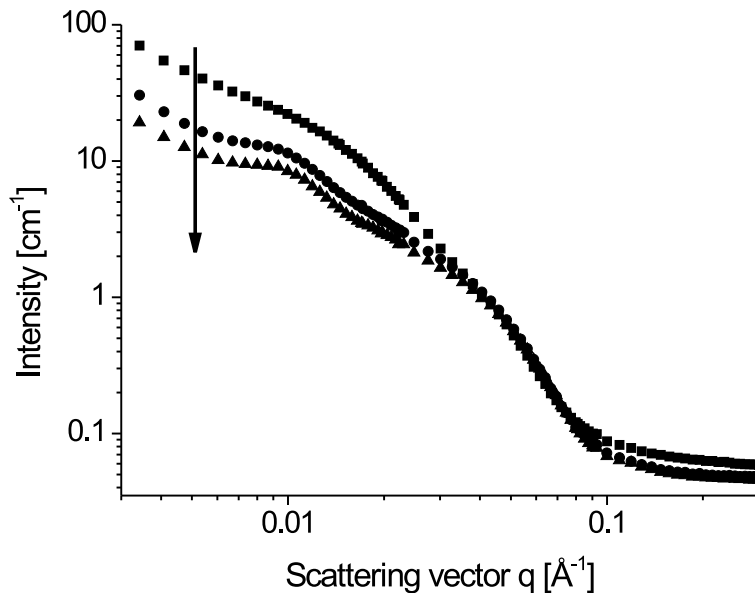


Fig. 5.13: Dependence of SANS for  $PIB_{30}-b-PMAA_{190}$  at  $c_{NaCl} = 0.1M$  at  $\alpha$  of 0.1, 0.65 and 1 (curves from top to bottom).

can be observed. With decreasing degree of neutralization the micelles scatter more, e.g. the particles increase in size, leading to increasing  $\overline{N_{agg}}$  and to denser micellar assemblies. The results of the evaluation of SANS curves are given in Table 5.4.

The  $\overline{N_{agg}}$  of the micelle increases with decreasing  $\alpha$  (1, 0.65, 0.1) from 85 to 110 and finally 165. As already discussed above, this can also be seen for the other polymers investigated in this work (see Table 5.4). Here the changes seem to slightly depend on the length of the PIB block. For the change of  $\alpha$  from 1 to 0.1, the values of  $\overline{N_{agg}}$  increase for 194 % in case of the PIB<sub>30</sub>-b-PMAA<sub>190</sub> and 185 % in case of the PIB<sub>75</sub>-b-PMAA<sub>190</sub>.

Quantitatively, comparison of the SANS results of the two polymers show a difference in size of the micellar assemblies. For PIB<sub>30</sub>-b-PMAA<sub>190</sub> the cores of the micelles are expectedly smaller than for the block copolymer with the longer PIB chain of 75 units. For different  $\alpha$  values, the size of the PIB core of the PIB<sub>x</sub>-b-PMAA<sub>y</sub> micelles with the longer PIB ( $\overline{DP}_n = 75$ ) can be evaluated as 8.7 nm (pH 10) up to 12.4 nm (pH 5.2). Compared to the shorter PIB ( $\overline{DP}_n = 30$ ), the core sizes higher for a factor of ca. 2 (4.0 nm at pH 10, 4.9 nm at pH 5.2). Even smaller is the  $R_c$  for the PIB with  $\overline{DP}_n = 20$  (3.0 nm, [10]).

An influence of the length of the PMAA block on the size of the micellar core can be seen from Table 5.4. Comparing the two diblock copolymers with a PIB block with  $\overline{DP}_n$  of 75 but different length of the PMAA block it is clear that an increase in  $\overline{DP}_n$  of PMAA block of about a factor of 3 results in a decrease of  $R_c$  for a factor of 1.7. This coincides with the theoretical predictions as already discussed in the DLS and SLS section. The enlargement of the area occupied by a PMAA block at the core-corona interface is nicely seen for PIB<sub>75</sub>-b-PMAA<sub>190</sub> 263 Å<sup>2</sup> at  $c_{NaCl} = 0.1$  M and 447 Å<sup>2</sup> for PIB<sub>75</sub>-b-PMAA<sub>615</sub> at the same ionic strength.

Another important issue is the influence of ionic strength on the size of the aggregates. As it can be seen from DLS measurements,  $R_h$  and  $D_{corona}$  decrease with increasing salt content for the PIB<sub>75</sub>-b-PMAA<sub>1600</sub>. By means of SANS measurements, the investigated  $q$ -range only allows to draw conclusions about the core of the micelle. From Figure 5.14 only a weak dependence of the shape of the scattering curve can be seen. In addition, due to an overlap of the PMAA arms of the micelles no correlation among the micelles can be observed (for this case the length of the stretched PMAA chain is about 2-3 times larger than the average distance between the micelles). Only in the low  $q$  region, where the influence of the PMAA polyelectrolyte corona on the scattering of the PIB core is seen, slight shifts to higher scattering intensity can be observed. This is again related to the  $q$  range used for SANS measurements, which does not allow to draw a reasonable inference about the overall size of the PIB<sub>x</sub>-b-PMAA<sub>y</sub> micelle.

Table 5.4 also shows the effect of  $c_{NaCl}$  on  $\overline{N_{agg}}$  of the PIB<sub>x</sub>-b-PMAA<sub>y</sub> micelles. For the block copolymer PIB<sub>75</sub>-b-PMAA<sub>615</sub> where the PMAA chain relatively long, the change in  $\overline{N_{agg}}$  resulting from changing the salt concentration from 0 up to 1 M NaCl is pronounced: from 72 to 99. Especially upon a large jump in the salt concentration from 0.5 M to 1.0 M NaCl the  $\overline{N_{agg}}$  changes by roughly 20%.

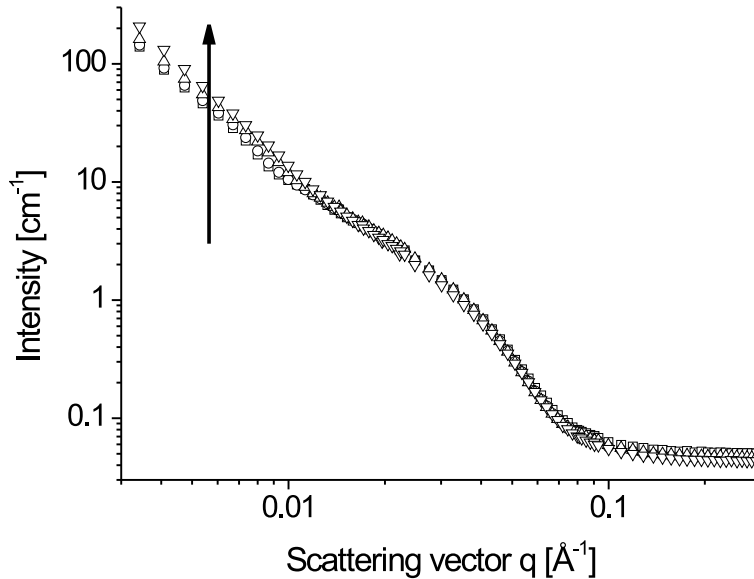


Fig. 5.14: SANS scattering curves of  $PIB_{75}$ - $b$ - $PMAA_{615}$ ,  $c_{TRIS} = 0.01M$  for salt concentrations of 0, 0.1, 0.5 and 1 M (from bottom to top).

Within this work, differences in the aggregation number obtained from SLS and SANS can be stated (see Tables 5.3 and 5.4). This can be due to the time frame between the preparation of the solutions and the measurements for both SLS and SANS. For SANS the samples had to be prepared in advance for assuring to keep the measurement time offered by the neutron facilities. For SLS, the samples were prepared and dialyzed one week before measurement. They were filtered one day before measurement to remove dust. By applying the shear forces to the samples, the micellar assemblies might have been changed. In addition, the concentration regime applied for SANS (1 - 2 wt-%) is far above the concentrations applied for SLS ( $\approx 0.02$  wt-%). We also investigated the concentration dependence in SANS measurements. As discussed above, the samples behave similar in the investigated regime. Measurements for lower concentrations could not be made due to low scattering power of the samples. Furthermore the difference of the data treatment has to be taken into account. For SLS, an evaluation according to Berry was applied. For SANS a theoretical model was applied that fits to our best knowledge to the structure of the samples.

#### 5.4 Conclusion

In this paper we report on  $PIB_x$ - $b$ - $PMAA_y$  diblock copolymers with low PDI, which self-assemble in aqueous solutions. The data we have obtained by means of SANS and DLS point to a dynamic behavior of such micelles reacting on changes in pH from 10 to 7 and 5 respectively. The response is not only related to a change of

the degree of neutralization of the PMAA block and therewith to a denser packing of these blocks in the corona. Quantitative evaluation of SANS curves also shows a change of the size of the hydrophobic core formed by the PIB blocks, due to a change of the aggregation numbers.

From cryo-TEM images, a spherical shape of the micelles is clearly seen. This allows us to evaluate the SANS data using a model of a spherical particle with protruding arms into the solvent. Evaluation of the SANS curves evidences about changes in  $\overline{N_{agg}}$  with pH and with ionic strength. The higher the pH is, the more the arms of the micelle repel their neighbors and the higher the area at the core-corona interface of the micelle is. This leads to decreasing values of  $\overline{N_{agg}}$  with rising pH. An increase in ionic strength has an opposite effect, resulting in higher  $\overline{N_{agg}}$  upon improving screening of the charges of the PMAA blocks.

DLS measurements also show the response of the corona of the micelle on external stimuli such as changes in pH or ionic strength. In principle, the PMAA block is more stretched the higher the number of charges on the arms of the micelles are. This also leads to an increasing  $R_h$ . Here the hydrophilic block dominates the response of the micellar aggregate. For DLS, the influence of the PIB core and therefore the changes in  $\overline{N_{agg}}$  can be neglected due to the longer PMAA block compared to the PIB block of the diblock copolymers used in this work.

Potentiometric titrations also show an effect of the ionic strength on the apparent  $pK_a$  value, shifting it to lower values with increasing  $c_{NaCl}$ , while the length of the hydrophilic block seems to play a minor role. The apparent  $pK_a$  values are found to be around 6.5 for all copolymers examined.

For the evaluation of the *cmc* for different diblock copolymers the PIB block determines the properties of the micellar assemblies as well. The *cmc* clearly depends on the length of the hydrophobic PIB block. The longer the block is, the lower the *cmc* is found to be.

### *Acknowledgment*

This work was supported by the European Union within the Marie Curie RTN Polyamphi and by DFG within the ESF EUROCORES Programme SONS. ILL is gratefully acknowledged for providing SANS beam time and travel support. Markus Ruppel and Oleg V. Borisov are acknowledged for fruitful discussions. D. V. P. thanks DFG for the financial support of his research stays at the Universität Bayreuth.

Supporting Information available: Synthesis of block copolymers. This information is available free of charge via the Internet at <http://pubs.acs.org>.

## BIBLIOGRAPHY

- [1] Gil, E.S.; Hudson, S.M.; *Prog. Polym. Sci.*, **2004**, *29*, 1173;
- [2] Blom, A.; Drummond, C.; Wanless, E.J.; Richetti, P.; Warr G.G.; *Langmuir*, **2005**, *21*, 2779;
- [3] Rigler, P.; Meier, W.; *J. Am. Chem. Soc.*, **2006**, *128*, 367;
- [4] Dwars, T.; Paetzold, E.; Oehme, G.; *Angew. Chem. Int. Ed.*, **2005**, *44*, 7174;
- [5] Förster, S.; Abetz, V.; Müller, A.H.E.; *Adv. Polym. Sci.*, **2004**, *166*, 173;
- [6] Shen, H.; Eisenberg, A.; *Macromolecules*, **2000**, *33*, 2561;
- [7] Colombani, O.; Ruppel, M.; Burkhardt, M.; Drechsler, M.; Schumacher, M.; Gradzielski, M.; Schweins, R.; Müller, A.H.E.; *Macromolecules*, **2007**, *40*, 4351;
- [8] Martinez-Castro, N.; Lanzendörfer, M.G.; Müller, A.H.E.; Cho, J.C.; Acar, M.H.; Faust, R.; *Macromolecules*, **2003**, *36*, 6985;
- [9] Pergushov, D.V.; Remizova, E.V.; Feldthusen, J.; Zezin, A.B.; Müller, A.H.E.; Kabanov, V.A.; *J. Phys. Chem. B*, **2003**, *107*, 8093;
- [10] Pergushov, D.V.; Remizova, E.V.; Feldthusen, J.; Gradzielski, M.; Lindner, P.; Zezin, A.B.; Müller, A.H.E.; Kabanov, V.A.; *Polymer*, **2004**, *45*, 367;
- [11] Schuch, H.; Klingler, J.; Rossmannith, P.; Frechen, T.; Gerst, M.; Feldthusen, J.; Müller, A.H.E.; *Macromolecules*, **2000**, *33*, 1734;
- [12] Wilhelm, M.; Zhao, C.-L.; Wang, Y.; Winnik, M.A.; Mura, J.-L.; Riess, G.; Croucher, M.D.; *Macromolecules*, **1991**, *24*, 1033;
- [13] Astafieva, I.; Zhong, X.F.; Eisenberg, A.; *Macromolecules*, **1993**, *26*, 7339;
- [14] Astafieva, I.; Khougaz, K.; Eisenberg, A.; *Macromolecules*, **1995**, *28*, 7127;
- [15] Kalyanasundaram, K.; Thomas, J.K.; *JACS*, **1977**, *99*, 2039;
- [16] Dong, D.C.; Winnik, M.A.; *Photochem Photobiol*, **1982**, *35*, 17;
- [17] Adrian, M.; Dubochet, J.; Lepault, J.; McDowell, A.W.; *Nature*, **1984**, *308*, 32;

- 
- [18] Jacrot, B.; Zacchai, G.; *Biopolymers*, **1981**, *20*, 2413;
- [19] Chen, S.-H.; Lin, T.-L.; *Methods of Experimental Physics*, **1987**, Academic Press, 489;
- [20] GRAS<sub>ans</sub>P; Charles Dewhurst; email: dewhurst@ill.fr; Institut Laue Langevin, Grenoble, France;
- [21] Feldthusen, J.; *Thesis*, **1998**, Makromolekulare Chemie II, Bayreuth;
- [22] Rosen, M.J.; *Surfactants and Interfacial Phenomena*, **2004**, 3rd Edition, Wiley;
- [23] Borisov, O.V.; Zhulina, E.B.; *Macromolecules*, **2002**, *35*, 4472;
- [24] Guo, X.; Ballauff, M.; *Phys. Rev. E*, **2001**, *64*, 051406;
- [25] Klein Wolterink, J.; van Male, J.; Cohen Stuart, M.A.; Koopal, L.K.; Zhulina, E.B.; Borisov, O.V.; *Macromolecules*, **2002**, *35*, 9176;
- [26] Plamper, F.A.; Becker, H.; Lanzendörfer, M.; Patel, M.; Wittemann, A.; Ballauff, M.; Müller, A.H.E.; *Macromol. Chem. Phys.*, **2005**, *206*, 1813;
- [27] Stepanek, M.; Podhajecka, K.; Prochazka, K.; Teng, Y.; Webber, S.E.; *Langmuir*, **1999**, *15*, 4185;
- [28] Förster, S.; Hermsdorf, N.; Böttcher, C.; Lindner, P.; *Macromolecules*, **2002**, *35*, 4096;
- [29] Guenuon, P.; Davis, H.T.; Tirrell, M.; Mays, J.W.; *Macromolecules*, **1996**, *29*, 3965;
- [30] Burchard, W.; *Adv. Polym. Sci.*, **1999**, *143*, 113;
- [31] Holtzer, A.; Hawkins, R.B.; *J. Am. Chem. Soc.*, **1996**, *118*, 4220;
- [32] Dautzenberg, H.; Jaeger, W.; Kötz, J.; Philipp, B.; Seidel, Ch.; Stscherbina, D.; *Polyelectrolytes - Formation, Characterization and Application*, **1994**, Hanser Publishers, Munich;
- [33] Förster, S.; Burger, C.; *Macromolecules*, **1998**, *31*, 879;
- [34] Schulz, G.V.; *Z. Phys. Chem.*; **1939 B 43**, 25;
- [35] Baba-Ahmed, L.; Benmouna, M.; Grimson, M.J.; *Phys. Chem. Liq.*; **1987 16**, 235;

## 5.5 Supporting Information

### 5.5.1 Synthesis

The PIB<sub>*x*</sub>-*b*-PMAA<sub>*y*</sub> used for the investigations in this work are shown in Table 5.5. The hydrophobic PIB block used as a macroinitiator as described elsewhere [1] was obtained by quenching the cationic polymerization of IB with thiophene. The PDI of approximately 1.12 to 1.19 are relatively low for cationic polymerization. For this work three PIB macroinitiators with  $\overline{DP}_n$  of 25, 30 and 75 were utilized as precursors for the amphiphilic diblock copolymers. Anionic polymerization resulted in rather monodisperse polymers of PDI of 1.03 to 1.14, except for polymer "3" with a PDI of 1.22, which is still narrow.

<i>Polymer</i>	$\overline{DP}_n$ , PIB	$\overline{DP}_n$ , PtBMA	$\overline{M}_n$ (GPC) $\frac{g}{mol}$	<i>PDI</i> (GPC)
PIB 1	25	-	1,340	1.16
PIB 2	30	-	1,740	1.19
PIB 3	75	-	4,270	1.12
1	75	615	57,000	1.05
2	75	1600	141,000	1.03
3	25	350	31,600	1.22
4	75	190	20,500	1.09
5	25	2600	222,000	1.02
6	30	190	18,000	1.14
7	30	170	16,400	1.12

Tab. 5.5: Molecular characteristics of the PIB<sub>*x*</sub>-*b*-PtBMA<sub>*y*</sub> used in this work

In Figure 5.15 representative GPC traces of PIB<sub>75</sub>-*b*-PtBMA<sub>1600</sub> are shown, with the dashed lines, representing the UV signal and the dotted lines, representing the RI response of the apparatus. For the PIB<sub>75</sub> precursor, the UV trace shows a small shoulder at higher  $M_n$ . The shoulder is placed at the position corresponding to double molecular weight of the main peak, suggesting coupling of two cationic PIB chains to one thiophene, as already reported by Martinez-Castro *et al.* [1]. The fact that this shoulder is not observed in RI trace implies that the amount of this double molecular weight product is not too high. The pronounced response in UV-trace is due to the strong response of the aromatic thiophene incorporated in the chain. A second PIB chain blocks the 5-position of the thiophene ring, hence it cannot be activated by BuLi for initiating the polymerization of *t*BMA.

The GPC traces obtained after purification of the diblock copolymer (Figure 5.15) show monomodal distribution. At 32 - 34 ml elution volume, almost no pre-

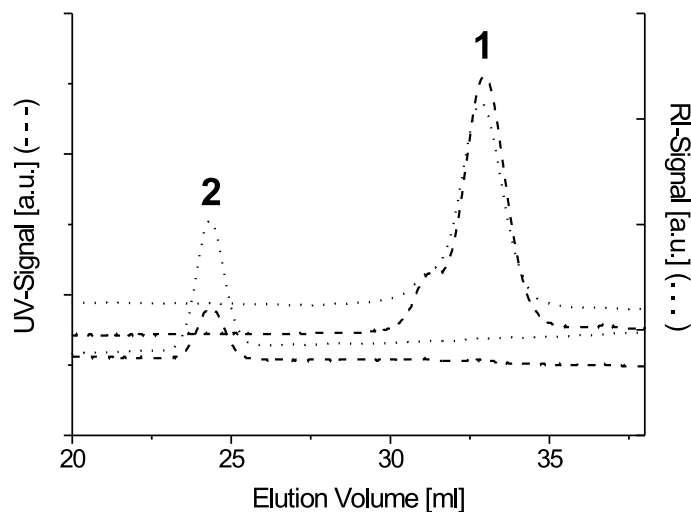


Fig. 5.15: GPC traces of the  $\text{PIB}_{75}$  precursor (1) for anionic polymerisation and purified  $\text{PIB}_{75}\text{-}b\text{-}P\text{tBMA}_{1600}$  block copolymer (2) obtained in THF; ( $\cdot \cdot \cdot$ ): RI-signal; ( $- -$ ): UV-signal ( $\lambda = 260$  nm).

cursor is left, except of a tiny peak that can be attributed to coupled PIB that could not initiate anionic polymerization of *t*BMA. After elimination of *t*-Bu moieties via hydrolysis of *Pt*BMA blocks with hydrochloric acid in dioxane at 80°C, PIB-*b*-PMAA diblock copolymer was obtained. The degree of hydrolysis obtained by means of IR spectroscopy provides evidence for nearly complete conversion ( $\approx 95$  %). The coupled PIB can be removed from PIB-*b*-PMAA by precipitation of this diblock copolymer into hexane [2].

## BIBLIOGRAPHY

- [1] Martinez-Castro, N.; Lanzendörfer, M.G.; Müller, A.H.E.; Cho, J.C.; Acar, M.H.; Faust, R.; *Macromolecules*, **2003**, *36*, 6985;
- [2] Feldthusen, J.; *Thesis*, **1998**, Makromolekulare Chemie II, Bayreuth;

## 6. WATER-SOLUBLE IPECS OF PIB<sub>X</sub>-B-PMAA<sub>Y</sub> MICELLES: FORMATION AND PROPERTIES

### **Water-Soluble Interpolyelectrolyte Complexes of Polyisobutylene-*block*-Poly(methacrylic acid) Micelles: Formation and Properties**

Markus Burkhardt<sup>1</sup>, Markus Ruppel<sup>1</sup>, Markus Drechsler<sup>1</sup>, Ralf Schweins<sup>2</sup>, Dmitry V. Pergushov<sup>3</sup>, Michael Gradzielski<sup>4</sup>, Alexander B. Zezin<sup>3</sup>, Axel H.E. Müller<sup>1</sup>

<sup>1</sup>*Makromolekulare Chemie II, Universität Bayreuth, D-95440 Bayreuth, Germany;*

<sup>2</sup>*Institut Laue-Langevin, 38042 Grenoble Cedex 9, France;*

<sup>3</sup>*Department of Polymer Science, School of Chemistry, Moscow State University, 119992 Moscow, Russia;*

<sup>4</sup>*Stranski Laboratorium Berlin, Technische Universität D-10623 Berlin, Germany*

\* e-mail: axel.mueller@uni-bayreuth.de

Markus Burkhardt: markus.burkhardt@uni-bayreuth.de;

Markus Ruppel: markus.ruppel07@imperial.ac.uk;

Sandrine Tea: sandrine.tea@uni-bayreuth.de;

Markus Drechsler: markus.drechsler@uni-bayreuth.de;

Ralf Schweins: schweins@ill.eu;

Dmitry V. Pergushov: pergush@genebee.msu.su;

Michael Gradzielski: michael.gradzielski@tu-berlin.de;

Alexander B. Zezin: zezin@genebee.msu.su;

## Abstract

We report on interpolyelectrolyte complexes (IPECs) formed by micelles of ionic amphiphilic diblock copolymers with polyisobutylene (PIB) and poly(sodium methacrylate) (PMANa) blocks interacting with quaternized poly(4-vinylpyridine) (P4VPQ). The interpolyelectrolyte complexation was followed by turbidimetry as well as small angle neutron scattering (SANS). The data obtained by means of a combination of SANS, dynamic light scattering (DLS), and cryogenic transmission electron microscopy (cryo-TEM) provide evidence on the core-shell-corona structure of the complex species with the shell assembled from fragments of electrostatically bound PMANa and quaternized P4VPQ fragments, original  $\text{PIB}_x\text{-}b\text{-PMAA}_y$  micelles apparently playing a lyophilizing part. The complex formation is followed by potentiometric titration as well. This process is initially kinetically controlled. In the second step larger aggregates rearrange in favor of smaller complexes with core-shell-corona structure, which are thermodynamically more stable. An increase in ionic strength of the solution results in dissociation of the complex species as proven by SANS and analytical ultracentrifugation (AUC). This process begins at the certain threshold ionic strength and proceeds via a salt-induced gradual release of chains of the cationic polyelectrolyte from the complex species.

**Keywords:** *micelles, amphiphilic, block copolymers, DLS, SANS, polyelectrolyte complexes, potentiometric titration*

## 6.1 Introduction

Ionic amphiphilic diblock copolymers are of considerable importance due to their numerous [1] possible promising applications in various fields, including industry, ecology, biotechnology, and medicine. Their properties, in particular, their self-assembly behavior in selective solvents, leading to the formation of macromolecular micelles, resemble those manifested by common low molecular weight surfactants though the formed polymeric micelles are considerably less responsive, i.e. the influence of variations of external conditions (pH, ionic strength, etc.) on their aggregation numbers is much less pronounced than for low molecular weight surfactant systems. A presence of a polyelectrolyte block in such copolymers provides a unique possibility to tune the characteristics of the formed macromolecular assemblies (e.g., their size, shape, and in some cases even aggregation number) via a simple variation of conditions of the surrounding solution (e.g., pH or ionic strength). Besides, the ionic amphiphilic diblock copolymers can obviously interact with oppositely charged molecules.

Several attempts have been reported to obtain polyelectrolyte complexes (PECs) of homopolymers with oppositely charged surfactants [2, 3]. Babak *et al.* reported on chitosan capsules stabilized by a shell formed by an electrostatic complex. The

complex is formed by chitosan as a semi-rigid positively charged polyelectrolyte and sodium dodecyl sulfate (SDS) as anionic surfactant. They report that the cationic polymer chains are cross-linked by a shell consisting of a network containing anionic surfactant micelles.

Special architectures like brushes were investigated as well [4]. Complexes with enzymes [5] or DNA [6] and their possible applications as carriers were also reported [7]. Another attempt, offering a novel route for a design of yet unexplored complex macromolecular architectures stabilized by interpolymer salt bonds, is the complexation of oppositely charged macromolecules. Such complex macromolecular assemblies are traditionally related to so-called interpolyelectrolyte complexes (IPECs).

The domain of IPECs has been very extensively investigated by a number of research groups during the last decades. The results of those studies have been exhaustively reviewed elsewhere [2, 8, 9], with the main attention devoted to the complex macromolecular architectures based on the oppositely charged linear homopolyelectrolytes. The structure and properties of IPECs are determined by a number of factors: the characteristics of the polymeric components (e.g. nature of their ionic groups, degrees of polymerization, charge density, etc.) and their concentrations, the ratio between amounts of the oppositely charged groups of polyelectrolytes, the conditions of the surrounding solution (e.g., ionic strength, degree of neutralization ( $\alpha$ ), pH, temperature, etc.), and in some cases the method of the preparation of such complex macromolecular assemblies. The use of ionic diblock copolymers, including ionic amphiphilic diblock copolymers self-assembling in aqueous media with the formation of macromolecular micelles, as polymeric components in interpolyelectrolyte complexation provides an attractive opportunity to design novel complex macromolecular architectures of micellar type [10] - [22], which are thought to be utilized as stimuli-responsive nano-carriers or nano-reactors.

In our previous papers [20] - [22], we have demonstrated that polyisobutylene-*block*-poly(sodium methacrylate) ( $PIB_x$ - $b$ - $PMANa_y$ ) micelles interacting with a linear cationic polyelectrolyte, viz. poly(N-ethyl-4-vinylpyridinium bromide) (P4VPQ), can form complex species in which the original  $PIB_x$ - $b$ - $PMANa_y$  micelles apparently play a lyophilizing part. The diblock copolymers were synthesized via combination of cationic polymerization of isobutylene followed by transfer to anionic polymerization to polymerize the second block, poly(*tert*-butyl methacrylate) (*Pt*BMA), as reported by Martinez-Castro *et al.* [23]. Thus, such novel complex macromolecular architectures represent a kind of polymeric hybrids combining features of the macromolecular micelles with those typical for the common IPECs. The experimental results obtained by a combination of various techniques (SANS, Fluorescence Spectroscopy (FS), DLS) have provided conclusive evidence on a peculiar core-shell-corona ("onion-like") structure of the formed complex species, with a core formed by

PIB blocks, a shell assembled from the coupled oppositely charged polyelectrolyte fragments, and a corona built up from the fragments of PMANa blocks not involved in interpolyelectrolyte complexation, the aggregation number of the original PIB<sub>x</sub>-b-PMANa<sub>y</sub> micelles appearing to remain nearly constant upon the interpolyelectrolyte complexation. Later, a similar core-shell-corona structure has been also suggested for the complex species derived from polystyrene-*block*-poly(N-ethyl-4-vinylpyridinium bromide) (PS-*b*-P4VPQ) micelles interacting with a linear anionic polyelectrolyte, viz. poly(sodium methacrylate) (PMANa) [24].

This paper considerably extends our previous investigations on IPECs based on the PIB<sub>x</sub>-b-PMANa<sub>y</sub> micelles, showing that the proposed core-shell-corona structure exists for a number of copolymers with different lengths of their blocks. Besides, we demonstrate that interpolyelectrolyte complexation apparently does not render the PIB<sub>x</sub>-b-PMANa<sub>y</sub> micelles from "dynamic" (as thoroughly discussed in [25]) to "frozen" ones: the number of the PIB<sub>x</sub>-b-PMANa<sub>y</sub> molecules incorporated into the complex species changes upon the variation of conditions of the surrounding solution (e.g., pH). In addition, we have examined salt-induced dissociation of such complex macromolecular architectures.

## 6.2 Experimental Part

### 6.2.1 Materials

Polyisobutylene-*block*-poly(*tert*-butyl methacrylate) diblock copolymers were synthesized via combination of living cationic and anionic polymerizations as described elsewhere [23, 26]. Size exclusion chromatography (SEC) was used to determine the molecular weight distributions of the PIB precursor (measured separately) and PIB-*b*-PtBMA using PIB and PtBMA standards. For the diblock copolymer, a weighted average of the homopolymer calibration curve was used. SEC was performed using PSS SDV-gel columns (5 μm, 60 cm, 1 x linear (10<sup>2</sup> – 10<sup>5</sup> Å), 1 x 100 Å) with THF as eluent at a flow rate of 1.0 ml/min at room temperature using UV (λ = 230 and 260 nm) and RI detection. The values of the number-average degree of polymerization,  $DP_n$ , of the blocks and the calculated number-average molecular masses,  $\overline{M}_n$ , for the corresponding hydrolyzed diblock copolymers PIB-*b*-PMAA are shown in Table 6.1. The values were calculated from the values of  $M_n$  for the corresponding values of  $M_n$  PIB-*b*-PtBMA diblock copolymers measured by means of SEC. The polydispersity indices of PIB-*b*-PtBMA are in the range of 1.03 to 1.22. After hydrolysis of the block copolymer with hydrochloric acid in dioxane at 80 °C for 24 hours polyisobutylene-*block*-poly(methacrylic acid) (PIB-*b*-PMAA) copolymer was obtained.

Poly(N-ethyl-4-vinylpyridinium bromide) (P4VPQ) was synthesized from poly(4-vinylpyridine) with weight-average molar mass  $M_w = 60\,000$  g/mol (Aldrich,  $DP_w$

<i>Polymer</i>	$DP_n, PIB$	$DP_n, PtBMA$	$PDI$ ( <i>GPC</i> )	$M_n(\text{calc.})$ $\frac{\text{g}}{\text{mol}}$
1*	20	100	1.16	9,620
2*	20	280	1.10	24,920
3*	20	425	1.20	37,250
4	25	350	1.22	31,600
5	30	190	1.14	18,000
6	30	170	1.12	16,400
7	75	190	1.09	20,500
8	75	615	1.05	57,000
9	75	1600	1.03	141,000

Tab. 6.1: Molecular characteristics of the polymers used in this work. \* These polymers were synthesized via a different route [26].

= 600) and  $M_w = 50\,000$  g/mol (Polysciences Inc.,  $DP_w = 500$ ) via its exhaustive quaternization with a 10-fold excess of ethyl bromide at 60°C in methanol. As determined by  $^1H$ -NMR spectroscopy, the molar fraction of quaternized pyridine units in the resulting polymer was close to 0.9, corresponding to about 540 and 450 charged monomer units per polymer chain, respectively.

### 6.2.2 Sample Preparation

To prepare a stock solution of the copolymer, PIB<sub>x</sub>-b-PMAA<sub>y</sub>, NaCl (Merck) and TRIS buffer (2-amino-2-(hydroxymethyl)-1,3-propanediol, Fluka) were dissolved in NaOH solutions at room temperature (RT) under continuous stirring for at least 24 h. The amount of NaOH was calculated according to the number of COOH groups of the weighed polymer. The solutions all showed low viscosity and were transparent.

For preparation of the complexes, a stock solution of the P4VPQ was prepared, dissolving a calculated amount of P4VPQ in Milli-Q water (resistance = 18 MΩ) containing NaCl and 0.01 M TRIS. The polymer dissolved immediately. The calculated amount of P4VPQ solution was added to the solution containing the micelles under vigorous stirring, until a slight turbidity could be seen. The solution was stirred until the solution was completely transparent again. Then more polycation solution was added to the complexes until the desired value of  $Z$  was achieved, where  $Z$  is the ratio of the molar concentrations of ionic groups of the oppositely charged polymeric components,  $Z = [P4VPQ]/[PIB\text{-}b\text{-}PMANa]$ .

### 6.2.3 Methods

#### *Potentiometric Titrations*

Potentiometric and turbidity titrations were conducted in aqueous solutions of the polymers employing a computer controlled titrator (Titrand 806, Metrohm). Potentiometric sodium ion selective measurements were performed with a Na<sup>+</sup>-selective polymer membrane electrode (6.0508.100, METROHM). Turbidity was monitored with a photometer (Spectrosense 523 nm, 6.1109.110, Metrohm). For complexation, a calculated amount of P4VPQ solution was added to the micellar solution applying the highest dosing rate (16 ml/min). The turbidity was monitored until a plateau was reached. Then further portions of the solution of P4VPQ were added to obtain complexes with higher *Z*-values.

#### *Cryogenic Transmission Electron Microscopy (Cryo-TEM) [27]*

Samples were prepared as described above. The polymers were dissolved in aqueous solutions of CsOH (Fluka). To achieve the desired ionic strength CsCl (Acros) was used. For cryo-TEM studies, a drop of the sample was placed on an untreated bare copper transmission electron microscopy (TEM) grid (600 mesh, Science Services, München, Germany). Most of the liquid was removed with blotting paper, leaving a thin film stretched over the grid holes. The specimens were shock vitrified by rapid immersion into liquid ethane and cooled to approximately 90 K by liquid nitrogen in a temperature controlled freezing unit (Zeiss Cryobox, Zeiss NTS GmbH, Oberkochen, Germany). The temperature was monitored and kept constant in the chamber during all of the sample preparation steps. After freezing the specimens, the remaining ethane was removed using blotting paper. The specimen was inserted into a cryo-transfer holder (CT3500, Gatan, München, Germany) and transferred to a Zeiss EM922 EF-TEM instrument. Examinations were carried out at temperatures around 90 K. The transmission electron microscope was operated at an acceleration voltage of 200 kV. Zero-loss filtered images ( $\Delta E = 0$  eV) were taken under reduced dose conditions (100 - 1000 e/nm<sup>2</sup>). All images were registered digitally by a bottom mounted CCD camera system (Ultrascan 1000, Gatan) combined and processed with a digital imaging processing system (Gatan Digital Micrograph 3.9 for GMS 1.4).

#### *Dynamic Light Scattering (DLS)*

Sample solutions for DLS experiments were obtained by an isoionic 50-fold dilution of the sample solutions prepared for the SANS measurements (1 wt-%, see Section 2.3.4 below) with corresponding aqueous H<sub>2</sub>O solutions of NaCl. The prepared sample solutions were thoroughly filtered by passing at least three times through a Nylon filter (13-HV, Millipore) with a pore size of 0.45  $\mu$ m. In addition, samples were also prepared as described above with an amount of polymer of about  $c_{Pol.} =$

0.02 wt-%. The DLS measurements were carried out in sealed cylindrical scattering cells ( $d = 10$  mm) at five scattering angles  $30^\circ$ ,  $60^\circ$ ,  $90^\circ$ ,  $120^\circ$  and  $150^\circ$  with the use of an ALV DLS/SLS-SP 5022F equipment consisting of an ALV-SP 125 laser goniometer, an ALV 5000/E correlator (cross correlation), and a He-Ne laser with the wavelength  $\lambda = 632.8$  nm. The CONTIN algorithm was applied to analyze the obtained correlation functions. Apparent hydrodynamic radii,  $R_h$ , of the macromolecular assemblies were calculated according to the Stokes-Einstein equation.

#### *Small Angle Neutron Scattering (SANS) [28, 29]*

Sample solutions for SANS experiments were prepared by dissolving PIB<sub>x</sub>-b-PMAA<sub>y</sub> in D<sub>2</sub>O (Aldrich), containing a desired amount of NaOH (Riedel-de Haën), at RT under continuous stirring overnight. P4VPQ was dissolved in D<sub>2</sub>O. The complexes were prepared as described above. The final concentration of the complex in the sample solutions was ca. 1.0 wt-%. In all cases, the prepared solutions were homogeneous, transparent, partially colored (slightly brownish), and of low viscosity.

The sample solutions were filled into quartz cells with 2 mm path length (Hellma). In case of samples at pH = 10 the pH value was controlled upon addition of 0.01 M of TRIS buffer (Merck) to the sample solutions. The ionic strength of the sample solutions was adjusted by adding NaCl (Merck). The SANS measurements were performed using the instrument D11 of the Institute Max von Laue-Paul Langevin (ILL, Grenoble, France) with a neutron wavelength  $\lambda = 6$  Å. Sample-to-detector distances of 1.1, 4, and 16 m were employed. With these configurations a total range of the magnitude of the scattering vector,  $q = 0.003 - 0.35$  Å<sup>-1</sup> was covered. The detector sensitivity and the intensity of the primary beam were calibrated by a comparison with the scattering from a 1 mm reference sample of water. The obtained data were radially averaged and corrected for the detector background, the detector dead time, and the scattering from an empty cell. They then were converted into absolute units by a comparison with the scattering from water according to standard routines supplied by the ILL [30] using the GRASP software. It should be noted that the SANS curves presented in this paper still contain the incoherent background scattering of the solvent and the sample.

#### *Analytical Ultracentrifugation (AUC)*

Sample solutions were obtained by mixing the stock solutions of PIB<sub>20</sub>-b-PMAA<sub>y</sub> and P4VPQ in the presence of the desired amount of NaCl, followed by a subsequent dilution of such mixtures with 0.01 M TRIS. The sedimentation experiments were carried out with a Beckman (Spinco, Model E) analytical ultracentrifuge equipped with a UV-vis absorption optical detector (Scan mode). The speed of rotor rotation was 48,000 rpm.

## 6.3 Results and Discussion

### 6.3.1 Complexation

#### Turbidimetric Titrations

Turbidimetric titrations allow an insight into the complexation phenomenon, as the turbidity of a solution is strongly related to the scattering properties and with this to the mass and size of the particles comprised. Even visually decreased transmittance (corresponding to increased turbidity) could be observed during complexation of the micellar solutions with addition of P4VPQ. The transmittance of the complex solution increased with time of stirring. Hence quantitative turbidimetric measurements were carried out. A certain amount of P4VPQ ( $V = 1.2$  ml,  $c \approx 2$  g/l) was added isoionically ( $c_{NaCl} = 0.1$  M) at the constant value of pH 9) within  $t \approx 5$  s to a micellar solution of  $PIB_{75}$ - $b$ - $PMAA_{1600}$  ( $V = 10$  ml,  $c \approx 2$ g/l) to obtain  $Z = 0.4$ . The polycation solution was added with highest rate of addition to enable fast mixing under vigorous stirring. As the addition of the polycation was started manually, the first few seconds of the measurement were taken as a background (Figure 6.1). Immediately after the start of the addition, a pronounced increase in turbidity could be observed. After reaching the minimum in transmittance at about  $T = 0.05$ , an

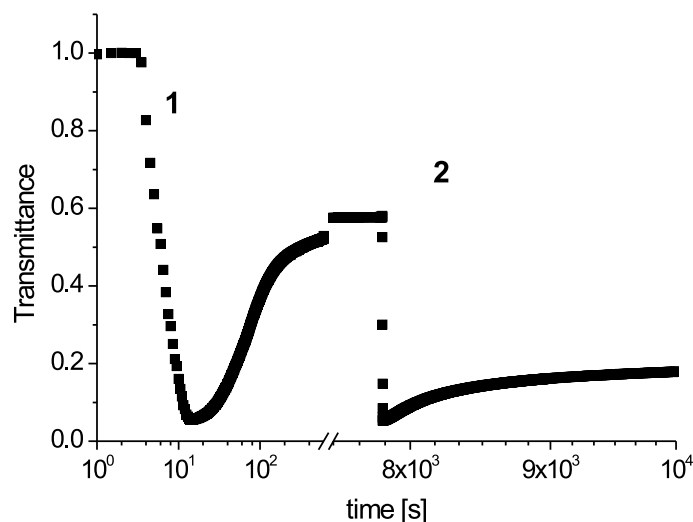


Fig. 6.1: Turbidimetric measurement of the complexation of  $PIB_{75}$ - $b$ - $PMAA_{1600}$  with addition P4VPQ to obtain  $Z = 0.4$  (1) and  $Z = 0.5$  (2) at  $c_{TRIS} = 0.01$  M,  $c_{NaCl} = 0.1$  M.

increase in transmittance could be observed, reaching a plateau at  $T = 0.57$  after 120 min.

The observed increase of turbidity (decrease in transmittance) on addition of P4VPQ into an aqueous solution of  $PIB_{75}$ - $b$ - $PMAA_{1600}$  micelles (Figure 6.1, the first drop) points to generation of large species with considerably larger mass (and

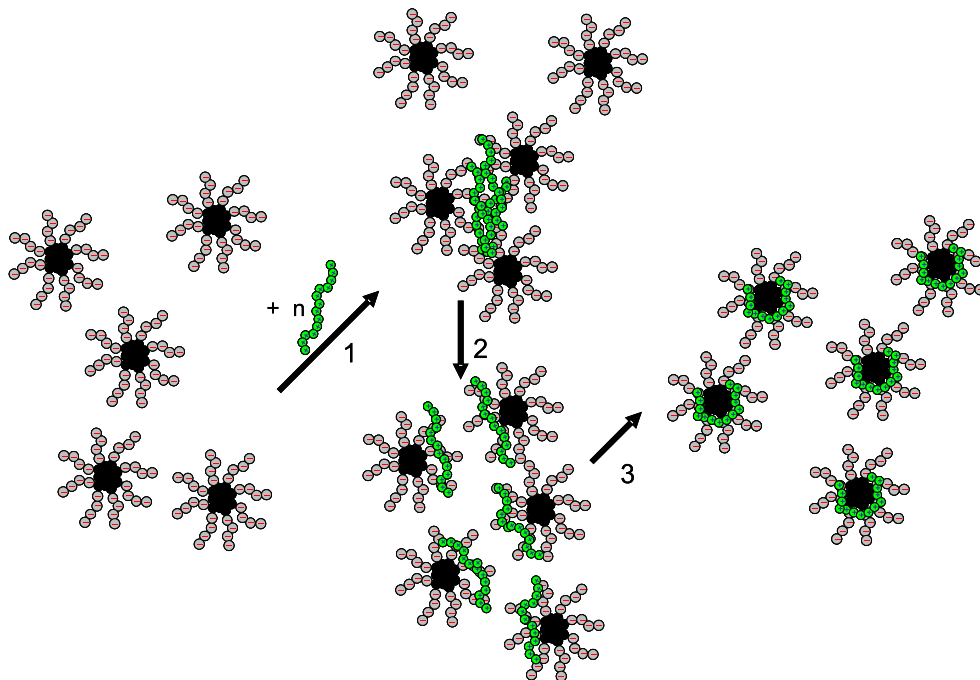


Fig. 6.2: Proposed mechanism of formation of IPECs of spherical negatively charged polyelectrolyte micelles with cationic polyelectrolyte. The use of five micelles is just arbitrarily and should just represent a part of the solution. The polycation added is also not represented quantitatively.

size) compared to the pure micelles, shown as a sketch in Figure 6.2 (Step 1). They might be formed as non-equilibrium structures due to non-ideal mixing resulting in the formation of multimicellar aggregates comprising  $\text{PIB}_{75}\text{-}b\text{-PMAA}_{1600}$  micelles bound each other through macromolecules of the cationic polyelectrolyte.

The following increase in transmittance (decrease in turbidity) reaching a plateau value of  $T = 0.55$  after 10 min indicates that the formed large species become smaller. This effect can be explained by disaggregation of these large species proceeding via so called polyion exchange reactions, that is, these multimicellar aggregates interacting with free  $\text{PIB}_{75}\text{-}b\text{-PMAA}_{1600}$  micelles present in the solution in an excess gradually split into smaller aggregates (Figure 6.2, Step 2). Such a rearrangement finally leading to the formation of equilibrium complex species from non-equilibrium large aggregates generated right away upon mixing aqueous solutions of the oppositely charged linear polyelectrolytes was previously described by Bakeev *et al.* [31].

At the same time, chains of P4VPQ bound at first to peripheral (outmost) parts of micellar corona of each  $\text{PIB}_{75}\text{-}b\text{-PMAA}_{1600}$  micelle are assumed then to penetrate deeper inside to be eventually located at the core-corona interface (Figure 6.2, Step 3). The reason for that is hydrophobic nature of the product of the interpolyelectrolyte complexation because of the charge neutralization. This favors the minimization of the interface toward the aqueous phase. This results in increasing

negative charge of the peripheral (outmost) parts of micellar coronas, leading, in turn, to separation of complex assemblies due to electrostatic repulsion and providing their stability in aqueous media.

To further complex the remaining charges up to  $Z = 0.5$ , another 0.3 ml of polycation was added, leading to a second decrease in transmittance down to  $T = 0.05$ . This mixture was also stirred to let the complexes relax to obtain equilibrium structures. This time a plateau value of  $T = 0.18$  was reached after 30 min. After addition of the second amount of P4VPQ a further increase in turbidity can be observed. Here also a complexation and formation of assemblies of complexes followed by rearrangement and decrease of size afterward can be stated. This shows that there are still vacant sites in the corona that can be complexed with the polycation. The increase of transmittance with time is not that pronounced as after addition of the first portion of P4VPQ, showing that there are larger aggregates after reaching the plateau compared to the aggregates after addition of the first portion of P4VPQ. It is remarkable that no precipitation was observed even at  $Z = 0.5$ . However, the size of the micellar complexes is comparable to the size of the precursor micelles as shown below by means of DLS. In this case, lower transmittance (or higher turbidity) means that the aggregates with larger inner dense nuclei (PIB core + complex shell) are generated.

### Cryo-TEM

For all investigations complexes were formed as described in the experimental part. The complex solutions were still transparent. It has to be pointed out that CsOH and CsCl were added to stain PMAA blocks forming coronae of the PIB-*b*-PMAA micelles, making them visible. Though the affinity of Cs<sup>+</sup> to PMAA is known to be lower than the affinity of Na<sup>+</sup> to PMAA, the results discussed in this paper do not change on the qualitative level.

Cryo-TEM images show micelles (Figure 6.3) and complexes (Figure 6.4), respectively. The micelles consist of a dark core, containing the water-insoluble PIB [25]. The surrounding slightly dark shade comprises denser parts of the corona consisting of PMACs, resulting in better electron contrast. The larger the distance of the PMACs from the core is, the less dense the corona is and the brighter the region appears in cryo-TEM images. The outer parts of the micelle disappear in the background scattering of the solvent, i.e. water and remaining Cs<sup>+</sup>- and Cl<sup>-</sup>-ions. The same can be seen in the case of the complexes (Figure 6.4). The core is surrounded by a corona of decreasing darkness. It was proposed by Pergushov *et al.* that the complexes in the equilibrium state possess a core-shell-corona structure [20, 21]. With cryo-TEM this cannot be demonstrated directly because the contrast (i.e. electron density) between the complex, core and the CsCl solution is too low. Additionally the scattering noise is overlaying the small differences in scattering

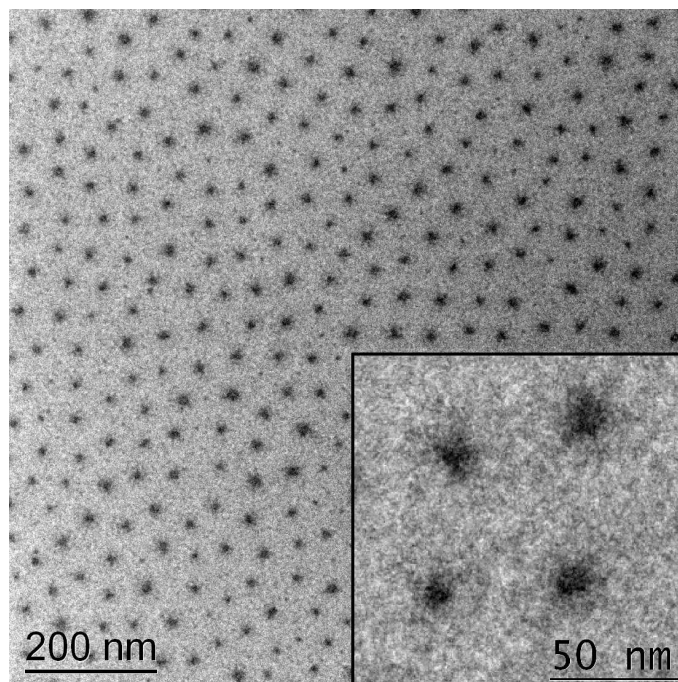


Fig. 6.3: Cryo-TEM image of  $PIB_{30}$ - $b$ - $PMACs_{170}$ ,  $c_{CsCl} = 0.1M$ ,  $CsOH$ ,  $\alpha = 1$ ,  $c_{Pol.} = 0.5$  wt-%.

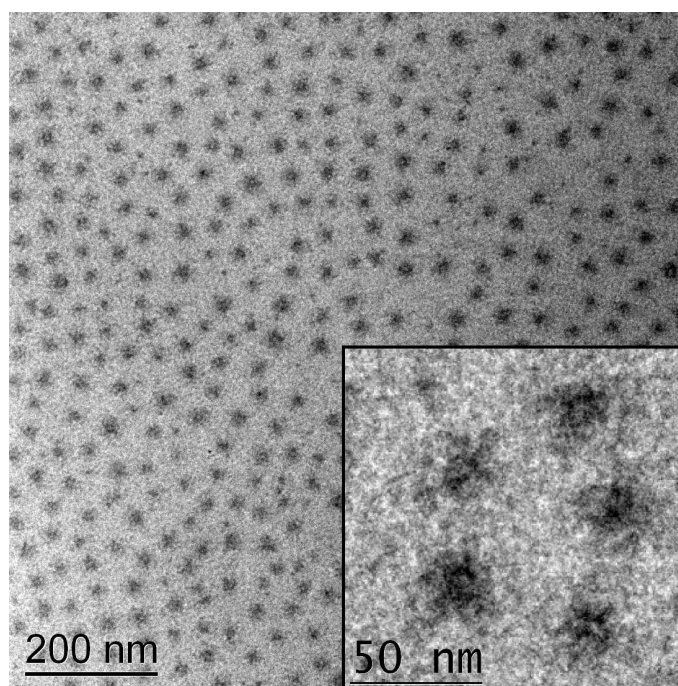


Fig. 6.4: Cryo-TEM image of complex of P4VPQ with  $PIB_{30}$ - $b$ - $PMACs_{170}$  at  $Z = 0.4$ ,  $c_{CsCl} = 0.1M$ ,  $CsOH$ ,  $\alpha = 1$ ,  $c_{Pol.} = 0.5$  wt-%.

power. By increasing the intensity of the electron beam to have a better signal to noise (S/N) ratio, the sample, especially the PIB core, is immediately destroyed by

radiation damage.

If a polycation was complexed in the corona of the micelle, a darker spot in the vicinity of the core should be seen. As no small dark spots in the corona region of the complexes can be found, this is in good agreement with the proposed core-shell-corona structure of such IPECs. Since the charge-neutral complex is hydrophobic, it is trying to decrease the interfacial area toward water. This happens by penetrating the corona of the micellar aggregate and wrapping around the hydrophobic PIB. So the energetically favored region where the complex is situated should be in the vicinity of the core.

The particles are still separated, showing no further aggregation or formation of superstructures. Thus, P4VPQ does not link several micelles resulting in generation of large aggregates. The narrow size distribution shown in the micrograph supports the equilibrium state of the complexes as well. In case of non-equilibrium state larger aggregates of several micelles cross-linked with one P4VPQ chain, resulting in high polydispersity in size, should be observed.

Comparing the cryo-TEM images for the complex and the precursor micelle, some differences can be seen. It has to be emphasized, that the imaging conditions for both images were the same. In the overview, the particles present in the image for complexes are arranged more densely than in the image for the pure micelles. After addition of P4VPQ to the solution of  $PIB$ - $b$ - $PMACs$  micelles, extended  $PMACs$  blocks undergo a certain shrinkage because of charge neutralization.

In the insets of the Figures 6.3 and 6.4, some of the micelles are zoomed. With respect to the darker areas of the inset (hydrophobic parts of the micellar assemblies) slight changes can be observed. For the pure micelles, the dark part is more compact, the change in scattering contrast is well defined. However the hydrophobic part of the complex micelles is less defined and the contrast boundaries are smoother. This is assumed to be due to the P4VPQ- $PMAA$  complex present in the vicinity of the  $PIB$  core. The electron density of the complex is higher than the one of the pure  $PMACs$  chains. Hence they appear as a darker region in the cryo-TEM image. Compared to the  $PIB$  core, they are less dense. Thus, the complex worsens the contrast between the hydrophobic part and the background.

### *Dynamic Light Scattering*

DLS measurements provide apparent hydrodynamic radii,  $R_h$ , of the micellar assemblies. The distribution of the complexed particle sizes is monomodal (Figure 6.5). Compared to the pure micellar solutions of  $PIB_x$ - $b$ - $PMAA_y$  diblock copolymer, the  $R_h$  appears to be slightly smaller, as seen from a shift of the decay curve to shorter times. It has to be pointed out, that all samples prepared for DLS were measured several days after the preparation to avoid any effects related to the kinetically driven formation of larger aggregates at the early stage of complex preparation.

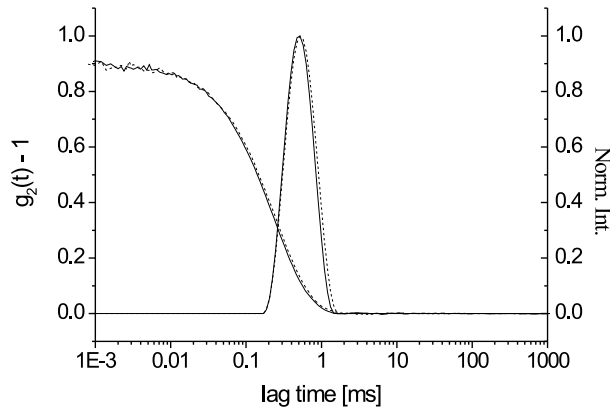


Fig. 6.5: Intensity autocorrelation function and CONTIN-plot of micellar solution (dashed) and IPEC with P4VPQ at  $Z = 0.4$  (solid) of  $PIB_{30}$ - $b$ - $PMANa_{170}$ ,  $c_{TRIS} = 0.01$  M,  $\alpha = 1$  with  $c_{NaCl} = 0.1$  M,  $\Theta = 90^\circ$ .

$\overline{DP}_n, PIB$	$\overline{DP}_n, PMANa$	$R_h, Micelle$ [nm]	$R_h, IPEC$ [nm]	$\frac{R_{IPEC}}{R_{Mic.}}$
20	100	22.5	19	0.80
20	280	37	29	0.78
20	425	46.5	33	0.71
30	170	40	38	0.95
30	190	41	39	0.95
75	190	42	40	0.95
75	615	88	71	0.81
75	1600	101.5	81	0.79

Tab. 6.2: Apparent hydrodynamic radii ( $R_h$ ) of  $PIB_x$ - $b$ - $PMANa_y$  micelles and their IPECs prepared at  $Z = 0.4$ , scattering angle  $\Theta = 90^\circ$ , RT,  $c_{NaCl} = 0.1$  M,  $c_{TRIS} = 0.01$  M obtained from DLS measurements at  $\alpha = 1$ .

In Table 6.2 values for  $R_{h,IPEC}/R_{h,Micelle}$  deduced from apparent hydrodynamic radii from DLS measurements are given. They show that the hydrodynamic radii of the micellar assemblies decrease but not significantly compared to those of the precursor micelles (not more than for 20%). The obvious reason for this is complexation of the PMANa chains with P4VPQ leading to a decrease of the number of free negative charges, and therefore to an effective shortening of the PMANa arms due to the fact, that 40 % of it are compacted into the complex shell. Hence they can arrange in a denser way, resulting to less extended micellar corona.

## Small Angle Neutron Scattering

SANS measurements are also suited to follow the complexation of  $\text{PIB}_x\text{-}b\text{-PMAA}_y$  with P4VPQ. The increase of  $M_w$  of the micelle due to complex formation results in higher scattering intensity at low  $q$ -values (Guinier region).

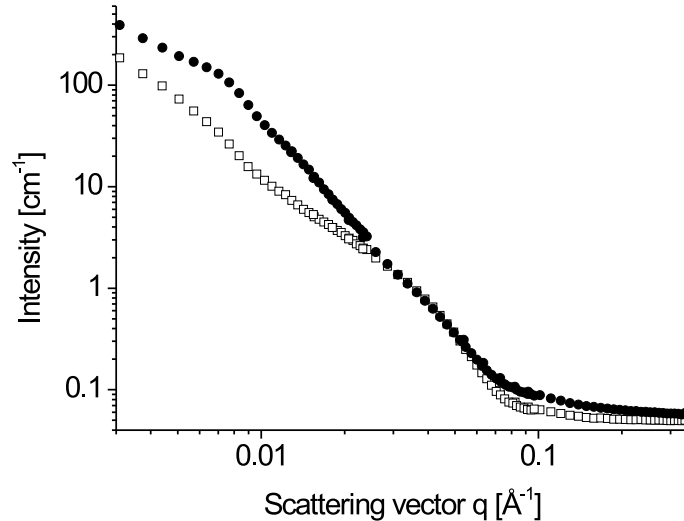


Fig. 6.6: SANS-curves of  $\text{PIB}_{75}\text{-}b\text{-PMANa}_{615}$  micelles ( $\square$ ) and their IPECs prepared at  $Z = 0.4$  ( $\bullet$ ),  $c_{\text{TRIS}} = 0.01\text{M}$ ,  $\alpha = 1$ ,  $c_{\text{NaCl}} = 0.1\text{M}$ .

In Figure 6.6 the micellar and complexed state of  $\text{PIB}_{75}\text{-}b\text{-PMANa}_{615}$  in higher  $q$ -region, representing the core of the micelle, show almost the same shape. Only at lower  $q$ -values, i.e. larger dimensions, an increase in scattering intensity can be observed. This is a clear sign for higher  $M_w$  of the micelle after interacting with P4VPQ, proving complexation of the positively charged P4VPQ with the carboxylic groups of the PMAA. This is similarly observed for the other samples.

The increase of the scattering intensity can also be seen upon increasing content of the cationic polyelectrolyte by stepwise addition to the micellar solutions (Figure 6.7). The more P4VPQ is added, the higher is the total scattering intensity. Again, in the higher  $q$ -region, the change of the curves is not that pronounced, showing almost no effect of complexation on the core of the micelle. When plotting the scattering intensity at the peak maximum ( $q = 0.0136 \text{ \AA}^{-1}$ ) against the  $Z$ -value, a linear dependence is observed (inset in Figure 6.7). Additionally, the position of the peak maximum does not change. This is a clear indication that the number density of complex micelles stays constant. Hence the aggregation number remains unchanged, even if  $Z$  changes from 0 up to 0.4.

In our previous work [25] we reported on the dynamic behavior of the micelles formed by the  $\text{PIB}_x\text{-}b\text{-PMAA}_y$  copolymer in aqueous solutions, i.e. the aggregation number,  $\overline{N_{agg}}$  was found to be sensitive to variations of external stimuli. In Figure 6.8 similar experiments were carried out for IPECs formed by  $\text{PIB}_{30}\text{-}b\text{-PMAA}_{190}$ ,

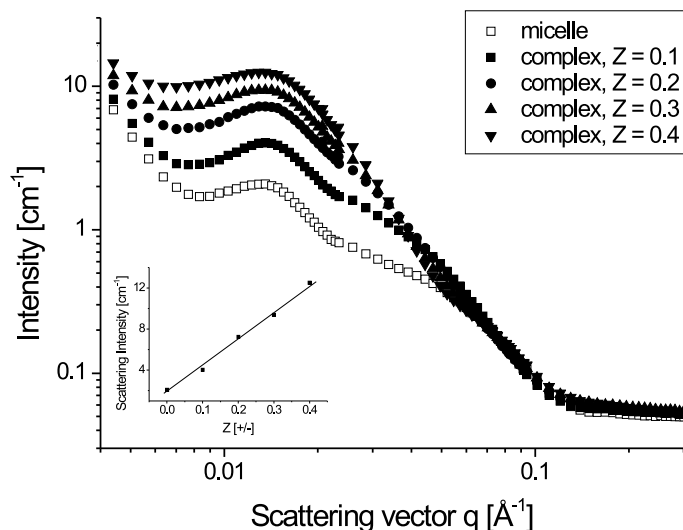


Fig. 6.7: SANS-curves of  $PIB_{20}$ - $b$ - $PMANa_{100}$  micelles,  $\alpha = 1.0$ , ( $\square$ ) and of their IPECs prepared at (from bottom to top)  $Z = 0.1, 0.2, 0.3$  and  $0.4$ ,  $c_{TRIS} = 0.01M$ ,  $c_{NaCl} = 0.1 M$ . Inset: Dependence of scattering intensity at  $q = 0.0136 \text{ \AA}^{-1}$  on  $Z$ .

complexed with P4VPQ,  $Z = 0.4$  at  $c_{NaCl} = 0.1 M$ . In these experiments, the

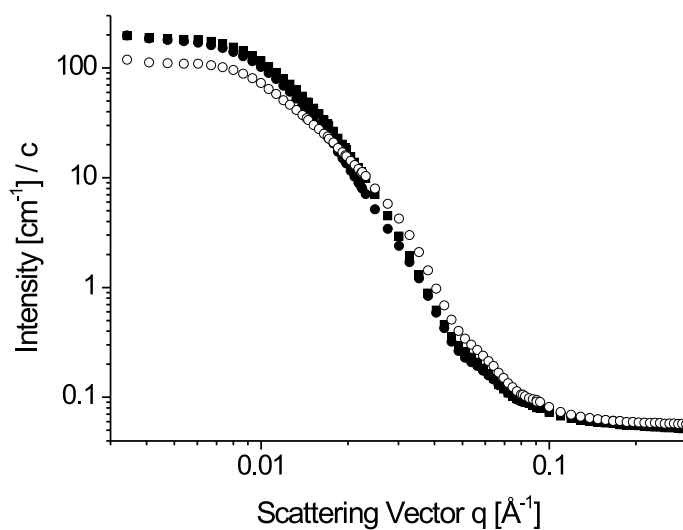


Fig. 6.8: SANS-curves of  $PIB_{30}$ - $b$ - $PMANa_{190}$  micellar solutions complexed with P4VPQ,  $Z = 0.4$ ,  $c_{NaCl} = 0.1 M$ , directly prepared at pH 10 ( $\circ$ ) and pH 7 (black square) and a sample prepared at pH 11.5 and brought to pH 7 ( $\bullet$ ).

scattering curves obtained from complex solutions directly prepared at pH 10 and 7, respectively, were compared to the scattering coming from a solution prepared at pH 11.5 and - after some days of equilibration, brought to pH 7. From Figure 6.8 it can be clearly seen that the scattering behavior for the two samples at pH 7, which were prepared in a different way, coincides. The most important point is that

the scattering curves in the range where the scattering coming from the PIB core is monitored superimpose. Thus it can be concluded that the core size of the two differently prepared samples is similar, whereas the scattering curve for the sample at pH 10 is clearly different.

## 6.3.2 Salt-Induced Dissociation of Complexes

## Small Angle Neutron Scattering

An interesting aspect of the complexes is their ability to respond on external stimuli, namely changes in ionic strength. In this work, we increased the ionic strength of our complex solutions up to  $c_{NaCl} = 0.6$  M. In Figure 6.9 SANS curves of samples with a selection of different salt contents are shown. The complexes consists of  $PIB_{20}$ - $b$ - $PMAA_{100}$  micelles and P4VPQ with a  $\overline{DP}_w$  of 500. The  $Z$ -value is set to 0.4, meaning that 40% of the negative charges on the PMAA chains are complexed. The salt concentration is increased from 0.1 M to 0.6 M NaCl (full symbols). The

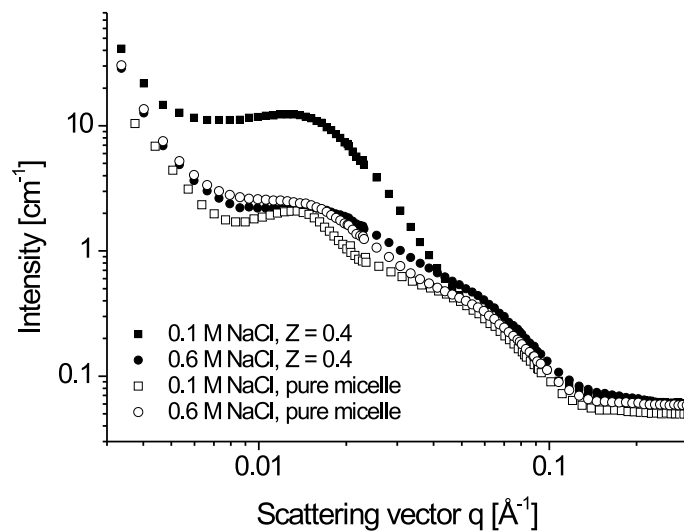


Fig. 6.9: Dissociation of complex formed by  $PIB_{20}$ - $b$ - $PMAA_{100}$  with P4VPQ,  $Z = 0.4$ ,  $c_{TRIS} = 0.01$  M. The SANS scattering curves represent (from top to bottom, full symbols)  $c_{NaCl} = 0.1$  M and 0.6 M. The open symbols represent (from top to bottom) the scattering curves obtained by micellar solutions of  $PIB_{20}$ - $b$ - $PMAA_{100}$ ,  $c_{NaCl} = 0.1$  M and 0.6 M,  $c_{TRIS} = 0.01$  M.

scattering curves represented by the open symbols correspond to solutions of the pure  $PIB_{20}$ - $b$ - $PMAA_{100}$  micelles at 0.1 M NaCl (open squares) and 0.6 M NaCl (open circles), respectively.

The most important change of the curves is the decrease of the scattering intensity in the intermediate  $q$ -range ( $0.01 - 0.03 \text{ \AA}^{-1}$ ). This correlation peak can be attributed to interactions between complexes. The decrease in scattering intensity can be seen in the low  $q$  region. As the scattering intensity is directly proportional to the molecular weight of the scattering particle, the  $\overline{M}_w$  of the complexes apparently decreases. The contribution of the free P4VPQ can be neglected to a first approximation, as the scattering intensity is far below the scattering coming from the pure micelles.

Another indication on changes in the superstructure is the slight shift of the peak maximum of the correlation peak in Figure 6.9. The movement from  $q = 0.0135 \text{ \AA}^{-1}$  (0.1 M NaCl) to  $q = 0.0105 \text{ \AA}^{-1}$  (0.3 M NaCl, not shown here) back to  $q = 0.0132 \text{ \AA}^{-1}$  represents a change in distance of the scattering centers from 46.5 nm to 59.8 nm and 48.6 nm, respectively. Thus, the average distance between the scattering centers increases slightly, seen by a shift of the correlation peak.

Gohy *et al.* [17] also reported on water-soluble complexes formed by sodium poly(4-styrenesulfonate) (PSS) and poly(2-vinylpyridinium)-*block*-poly(ethylene oxide) (P2VP-*b*-PEO). They observed monodisperse spherical micelles, their stability depending on the pH and ionic strength. The complexes dissociate above a critical salt concentration, seen by a decrease in scattering intensity of the solutions. Thus they conclude that the micelles with the complex core are dissolved. Kabanov *et al.* [32] reported on changes of structures of complexes consisting of poly(acrylic acid) (PAA) and poly(ethylene imine) (PEI) with increasing salt concentration. They investigated their behavior in aqueous media with low ionic strength as well as in intermediate region. Here they observed a rearrangement of the charged chains. The dissociation of the complex was reported to occur at high salt concentrations, resulting in separated polyelectrolytes.

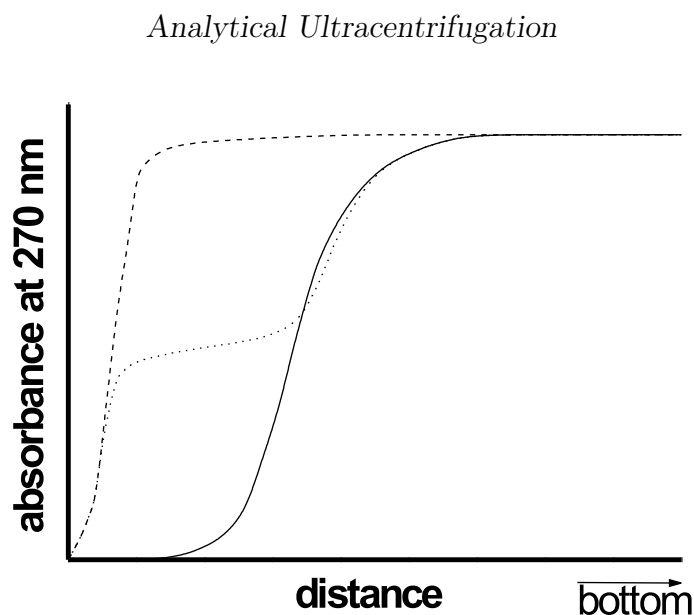


Fig. 6.10: Typical sedimentation patterns (scan mode, detection at  $\lambda = 270 \text{ nm}$ ) for the aqueous mixtures of complexes of  $PIB_{20}$ - $b$ - $PMAA_{100}$  micelles and P4VPQ at  $Z = 0.4$  obtained at  $c_{NaCl} = 0.1 \text{ M}$  (line) and  $0.4 \text{ M}$  NaCl (dotted),  $c_{TRIS} = 0.01 \text{ M}$  and pure P4VPQ (dashed).

Figure 6.10 shows typical sedimentation patterns obtained in the scan mode for solutions of IPECs based on  $PIB_{20}$ - $b$ - $PMAA_{100}$  micelles at relatively low (line) and

high (dotted) concentration of NaCl, i.e. at 0.1 and 0.4 M NaCl, respectively. As is seen, only one type of the sedimenting particles (one step in Figure 6.10) with sedimentation coefficient ( $S \approx 25$  Sv) considerably exceeding that of the free cationic macromolecules ( $S \approx 1.5 - 2$  Sv; sedimentation pattern is given in Figure 6.10 by a dashed line) is observed at 0.1 M NaCl. These species sedimenting with rather high sedimentation velocity represent particles of micellar interpolyelectrolyte complex. At the same time, two types of sedimenting particles (two steps in Figure 6.10, dotted) with pronouncedly different sedimentation coefficients of ca. 1.5 and ca. 23 Sv are clearly detected at 0.4 M NaCl. The species with low sedimentation coefficient are assigned to free cationic macromolecules while those with high sedimentation coefficient are considered to be particles of micellar interpolyelectrolyte complex. At relatively high concentrations of NaCl, therefore, free cationic macromolecules appear to release from the complex species, thus coexisting with them. The relative height of the first step in the sedimentation pattern shown in Figure 6.10 represents a fraction  $f$  of free cationic macromolecules. They behave similarly as the complexes of poly(methacrylic acid) and P4VPQ, reported by Pergushov *et al.* [33].

The stoichiometry of the complex species  $\varphi$  defined as a ratio of the pyridinium groups to carboxylate groups incorporated in the IPEC can be calculated according to equation 1:

$$\varphi = Z \cdot (1 - f). \quad (6.1)$$

Figure 6.11 demonstrates the dependence of  $\varphi$  on the concentration of NaCl in the

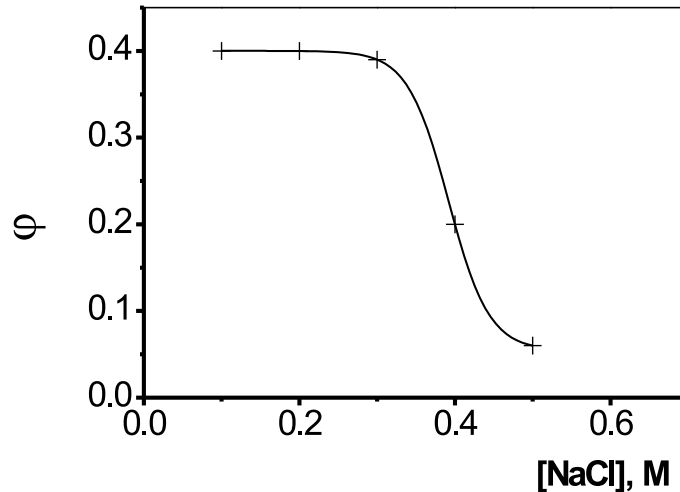


Fig. 6.11: Dependence of the stoichiometry of IPEC species of  $PIB_{20}$ - $b$ - $PMAA_{100}$  at  $Z = 0.4$  on the concentration of NaCl;  $c_{TRIS} = 0.01$  M.

aqueous mixtures of  $PIB_{20}$ - $b$ - $PMAA_{100}$  micelles and P4VPQ. For  $c_{NaCl} < 0.3$  M, the values of  $\varphi$  remain constant and coincide with  $Z$  while for  $c_{NaCl} \geq 0.3$  M,  $\varphi$  gradually decreases with increasing ionic strength, approaching finally a value of  $\varphi \sim 0$  at  $c_{NaCl} \approx 0.6$  M. This finding undoubtedly indicates that IPECs undergo

complete dissociation to their polymeric constituents, that is,  $\text{PIB}_{20}\text{-}b\text{-PMAA}_{100}$  micelles and P4VPQ, at relatively high ionic strength. The obvious reason for that is the effective screening of the electrostatic interaction between PMAA blocks and P4VPQ chains by small ions, which increase the relative solubility of the P4VPQ in the solvent.

### Titration

The dissociation of the complex can also be seen from potentiometric titrations of complexes with NaCl solutions. The activity of the  $\text{Na}^+$  ions was monitored with a  $\text{Na}^+$ -selective electrode. Relative to the background curve (pure NaCl) an increase of the signal can be observed (not shown here). However, in the intermediate range at a salt concentration of 0.5 M NaCl a small bump can be detected. This is obvious in Figure 6.12. Here, a curve representing a difference between the complex solution

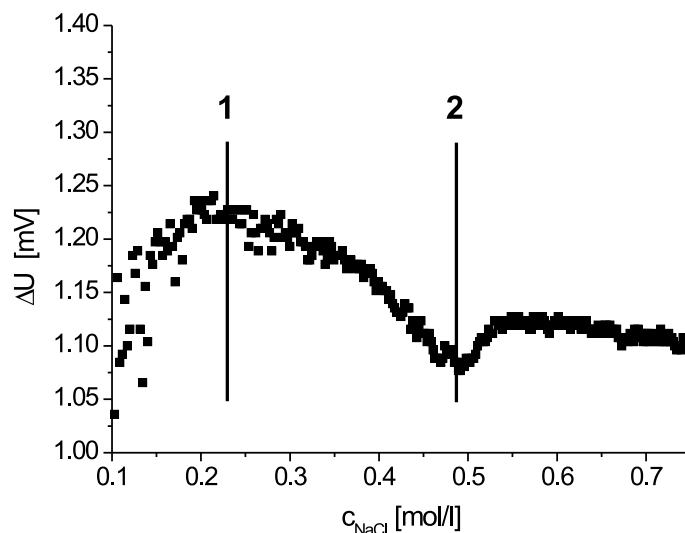


Fig. 6.12: Difference of potentiometric titration (voltage U) curves of mixtures of  $\text{PIB}_{75}\text{-}b\text{-PMAA}_{1600}$  and P4VPQ ( $Z = 0.4$ ) depending on the concentration of NaCl with sodium-selective electrode. A relative maximum (1) and a minimum (2) of the difference is observed.

and the background is depicted. The main reason that the complex shows a higher activity compared to the background solution is the fact that NaCl is produced during the neutralization of the polyacid. The amount of the NaCl is around  $n_{\text{NaCl}} = 2.3 \cdot 10^{-4}$  mol. In the graph shown, two distinct regions can be stated. The first maximum in the relative response occurs at a salt concentration of 0.23 M. Starting from this point, the slope of the titration curve of the complex is smaller than the slope of the background measurement. This results in a decrease of the differential signal seen in the graph.

This phenomenon can be explained by the activity of  $\text{Na}^+$  ions in both solutions.

The rate of addition of the brine solution was the same in both cases. Hence the overall amount of  $Na^+$ -ions in the solution is the same. The only difference is their contribution to the activity. In the reference solution, all sodium ions are measured. In case of the complex, at the beginning of the titration, all sodium ions contribute to the activity of the solution. Starting from a certain point (1), the complex slowly starts dissociating upon addition of further salt. Thus the additional negative charges of the PMAA chains are able to condense  $Na^+$  ions. Once trapped by the micellar corona, the sodium ions do not contribute to the  $Na^+$  activity in the solution any more. Hence, compared to the background measurement, the relative activity of the sodium ions decreases.

$PIB_x$ - $b$ - $PMAA_y$	Titration	Titration	SANS	SANS
	Start Diss.	End Diss.	Start Diss.	End Diss.
	$c_{NaCl}$ [M]	$c_{NaCl}$ [M]	$c_{NaCl}$ [M]	$c_{NaCl}$ [M]
75-1600	0.23	0.49	-	-
75-615	0.30	0.50	-	-
25-325	0.27	0.50	-	-
30-190	-	0.49	-	-
20-100	-	-	> 0.2; < 0.3	> 0.4; $\approx$ 0.5

Tab. 6.3: Comparison of the different stages of the dissociation process of the complex formed by different  $PIB_x$ - $b$ - $PMAA_y$  diblock copolymers by means of SANS and potentiometric titration.

This effect remains until a minimum of the curve (2) is reached. Starting from this point, the curve slightly increases until a plateau is reached. The minimum at a salt concentration of  $c_{NaCl} = 0.49$  M can be explained by the end of dissociation of the complex. Any further  $Na^+$  ion added to the solution of the complex now contributes to the activity of the solution in the same way as for the background solution. The slight increase of the curve is related to the fact that the  $PIB_x$ - $b$ - $PMAA_y$  micelles also react on changes in ionic strength of the solvent [25]. The increased screening effect of the charges along the PMAA chains due to Manning condensation enable the arms to arrange more densely. Therefore, solvent containing also sodium ions is expelled from the corona. Hence the  $Na^+$  ions are again detectable by the Na-selective electrode and contribute to the activity of the solution. The same behavior can be observed for all measured complexes (Figure 6.13).

The values obtained by titration nicely agree with the results obtained from SANS data (Figure 6.9). In Table 6.3 a comparison of the starting points and the end of the dissociation process of the complexes are shown. From SANS data a start of dissociation above a salt concentration of beyond 0.2 M can be observed as well.

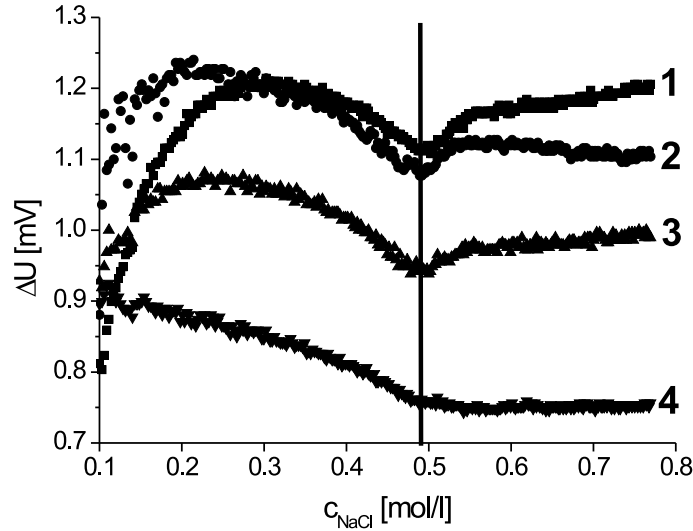


Fig. 6.13: Difference of titration curves with sodium-selective electrode for complexes formed with  $\text{PIB}_{75}\text{-}b\text{-PMAA}_{615}$  (1),  $\text{PIB}_{75}\text{-}b\text{-PMAA}_{1600}$  (2),  $\text{PIB}_{25}\text{-}b\text{-PMAA}_{325}$  (3) and  $\text{PIB}_{30}\text{-}b\text{-PMAA}_{190}$  (4),  $Z = 0.4$ .

Above a salt concentration of 0.5 M no noticeable change in the scattering behavior can be observed. This is another indication that the dissociation of the complexes takes place between 0.2 and 0.5 M salt content of the complex solution.

As already reported by Kabanov *et al.* [32], the driving force for the formation of complexes is the release of counterions of the polyelectrolyte species. This leads to an increase in entropy of the whole system. In complex particles, the counterions are replaced by an oppositely charged polyelectrolyte. The released counterions are contributing to the activity of the ions present in the solution. During the process of dissociation of the complex, the counterions, according to Manning [34], should be partially condensed on the polyelectrolyte chains. For polyelectrolyte brushes and stars, the fraction of condensed counterions has been found to be  $> 90\%$  [35, 36].

## 6.4 Conclusion

In this paper a detailed investigation of the formation, structure and dissociation of IPECs formed by  $\text{PIB}_x\text{-}b\text{-PMAA}_y$  with P4VPQ is presented.  $\text{PIB}_x\text{-}b\text{-PMAA}_y$  diblock copolymers with a large variation of  $\overline{DP}_n$  of both hydrophobic PIB and hydrophilic PMAA blocks are used to form water soluble complexes with core-shell-corona structure. From cryo-TEM images, a spherical shape of the IPECs can be concluded.

The process of formation of complexes can be subdivided in a kinetically driven and a thermodynamically driven process. Upon addition of the polycation solution to the micellar  $\text{PIB}_x\text{-}b\text{-PMAA}_y$  solution, first an increase in turbidity of the solution

can be observed. In this kinetically driven regime, large assemblies of micelles are formed. With time, these aggregates are equilibrating toward the thermodynamically more stable species of a single micelle with a complex shell formed around the hydrophobic PIB core. The formation process can also be seen by means of SANS, leading to higher scattering intensity with increasing  $Z$ . By means of SANS it was shown, that the complexes formed remain dynamic with respect to external stimuli as pH-jumps, as already reported for the pure micellar system [25].

SANS was also used to follow the salt-induced dissociation of the complex. Increasing the ionic strength of the IPEC solution leads to a release of the polycation, starting from about 0.2 M NaCl. Beyond 0.5 M NaCl, almost no difference in scattering behavior of the IPEC solution compared to pure micellar solution can be stated. This strongly suggests a total dissociation of the IPEC. By means of titration with a sodium selective electrode, the decrease of the activity of the Na<sup>+</sup> ions can be explained by substitution of the polycation due to Manning condensation. After complete dissociation of the IPEC, the activity of the IPEC solution, upon addition of further NaCl, follows the behavior of a background solution.

Comparing different techniques, a starting point of the complex dissociation at an ionic strength of about 0.2 M can be concluded. Independent on the block lengths of both PIB and PMAA the IPEC is completely dissociated at  $c_{NaCl} \sim 0.5$  M.

### *Acknowledgment*

This work was supported by the European Union within the Marie Curie RTN Polyamphi and by DFG within the ESF EUROCORES Programme SONS. ILL is gratefully acknowledged for providing SANS beam time and travel support. D. V. P. thanks DFG for the financial support of his research stays at the Universität Bayreuth.

## BIBLIOGRAPHY

- [1] Förster, S.; Abetz, V.; Müller, A.H.E.; *Adv. Polym. Sci.*, **2004**, *166*, 173;
- [2] Thünemann, A.F.; Müller, M.; Dautzenberg, H.; Joanny, J.-F.; Löwen, H.; *Adv. Pol. Sci.*, **2004**, *166*, 113;
- [3] Babak, V.G.; Merkovich, E.A.; Desbrieres, J.; Rinaudo, M.; *Pol. Bull.*, **2000**, *45*, 77;
- [4] Konradi, R.; Rühle, J.; *Macromolecules*, **2005**, *38*, 6140;
- [5] Matsudo, T.; Ogawa, K.; Kokufuta, E.; *Biomacromolecules*, **2003**, *4*, 1794;
- [6] Gossl, I.; Shu, L.; Schlüter, A.D.; Rabe, J.P.; *J. Am. Chem. Soc.*, **2002**, *124*, 6860;
- [7] Sonoda, T.; Niidome, T.; Katayama, Y.; *Recent Research Developments in Bioconjugate Chemistry*, **2005**, *2*, 145;
- [8] Smid, J.; Fish, D.; In: H.F. Mark, N.M. Bikales, C.G. Overberger, G. Menges; *Encyclopedia of polymer science and engineering*, Vol. 11; New York; Wiley; **1988**, 720;
- [9] Philipp, B.; Dautzenberg, H.; Linow, K.-J.; Koetz, J.; Dawydoff, W.; *Prog. Polym. Sci.*; **1989**, *14*, 91;
- [10] Harada, A.; Kataoka, K.; *Macromolecules*, **1995**, *28*, 5294;
- [11] Kataoka, K.; Togawa, H.; Harada, A.; Yasugi, K.; Matsumoto, T.; Katayose, S.; *Macromolecules*, **1996**, *29*, 8556;
- [12] Kabanov, A.V.; Bronich, T.K.; Kabanov, V.A.; Yu, K.; Eisenberg, A.; *Macromolecules*, **1996**, *29*, 288;
- [13] Harada, A.; Kataoka, K.; *Macromolecules*, **1998**, *31*, 6140;
- [14] Cohen Stuart, M.A.; Besseling, N.A.M.; Fokink, R.G.; *Langmuir*, **1998**, *14*, 6846;
- [15] Harada, A.; Kataoka, K. ; *Langmuir*, **1999**, *15*, 4208;

- 
- [16] Bronich, T.K.; Nguen, H.K.; Eisenberg, A.; Kabanov, A.V.; *J. Am. Chem. Soc.*, **2000**, *122*, 8339;
- [17] Gohy, J.-F.; Varshney, S.K.; Antoun, S.; Jerome, R.; *Macromolecules*, **2000**, *33*, 9298;
- [18] Talingting, M.R.; Voigt, U.; Munk, P.; Webber, S.E.; *Macromolecules*, **2000**, *33*, 9612;
- [19] Gohy, J.-F.; Varshney, S.K.; Jerome, R.; *Macromolecules*, **2001**, *34*, 2745;
- [20] Pergushov, D.V.; Remizova, E.V.; Feldthusen, J.; Zezin, A.B.; Müller, A.H.E.; Kabanov, V.A.; *J. Phys. Chem. B*, **2003**, *107*, 8093;
- [21] Pergushov, D.V.; Remizova, E.V.; Feldthusen, J.; Gradzielski, M.; Lindner, P.; Zezin, A.B.; Müller, A.H.E.; Kabanov, V.A.; *Polymer*, **2004**, *45*, 367;
- [22] Pergushov, D.V.; Gradzielski, M.; Burkhardt, M.; Remizova, E.V.; Zezin, A.B.; Kabanov, V.A.; Müller, A.H.E.; *Pol. Prepr.*, **2004**, *45*, 236;
- [23] Martinez-Castro, N.; Lanzendörfer, M.G.; Müller, A.H.E.; Cho, J.C.; Acar, M.H.; Faust, R.; *Macromolecules*, **2003**, *36*, 6985;
- [24] Lysenko, E.A.; Chelushkin, P.S.; Bronich, T.K.; Eisenberg, A.; Kabanov, V.A.; Kabanov, A.V.; *J Phys Chem B*; **2004**, *108*, 12352;
- [25] Burkhardt, M.; Martinez-Castro, N.; Tea, S.; Drechsler, M.; Babin, I.; Grishagin, I.; Schweins, R.; Pergushov, D.V.; Gradzielski, M.; Zezin, A.B.; Müller, A.H.E.; submitted to *Langmuir*;
- [26] Feldthusen, J.; Ivan, B.; Müller, A.H.E.; *Macromolecules*, **1998**, *31*, 578;
- [27] Adrian, M.; Dubochet, J.; Lepault, J.; McDowall, A.W.; *Nature*, **1984**, *308*, 32;
- [28] Jacrot, B.; Zacchai, G.; *Biopolymers*, **1981**, *20*, 2413;
- [29] Chen, S.-H.; Lin, T.-L.; *Methods of Experimental Physics*, **1987**, Academic Press, 489;
- [30] GRAS<sub>ans</sub>P; Charles Dewhurst; email: dewhurst@ill.fr; Institut Laue Langevin, Grenoble, France;
- [31] Bakeev, K.N.; Izumrudov, V.A.; Kuchanov, S.I.; Zezin, A.B.; Kabanov, V.A.; *Macromolecules*; **1992**, *25*, 4249;
- [32] Kabanov, V.A.; Zezin, A.B.; *Pure Appl. Chem*; **1984**, *56*, 343;

- 
- [33] Pergushov, D.V.; Izumrudov, V.A.; Zezin, A.B.; Kabanov, V.A.; *Pol. Sci. A*; **1995**, *37*, 1081;
- [34] Ray, J.; Manning, G.S.; *Macromolecules*; **1999**, *32*, 4588;
- [35] Das, B.; Guo, X.; Ballauff, M.; *Prog. Colloid Polym. Sci.*; **2002**, *121*, 34;
- [36] Plamper, F.A.; Schmalz, A.; Penott-Chang, E.; Drechsler, M.; Jusufi, A.; Ballauff, M.; Müller, A.H.E.; *Macromolecules*; submitted;

## 7. SOLUTIONS OF PIB-*B*-PAA: FORMATION OF NON-EQUILIBRIUM ASSEMBLIES

### **Aqueous Solutions of Polyisobutylene-*block*-Poly(acrylic acid) Diblock Copolymers: Path Dependent Formation of Non-Equilibrium Assemblies**

Markus Burkhardt<sup>1</sup>, Roland Walker<sup>1</sup>, Markus Drechsler<sup>1</sup>, Ralf Schweins<sup>2</sup>, Dmitry Pergushov<sup>3</sup>, Alexander B. Zezin<sup>3</sup>, Michael Gradzielski<sup>4</sup>, Axel H.E. Müller<sup>1</sup>

<sup>1</sup>*Makromolekulare Chemie II, Universität Bayreuth, D-95440 Bayreuth, Germany;*

<sup>2</sup>*Institut Laue-Langevin, 38042 Grenoble Cedex 9, France;*

<sup>3</sup>*Department of Polymer Science, School of Chemistry, Moscow State University, 119991 Moscow, Russia;*

<sup>4</sup>*Stranski Laboratorium für Physikalische und Theoretische Chemie, Institut für Chemie, Technische Universität Berlin, D-10623 Berlin, Germany;*

\* e-mail: axel.mueller@uni-bayreuth.de

Markus Burkhardt: markus.burkhardt@uni-bayreuth.de;

Roland Walker: Roland.Walker@uni-bayreuth.de;

Markus Drechsler: markus.drechsler@uni-bayreuth.de;

Ralf Schweins: schweins@ill.eu;

Dmitry V. Pergushov: pergush@genebee.msu.su;

Michael Gradzielski: michael.gradzielski@tu-berlin.de;

Alexander B. Zezin: zezin@genebee.msu.su;

## Abstract

We report on first results of the micellization of polyisobutylene-*block*-poly(acrylic acid) (PIB-*b*-PAA) diblock copolymer, synthesized via combination of cationic polymerization of isobutylene (IB) and anionic polymerization of *tert*-butyl acrylate (*t*BuA). After hydrolysis of the *t*-butyl protection group, we obtained an amphiphilic diblock copolymer, which is water soluble at room temperature (RT). Upon addition of salt (NaCl) an interesting phenomenon is observed. Related to the point of time of addition of the salt, i.e. before or after dissolution of the polymer, differently sized aggregates are obtained. By means of cryogenic transmission electron microscopy (cryo-TEM), it is revealed, that also the counterion has an effect on the formation of equilibrium structures. Dynamic light scattering (DLS) and small angle neutron scattering (SANS) give an insight into the size and shape of the assemblies formed in aqueous solution for both methods of sample preparation at high pH. Additionally a pronounced effect of the solvent (H<sub>2</sub>O, D<sub>2</sub>O) on the size of the species is revealed by means of SANS and DLS.

**Keywords:** *micelles, amphiphilic, block copolymers, DLS, SANS, cryo-TEM, salt effect*

## 7.1 Introduction

Amphiphilic diblock copolymers with a polyelectrolyte block have attracted increasing scientific interest [1] due to their various fields of application in industry as lubricants [2], emulsifiers, for drug delivery [3], as templates for biomimetic nanostructures or for removal of ionic dyes from water [4]. Within this scope, various diblock copolymers synthesized via the use of different polymerization techniques and even combinations of them were used to obtain well defined polymers. Investigations of solution behavior of the water-soluble diblock copolymers were extended to studies of the stimuli responsiveness on external stimuli, such as changes in ionic strength, pH or temperature in aqueous solutions [1, 8].

Especially, the self-assembling behavior of such copolymers resulting in formation of various macromolecular assemblies (star-like micelles, crew-cut micelles, vesicles) is of interest as tailoring the block length ratio of the hydrophobic and the hydrophilic part of the copolymers can easily lead to their different morphology [5] - [9]. The investigations reported were mostly compared to theories of equilibrium structures [10, 11]. In contrary to that for polystyrene (PS)-containing diblock copolymers in aqueous solutions [12] at room temperature, RT, the hydrophobic part is far below the glass transition temperature,  $T_g$ , and therefore "frozen", i.e. no exchange of unimers between the micelles formed is possible. In the last years, different groups focused on investigations of diblock copolymers with a polymer for the hydrophobic block that has a  $T_g$  below RT. Especially Richter *et al.* investigated the dynamic behavior of diblock copolymer micelles by means of SANS techniques [13, 14]. They report on chain exchange kinetics of poly(ethylene-propylene)-poly(ethylene oxide) (PEP-PEO) micelles in aqueous solutions. In our earlier work, the core was also reported to be able to change the aggregation number,  $\overline{N_{agg}}$ , upon external stimuli as pH change as reported [15]. This phenomenon was also clearly seen for our system containing polyisobutylene (PIB) as hydrophobic block and poly(methacrylic acid) (PMAA) as the hydrophilic part. Colombani *et al.* reported another approach to obtain responsive copolymer micelles [16, 17]. In this work, they investigated poly(*n*-butyl acrylate)-*block*-poly(acrylic acid) (P*n*BA-*b*-PAA) diblock copolymers synthesized via atom transfer radical polymerization (ATRP). The structures formed in aqueous solutions of this system strongly depend on the way of preparation of the solutions, i.e. point of time of addition of salt. For solutions, where NaCl was added after complete dissolution of the diblock copolymer, well defined structures were obtained. In contrast to this, for samples, in which the salt was added before addition of water, larger assemblies were found to exist.

In this work we report on first investigations on a new diblock copolymer, polyisobutylene-*block*-poly(acrylic acid) (PIB<sub>*x*</sub>-*b*-PAA<sub>*y*</sub>) synthesized via combination of cationic polymerization of isobutylene, followed by anionic polymerization of *t*-butyl acrylate as described elsewhere [18, 19]. A special interest in this work was

the effect of way of preparation, i.e. point of time of addition of salt. The samples obtained were investigated by means of DLS, cryo-TEM and SANS.

## 7.2 Experimental Part

### 7.2.1 Materials

Polyisobutylene-*block*-poly(*tert*-butyl acrylate) diblock copolymers (PIB-*b*-PtBA) were synthesized as described before [18, 19]. Therefore a macroinitiator, synthesized by endcapping cationic polymerization of isobutylene (IB) with thiophene (T), was activated with *n*-butyl lithium (BuLi). The *t*BA was polymerized anionically in THF containing LiCl with a concentration of 4 mM. The LiCl stock solution,  $c_{LiCl} = 16$  mM, was prepared from LiCl salt dried in HV at 300 °C for 2 days followed by condensing dried THF into the transfer ampoule. Size exclusion chromatography (SEC) was used to determine the molecular weight distributions of the PIB precursor (measured separately) and PIB-*b*-PtBA using PIB and PtBA standards. For the diblock copolymer, a weighted average of the homo polymer calibration curves was used. SEC was performed using PSS SDV-gel columns (5  $\mu$ m, 60 cm, 1 x linear (10<sup>2</sup> – 10<sup>5</sup> Å), 1 x 100 Å) with THF as eluent at a flow rate of 1.0 ml/min at room temperature using UV ( $\lambda = 230$  and 260 nm) and RI detection. The value of number-average molecular weight,  $\overline{M}_n$ , for PIB and PtBA polymers were determined to be 1740 g/mol ( $\overline{DP}_n = 30$ ) and 54.900 g/mol ( $\overline{DP}_n = 430$ ), respectively. The polydispersity indices,  $\overline{PDI}$ , of PIB and PIB-*b*-PtBA are 1.19 and 1.15, respectively. After hydrolysis of the *t*-butyl groups with hydrochloric acid in dioxane at 80 °C for 24 hours ( $c_{P_{ol.}} = 10$  wt-%) polyisobutylene-*block*-poly(acrylic acid) (PIB<sub>30</sub>-*b*-PAA<sub>430</sub>) was obtained.

### Sample Preparation

To prepare a stock solution of the copolymer, PIB<sub>30</sub>-*b*-PAA<sub>430</sub> was dissolved in aqueous NaOH solution at RT under continuous stirring for at least 24 h. The amount of NaOH was calculated according to the number of COOH-groups of the weighed polymer. In this work, two ways of sample preparation were compared. It has to be pointed out, that the samples were stirred vigorously until the polymer was dissolved completely. For the first method the polymer was dissolved in NaOH directly without addition of buffer or salt. After complete dissolution of the polymer, the ionic strength was adjusted upon addition of NaCl (Merck) and TRIS buffer (2-amino-2-(hydroxymethyl)-1,3-propanediol, Fluka). As the salt is added after dissolution of the polymer, this method will be discussed in the following as "post-dissolution" method (PD). For the second method, the salt was added to the weighed polymer before addition of NaOH solutions. This method, where salt is added before dis-

solution of the polymer, will be discussed in the following as "before dissolution" method (BD). Salt was always added as a powder for both preparation methods. The solutions with added salt all showed low viscosity. Solutions without added NaCl showed higher viscosity, but this was not investigated any further within this work.

### 7.2.2 Methods

#### *Cryogenic Transmission Electron Microscopy (Cryo-TEM) [20]*

For cryo-TEM studies, a drop of the sample ( $c = 0.5$  wt-%) was placed on an untreated bare copper TEM grid (600 mesh, Science Services, München, Germany), where most of the liquid was removed with blotting paper, leaving a thin film stretched over the grid holes. The specimens were shock frozen by rapid immersion into liquid ethane and cooled to approximately 90 K by liquid nitrogen in a temperature controlled freezing unit (Zeiss Cryobox, Zeiss NTS GmbH, Oberkochen, Germany). The temperature was monitored and kept constant in the chamber during all of the sample preparation steps. After freezing the specimens, the remaining ethane was removed using blotting paper. The specimen was inserted into a cryo-transfer holder (CT3500, Gatan, München, Germany) and transferred to a Zeiss EM922 EF-TEM instrument. Examinations were carried out at temperatures around 90 K. The transmission electron microscope was operated at an acceleration voltage of 200 kV. Zero-loss filtered images ( $\Delta E = 0$  eV) were taken under reduced dose conditions (100 - 1000 e/nm<sup>2</sup>). All images were registered digitally by a bottom mounted CCD camera system (Ultrascan 1000, Gatan) combined and processed with a digital imaging processing system (Gatan Digital Micrograph 3.9 for GMS 1.4). For preparation of the samples either NaCl and NaOH or CsOH and CsCl were used.

#### *Dynamic Light Scattering (DLS)*

Sample solutions for DLS experiments were prepared as described above with an amount of the copolymer in the range of  $c_{Pol.} = 0.02$  wt-% for both methods. The prepared sample solutions were thoroughly filtered by passing at least three times through a nylon filter (13-HV, Millipore) with a pore size of 0.45  $\mu\text{m}$ . The DLS measurements were carried out in sealed cylindrical scattering cells ( $d = 10$  mm) at five scattering angles (30°, 60°, 90°, 120° and 150°) with the use of an ALV DLS/SLS-SP 5022F equipment consisting of an ALV-SP 125 laser goniometer, an ALV 5000/E correlator, and a He-Ne laser with the wavelength  $\lambda = 632.8$  nm. The CONTIN algorithm was applied to analyze the obtained correlation functions. Apparent hydrodynamic radii,  $R_h$ , were calculated according to the Stokes-Einstein equation.

### *Small-Angle Neutron Scattering (SANS) [21, 22]*

Sample solutions for SANS experiments were prepared by dissolving PIB<sub>30</sub>-*b*-PAA<sub>430</sub> in D<sub>2</sub>O (Aldrich), containing a desired amount of NaOH (Riedel-de Haën), at RT under continuous stirring overnight. For both methods of sample preparation, as described above, the amount of salt was added either before (BD) or after dissolution of the polymer (PD). The final concentration of the copolymer in the sample solutions was ca. 0.9 - 1 wt-%. In all cases, the prepared solutions were homogeneous, transparent, and of low viscosity. The sample solutions were put into quartz cells with 2 mm path length (Hellma). The degree of neutralization,  $\alpha$ , of the PAA blocks of the copolymers was controlled by the amount of NaOH solution. The ionic strength of the sample solutions was adjusted by adding NaCl (Merck) according to the AD and BD method, respectively. The SANS measurements were performed using the instrument D11 of the Institute Max von Laue-Paul Langevin (ILL, Grenoble, France) with neutron wavelength  $\lambda = 6 \text{ \AA}$ . Sample-to-detector distances of 1.1, 4, and 16 m were employed. With these configurations a total range of the magnitude of the scattering vector,  $q = 0.003 - 0.35 \text{ \AA}^{-1}$  was covered. The detector sensitivity and the intensity of the primary beam were calibrated by a comparison with the scattering from a 1 mm reference sample of water. The obtained data were radially averaged and corrected for the detector background, the detector dead time, and the scattering from an empty cell. They then were converted into absolute units by a comparison with the scattering from water according to standard routines supplied by the ILL [23] using GRASP software. It should be noted that the SANS curves presented in this paper still contain the incoherent background scattering of solvent and sample.

## 7.3 Results and Discussion

As reported in our earlier work [15], PIB<sub>*x*</sub>-*b*-PMAA<sub>*y*</sub> diblock copolymers form well-defined, dynamic spherical micelles in aqueous solutions at high pH, independent of the point of time of addition of salt. The solutions are homogeneous and almost no turbidity can be observed.

### 7.3.1 Cryo-TEM of CsCl-solutions

We prepared solutions from the copolymer investigated in this work, PIB<sub>30</sub>-*b*-PAA<sub>430</sub>, where we added CsCl as salt before (BD) or after (PD) complete dissolution of the polymer. In the cryo-TEM images shown in Figures 7.1 and 7.2 the two samples are depicted. The solutions were examined with the same polymer concentration at  $c \approx 0.5 \text{ wt-%}$ .

In Figure 7.1 an image of a polymer solution prepared according to PD with CsCl

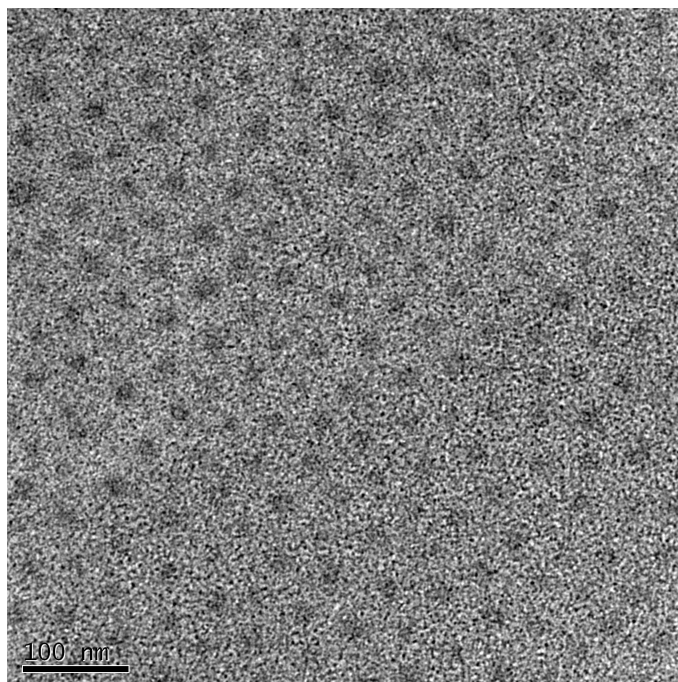


Fig. 7.1: Cryo-TEM image of  $PIB_{30}\text{-}b\text{-}PAA_{430}$ ,  $c_{Pol.} = 0.5$  wt-%,  $\alpha = 1$ ,  $c_{CsCl} = 0.1$  M,  $c_{TRIS} = 0.01$  M. Here, salt was added after total dissolution of the polymer (PD).

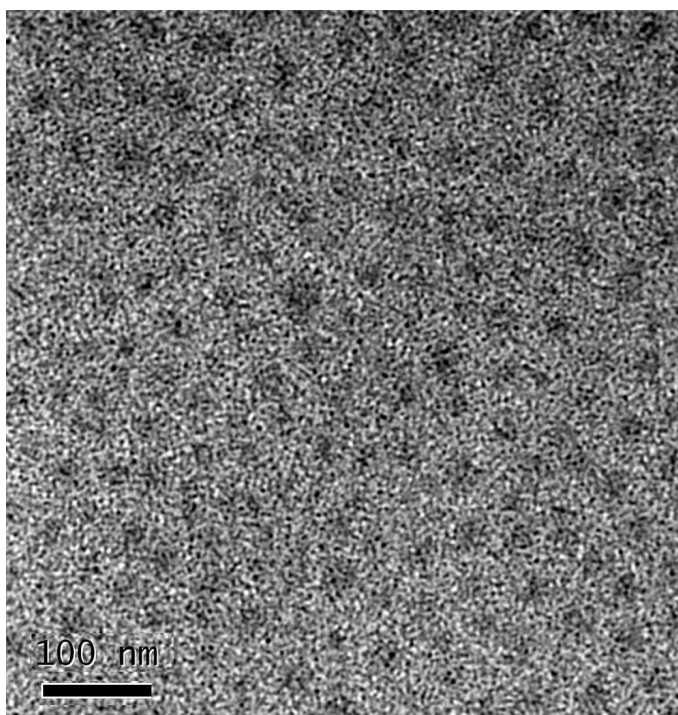


Fig. 7.2: Cryo-Tem image of  $PIB_{30}\text{-}b\text{-}PAA_{430}$ ,  $c_{Pol.} = 0.5$  wt-%,  $\alpha = 1$ ,  $c_{CsCl} = 0.1$  M,  $c_{TRIS} = 0.01$  M. Here, salt was added before dissolution of the polymer.

is shown. CsCl was chosen to increase the contrast between the PAA chains and the aqueous background. The sample was homogeneous and transparent, similar

to the samples described in our former work [15]. In the cryo-TEM image, clearly spherical particles with rather low polydispersity can be seen. Only in some areas of the cryo-TEM grid few larger aggregates can be found. The darker region of the spherical micellar assembly can be attributed to the hydrophobic PIB block of the diblock copolymer, forming the dense core of the micelle. The surrounding corona of PAA can not be seen due to too little contrast between the background solution (water, CsCl) and the PAA chains, which are stretched out into the solvent. As the coronae of the micelles are already overlapping, the PAA chains form a homogeneous background of the images. The almost regular arrangement of the micellar assemblies is due to the sample preparation for cryo-TEM. The blotting of excess solution from the TEM grid leads to a thin film with a thickness in the range of a monolayer of the micelles. Due to the high concentration the coronas are already in contact, forcing the assemblies to arrange in a dense regular packing.

The BD sample prepared for the cryo-TEM images shown in Figure 7.2 with Cs<sup>+</sup> as counterion, also show regularly shaped micellar assemblies with low PD. In the case of CsCl it can be stated that the BD and PD samples both were transparent and no precipitation occurred. Additionally the point of time of addition of the salt does not influence the shape and the size of the particles.

Assuming that the micelles seen in the cryo-TEM image in Figure 7.1 are forced to arrange in a dense packing, the coronae of the micellar assemblies should touch each other. Therefrom a radius  $R_{cryo}$  of the assemblies can be evaluated, being half the distance between two cores, evaluated to be mostly between 25 and 40 nm. Taking into account the bad contrast of the samples these results can be compared to DLS (see below).

### 7.3.2 Small Angle Neutron Scattering

In Figure 7.3 the scattering curves obtained from D<sub>2</sub>O samples prepared according PD method of PIB<sub>30</sub>-*b*-PAA<sub>430</sub> are shown. Already from qualitative evaluation an idea of the behavior and the changes of shape and size of the particles can be attained. The curves depicted are comparable to those measured with SANS of PIB<sub>*x*</sub>-*b*-PMAA<sub>*y*</sub> in our earlier work [15]. There, the curves were quantitatively treated with a model of a spherical core-shell structure with a PIB core and PMAA block forming the corona of the micellar assembly. Thus, in agreement with the cryo-TEM images, for PIB<sub>30</sub>-*b*-PAA<sub>430</sub> spherical micelles can be assumed as well.

An important result is the absence of a change in core size with increasing salt concentration, as the shapes of the scattering curves in the higher  $q$ -range ( $q > 0.02\text{\AA}^{-1}$ ) totally coincide. This strongly suggests, that the degree of aggregation,  $N_{agg}$ , does not change with increasing salt concentration. This indicates that the micelles are thermodynamically trapped, i.e. no exchange of unimers and therewith no change in the aggregation number and  $R_c$  is possible within the time-

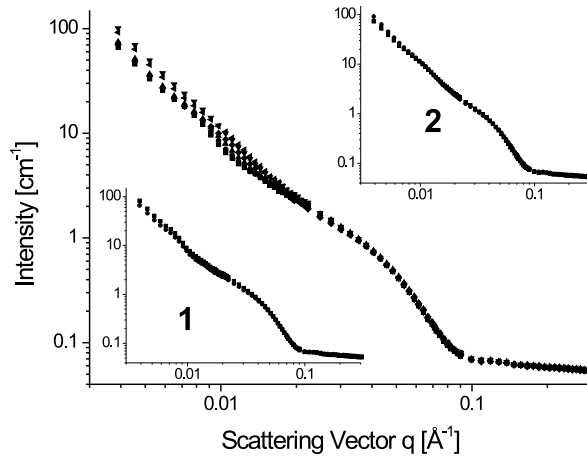


Fig. 7.3: SANS curves obtained from  $D_2O$  solutions (PD method) of  $PIB_{30}\text{-}b\text{-}PAA_{430}$  with different salt concentrations ranging from 0.1 M NaCl to 1.0 M NaCl (bottom to top). Insets: SANS curves from  $D_2O$  solutions of  $PIB_{30}\text{-}b\text{-}PAA_{430}$  at  $c_{NaCl} = 0.1$  M (1) and  $c_{NaCl} = 1.0$  M (2) prepared with PD (■) and BD (●) method,  $c_{POL.} = 1$  wt-%.

frame of the experiment. This is in striking contrast to the dynamic behavior of  $PIB_x\text{-}b\text{-}PMAA_y$ , where it was found that  $\overline{N_{agg}}$  changes upon external stimuli [15].

For comparison, also SANS samples according to method BD were prepared. In the insets in Figure 7.3 the samples with  $c_{NaCl} = 0.1$  M (1) and  $c_{NaCl} = 1.0$  M (2) for the BD (●) and PD (■) samples are presented. For both salt concentrations almost no difference in the scattering behavior can be seen. This strongly suggests that for the  $D_2O$  solutions the exchange of unimers leads to assemblies with almost the same size and structure and therewith scattering behavior.

### 7.3.3 Dynamic Light Scattering

For our measurements the samples were filtered (pore size 0.45  $\mu\text{m}$ ) prior to the measurements. This has to be taken into account when comparing the results with the results obtained from cryo-TEM images and SANS.

From the samples prepared for SANS, DLS measurements were carried out after a 50-fold dilution, leading to a final concentration of  $c_{Pol.} = 0.02$  wt-%. In Figure 7.4, for reasons of clarity, only the samples with  $c_{NaCl} = 0.2$  M for PD and BD samples are shown. Both samples were transparent and even after six months no precipitation occurred. From the slope of the plot of the decay rate,  $\Gamma$ , versus the square of the scattering vector,  $q$ , the diffusion coefficient of the species can be obtained. The slight deviation of the linear plot from a fit through the origin may come from a slight curvature of the measured points. This deviations can be attributed to the fact that the decay rate seen is an average decay rate of different diffusive species,

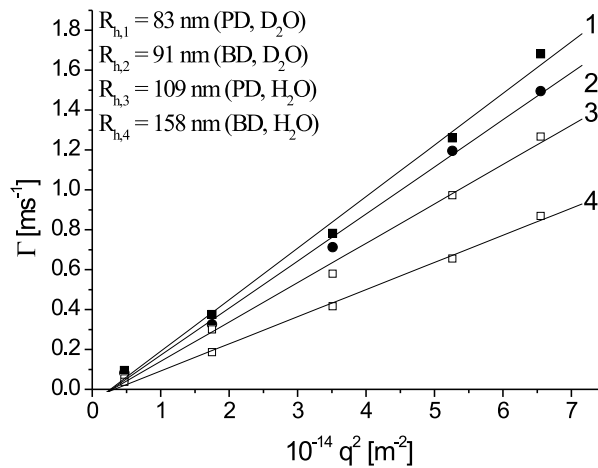


Fig. 7.4: Plot of decay rate  $\Gamma$  against  $q^2$  of  $\text{PIB}_{30}\text{-}b\text{-PAA}_{430}$  assemblies in  $\text{D}_2\text{O}$  solutions prepared according to PD (■) and BD (●) method and in  $\text{H}_2\text{O}$  solutions prepared according to PD (□) and BD (○) method at  $\text{pH} = 9$ ,  $c_{\text{NaCl}} = 0.2 \text{ M}$ ,  $c_{\text{Pol.}} = 0.02 \text{ wt-\%}$ .

as discussed later in this section.

Comparing the two curves, it can be stated that the overall size of the diffusing species is slightly smaller for the PD samples. This indicates a slight influence of the point of time of addition of salt in  $\text{D}_2\text{O}$ . Compared to the DLS results from the  $\text{H}_2\text{O}$  samples, the species are much smaller. The  $R_h$  of the  $\text{D}_2\text{O}$  samples can be evaluated from the diffusion coefficient with the Stokes-Einstein Equation to be 83 nm for the PD and 91 nm for the BD samples. The difference is not that pronounced as in the case of the  $\text{H}_2\text{O}$  samples with 109 nm (PD) and 158 nm (BD), respectively. One always has to keep in mind that the species seen from the evaluation from the slope of the plot of the decay rate versus  $q^2$  is an average of all species contributing to scattering, whether the distribution of the particle sizes is monomodal or multimodal.

Compared to cryo-TEM, the DLS results for the  $\text{D}_2\text{O}$  samples do not well agree on first glance. However, a weight-averaged distribution of radii can be obtained from the CONTIN-plot, derived from the intensity-weighted primary data by dividing by  $R^3$ . There the single peak from the rate distribution is split into a contribution from smaller particles and from larger assemblies. The latter ones are always in the range of more than 200 nm. The smaller micelles are evaluated to be around 30 to 40 nm for all samples. This result coincides with cryo-TEM, where particle radii in the range of 30 to 40 nm can be seen as well. As already mentioned, larger particles could also be stated in some regions of the TEM grid. Nevertheless the large assemblies cannot be incorporated in film of around 100 nm thickness, hence they will be removed during the film preparation process. The discrepancy with the results obtained from Figure 7.4 again can be explained by the fact that the average decay

rate for all species in the solution was used for the evaluation of this DLS. As the decay rate cannot be separated into different contributions from different species, this leads to a higher  $R_h$  due to the influence of larger particles.

After preparation of samples for DLS according to BD and PD method with NaCl as salt, it turned out that the behavior of those samples in water seems to be different. For solutions prepared according to the BD procedure, the samples

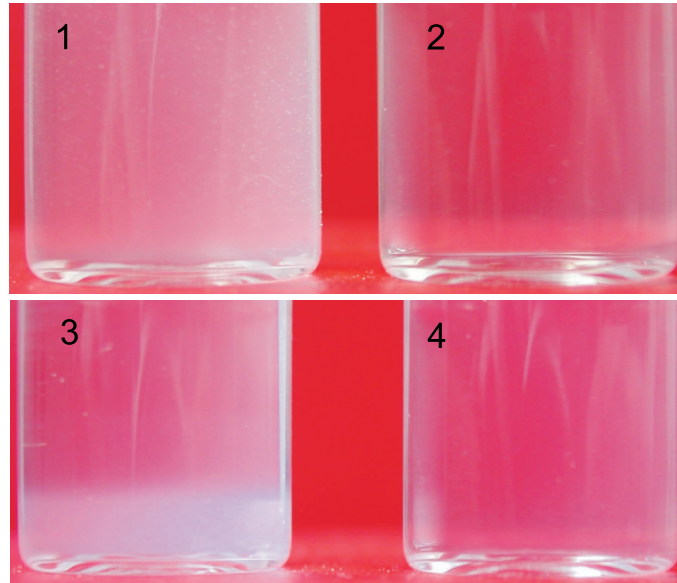


Fig. 7.5:  $PIB_{30}\text{-}b\text{-}PAA_{430}$  dissolved in NaOH after addition of salt (1, 3; BD) and before addition of salt (2, 4; AD). The final salt concentration was  $c_{NaCl} = 0.1\text{ M}$ ,  $pH = 9$ ,  $c_{TRIS} = 0.01\text{ M}$ ,  $c_{Pol.} = 0.2\text{ wt-}\%$ . Photos on top represent samples, which are freshly stirred, the photos below represent samples after one day without stirring.

are opaque, as shown in Figure 7.5, (image 1). This points to larger aggregates compared to the ones found for  $PIB_x\text{-}b\text{-}PMAA_y$  or to the proximity to a phase transition. Image (2) shows a polymer solution of identical composition prepared according to the PD procedure, i.e. salt is added after complete dissolution of the polymer. This solution optically behaves like the PMAA-based diblock copolymers investigated in our former work [15]. It is stable and no precipitation is observed (Figure 7.5 (image 4)) after stopping the stirring. In contrast to that, Figure 7.5 (image 3) shows the sample obtained from BD after one day without stirring. A clear zone of sedimented species can be seen. This strongly suggests non-equilibrium state of the system.

Additionally the behavior of BD samples with increasing salt concentration was investigated. Figure 7.6 shows aqueous solutions of freshly stirred solutions with (from left to right)  $c_{NaCl} = 0.1\text{ M}$ ,  $0.5\text{ M}$ , and  $1.0\text{ M}$ . With increasing salt concentration the turbidity of the solution increases. This suggests an increase in average size of the scattering particles.

An opportunity to make a system more dynamic is to increase its inner energy by

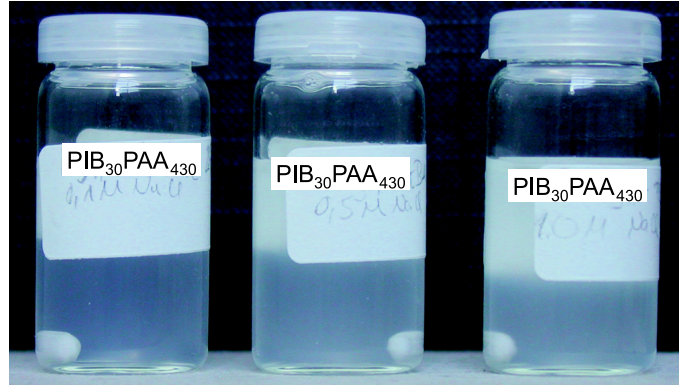


Fig. 7.6: Aqueous BD solutions of PIB<sub>30</sub>-*b*-PAA<sub>430</sub> with (from left to right)  $c_{NaCl} = 0.1$  M, 0.5 M and 1.0 M,  $c_{TRIS} = 0.01$  M,  $c_{Pol.} = 0.2$  wt-%.

heating it up. Therefore a more probable exchange between the different aggregates existing in solution may enable the equilibrium to be reached. But even heating up BD samples ( $c_{NaCl} = 0.1$  and 1.0 M) up to 80 °C for three days did not change the turbidity of the sample. The same can be stated by dialysis experiments. A sample prepared at  $c_{NaCl} = 0.5$  M was dialyzed over weeks against solutions with decreasing salt concentration, finally against Milli-Q water for one week. Here, also no change in turbidity of the samples could be observed. The fact, that the system does not change with temperature and ionic strength after addition of salt is a clear hint, that the preparation at higher ionic strength leads to "frozen" micelles that may not exist in equilibrium.

#### 7.3.4 Cryo-Transmission Electron Microscopy of H<sub>2</sub>O/NaCl-solutions

For comparison, samples with added NaCl (BD method) were investigated by means of cryo-TEM. From samples prepared according to BD with NaCl, after complete dissolution of the polymer and relaxation of the solution, a region with sedimentation is observed. To have an insight in the particle composition and shape, cryo-TEM images were taken from both supernatant solution and sedimented particles, shown in Figures 7.7 and 7.8, respectively. Comparing the two images, a clear difference in size of the particles can be seen. The aggregates show in Figure 7.7 are much smaller. Also the size distribution is more narrow for the particles in the supernatant solution. For the assemblies in the sedimented solution, some large aggregates in the range of 500 nm can be seen, explaining the more pronounced scattering of visible light and therewith the decreased transparency of the solution. In addition, the shape of the particles in Figure 7.8 is more irregular.

Compared to Figure 7.1, the difference is even more pronounced. On the one hand, the shape of the particles prepared according to PD is spherical, whereas the shape of the assemblies found in the BD sample is quite irregular. On the other hand, the size differs as well. Whereas in Figure 7.1 the size of the dark region,

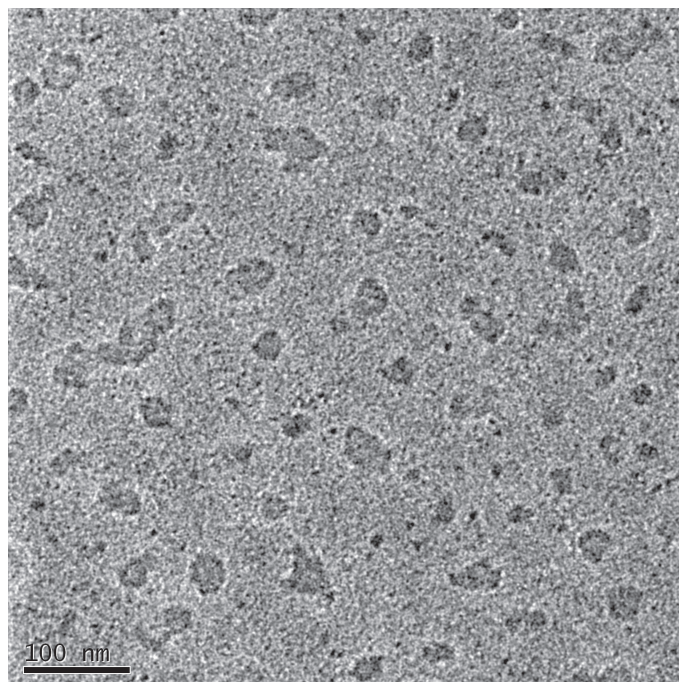


Fig. 7.7: Cryo-TEM image of the supernatant of PIB<sub>30</sub>-*b*-PAA<sub>430</sub> solution,  $c_{Pol.} = 0.5$  wt-%,  $\alpha = 1$ ,  $c_{NaCl} = 0.1$  M,  $c_{TRIS} = 0.01$  M. Here, salt was added before dissolution of the polymer (BD).

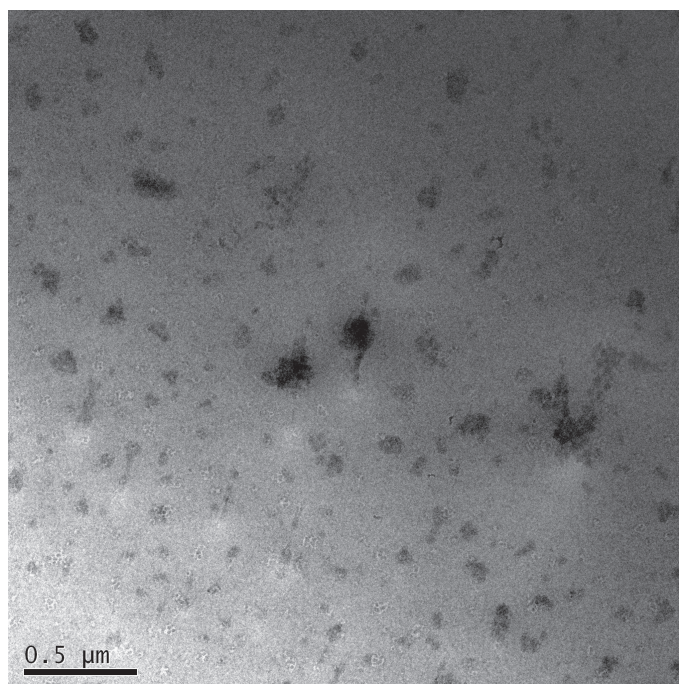


Fig. 7.8: Cryo-TEM image of the sedimented solution of PIB<sub>30</sub>-*b*-PAA<sub>430</sub> solution,  $c_{Pol.} = 0.5$  wt-%,  $\alpha = 1$ ,  $c_{NaCl} = 0.1$  M,  $c_{TRIS} = 0.01$  M. Here, salt was added before dissolution of the polymer (BD).

attributed to the core of the micelle, is in the range of 20 nm, in Figure 7.7 the core sizes mostly are 50-100 nm range. For both BD images, the size distribution is also broader than for the PD sample.

All these observations strongly suggest a strong influence of the point of time of addition of salt to the polymer on the structure of the polymeric assemblies formed in aqueous solutions. For the PD sample, an equilibrium state can be stated before addition of salt, shown by the low polydispersity as well as the regular shape of the assemblies. For the BD sample the investigation strongly points to non-equilibrium structures. The requirement for a thermodynamic equilibrium state, the possibility of exchange of unimers between the single assemblies, seems to be influenced by the added salt. The screening of the charges on the PAA chain of the diblock copolymer seems to hinder the expulsion of unimers.

Colombani *et al.* [16] reported on the micellisation of P*n*BA-*b*-PAA diblock copolymers. They also observed different sizes of the structures formed, depending on point of time of addition of salt. In their case, the spherical micelles obtained with the PD method are monodisperse and randomly distributed in the cryo-TEM images. On the contrary, the micelles obtained shortly after the dissolution of the polymer using the BD method are larger and they additionally tend to aggregate into clusters of micelles. They also report that neither light scattering, nor neutron scattering, nor cryo-TEM provides any significant evidence for structural rearrangements of the BD samples with respect to aggregation number and morphology upon external stimuli, which is typical for "frozen" micelles. The authors propose that the kinetics of unimer exchange is slower in the presence of added salt, attributed to the less hydrophilic nature of the PAA shell when charges are screened. Unimers are more easily expelled from micelles via Coulombic repulsion in salt-free solution, whereas they undergo hydrophobic attraction in a screened corona.

The same phenomenon can be seen in the work reported in this article. We also used PAA as hydrophilic block. Additionally, the core-forming block in our case is much more hydrophobic. To solubilize this PIB block additional energy is needed to bring it in an unfavorable polar surrounding. This may even lower the exchange rate, that is already reported to be quite low in the case of P*n*BA. Therefore the solutions may not be able to equilibrate after addition of salt.

### 7.3.5 Influence of Solvent and Counterion

This may also help explaining the difference observed for NaCl and CsCl containing samples. The BD sample prepared for the cryo-TEM images shown in Figure 7.2 with Cs<sup>+</sup> as counterion, also show regularly shaped micellar assemblies with low PD. As, related to the Bodenstein series of the alkaline metals, Na<sup>+</sup> is a much smaller and therefore harder ion compared to Cs<sup>+</sup>, the nature of interaction may change the behavior of the polymer.

For low molecular weight surfactants it is known, that surfactants with Cs<sup>+</sup> as a counterion are less soluble than those with Na<sup>+</sup>. This would be contradictory to our results, where the Na<sup>+</sup> species is less soluble. Up to now, this phenomenon cannot

be explained properly, although the results are reproducible. The effect of different counterions on the polyelectrolyte block still has to be investigated in more details.

The same can be stated for the influence of solvent nature on the micellar assemblies. Although it is already reported, that proteins behave differently in H<sub>2</sub>O and D<sub>2</sub>O solutions [24], the nature of the effect is not totally understood yet. It only can be stated that a difference in size for PD and BD solutions exists for both H<sub>2</sub>O and D<sub>2</sub>O as solvent and that this difference is larger for H<sub>2</sub>O.

The only two differences are the extent of difference in radius for PD and BD and the overall size. This would indicate a closer to equilibrium state for the D<sub>2</sub>O samples. As already mentioned more detailed investigations have to be carried out.

### 7.3.6 Comparison to PIB<sub>*x*</sub>-*b*-PMAA<sub>*y*</sub>

The behavior of PIB<sub>*x*</sub>-*b*-PAA<sub>*y*</sub> is rather unexpected, if compared to the solution behavior of a similar diblock copolymer, namely PIB<sub>*x*</sub>-*b*-PMAA<sub>*y*</sub>, as reported in our former work [15]. We observed no influence of the point of time of addition of salt to the polymer. Independent of counterion, always spherical particles as seen by means of cryo-TEM and SANS were obtained. Up to now it is not totally clear, why the PAA containing diblock behaves that differently.

With regard to the  $\alpha$ -methyl group of the PMAA it was already reported that the titration curves of both homopolymers are different, as the methyl group of the methacrylic moiety tends to change the conformation at lower pH values. This missing methyl group for the PAA containing block copolymer might have an lyophilizing influence on the polymer. Therefore the expulsion of unimeric polymer chains from assemblies might be energetically less favorable due to a higher energetic demands to solubilize the PIB. For the PMAA containing polymer, the methyl groups might facilitate this process. The added salt additionally screens the charges and hence makes the polymer chain even more hydrophobic and hence less mobile. This can only be stated by investigations of diblock copolymers with different PAA chains length to turn out the influence of the block length on the equilibration process of polymer solutions.

## 7.4 Conclusion

In this work the influence of point of time of addition of salt to an aqueous solution of a new diblock copolymer, namely Polyisobutylene-*block*-poly(acrylic acid) (PIB<sub>*x*</sub>-*b*-PAA<sub>*y*</sub>), is presented. By means of cryo-TEM of samples with CsCl as added salt, no effect on the shape of the particles formed in solution could be obtained, whether the salt was added before dissolution (BD) or after dissolution of the polymer (PD). For the BD samples, a relatively high polydispersity of the particles can be seen from cryo-TEM images. By means of SANS it can be stated, that for both

pathways of preparation of samples almost no difference in scattering behavior can be observed.

Investigations on polymer samples with NaCl in H<sub>2</sub>O solutions revealed an unexpected behavior of the polymer. Here, samples dissolved before addition of salt contain spherical micelles whereas for samples with salt added before dissolution of the diblock copolymer non-equilibrium structures are obtained. Additionally, for those samples, the sedimentation of a certain part of the polymer is another hint on larger aggregates, which are partially insoluble. For the PD samples, spherical micelles with a core-corona structure are visible in cryo-TEM images. Their PDI is quite low. This suggests that interparticle exchange of unimers between the micelles is possible, at least before addition of the NaCl.

Additionally it turned out, that samples in D<sub>2</sub>O result in smaller aggregates compared to H<sub>2</sub>O samples. For the latter one the difference in size of the assemblies formed for PD and BD samples is much more pronounced than for D<sub>2</sub>O samples.

Furthermore, it was shown, that changing the counterion to the "harder" Na<sup>+</sup> in H<sub>2</sub>O does not allow the formation of equilibrium structures for BD samples, as seen from the non-spherical structure in cryo-TEM images. Hence it can be concluded that the PIB<sub>*x*</sub>-*b*-PAA<sub>*y*</sub> solution behavior strongly depends on the treatment and way of preparation of the sample. Therefore it depends on the addition of salt, nature of counterion and solvent, whether equilibrium state of the solution can be obtained.

Compared to the results obtained from investigations on PIB<sub>*x*</sub>-*b*-PMAA<sub>*y*</sub>, the PIB<sub>*x*</sub>-*b*-PAA<sub>*y*</sub> copolymer behaves totally different. Especially the effect of the point of time of addition of salt is unexpected, as for PIB<sub>*x*</sub>-*b*-PMAA<sub>*y*</sub> solutions always equilibrated spherical particles were obtained.

### *Acknowledgment*

This work was supported by the European Union within the Marie Curie RTN Polyamphi and by DFG within the ESF EUROCORES Programme SONS. ILL is gratefully acknowledged for providing SANS beam time and travel support.

## BIBLIOGRAPHY

- [1] S. Förster, V. Abetz, A.H.E. Müller; *Adv. Polym. Sci.*, **2004**, *166*, 173;
- [2] A. Blom, C. Drummond, E.J. Wanless, P. Richetti, G.G. Warr; *Langmuir*, **2005**, *21*, 2779;
- [3] P. Rigler, W. Meier; *J. Am. Chem. Soc.*, **2006**, *128*, 367;
- [4] P. Pandit, S. Basu; *Environ. Sci. Technol.*, **2004**, *38*, 2435;
- [5] D.V. Pergushov, E.V. Remizova, J. Feldthusen, A.B. Zezin, A.H.E. Müller, and V.A. Kabanov; *J. Phys. Chem. B*, **2003**, *107*, 8093;
- [6] D.V. Pergushov, E.V. Remizova, J. Feldthusen, M. Gradzielski, P. Lindner, A.B. Zezin, A.H.E. Müller, and V.A. Kabanov; *Polymer*, **2004**, *45*, 367;
- [7] H. Schuch, J. Klingler, P. Rossmannith, T. Frechen, M. Gerst, J. Feldthusen, A.H.E. Müller; *Macromolecules*, **2000**, *33*, 1734;
- [8] D. Wang, J. Yin, Z. Zhu, Z. Ge, H. Liu, S.P. Armes, S. Liu; *Macromolecules*, **2006**, *39*, 7378;
- [9] S. Förster, N. Hermsdorf, C. Böttcher, P. Lindner; *Macromolecules*, **2002**, *35*, 4096;
- [10] O.V. Borisov, E.B. Zhulina; *Macromolecules*, **2002**, *35*, 4472;
- [11] E.B. Zhulina, O.V. Borisov; *Macromolecules*, **2002**, *35*, 9191;
- [12] H. Shen, A. Eisenberg; *Macromolecules*, **2000**, *33*, 2561;
- [13] R. Lund, L. Willner, J. Stellbrink, P. Lindner, D. Richter; *Phys. Rev. Lett.*, **2006**, *96*, 068302;
- [14] R. Lund, L. Willner, E.E. Dormidontova, D. Richter; *Macromolecules*, **2006**, *39*, 4566;
- [15] M. Burkhardt, N. Martinez-Castro, S. Tea, M. Drechsler, I. Babin, I. Grishagin, R. Schweins, D.V. Pergushov, M. Gradzielski, A.B. Zezin, A.H.E. Müller; *Langmuir*, submitted;

- 
- [16] Colombani, O.; Ruppel, M.; Schubert, F.; Zettl, H.; Pergushov, D.V.; Müller, A.H.E.; *Macromolecules*, **2007**, *40*, 4338;
- [17] O. Colombani, M. Ruppel, M. Burkhardt, M. Drechsler, M. Schumacher, M. Gradzielski, R. Schweins, A.H.E. Müller; *Macromolecules*, **2007**, *40*, 4351;
- [18] N. Martinez-Castro, M.G. Lanzendörfer, A.H.E. Müller, J.C. Cho, M.H. Acar, R. Faust; *Macromolecules*, **2003**, *36*, 6985;
- [19] X.F. Zhong, S.K. Varshney, A. Eisenberg; *Macromolecules*, **1992**, *25*, 7160;
- [20] M. Adrian, J. Dubochet, J. Lepault, A.W. McDowell; *Nature*, **1984**, *308*, 32;
- [21] B. Jacrot, G. Zacchai; *Biopolymers*, **1981**, *20*, 2413;
- [22] S.-H. Chen, T.-L. Lin; *Methods of Experimental Physics*, **1987**, Academic Press, 489;
- [23] GRAS<sub>ans</sub>P; Charles Dewhurst; email: dewhurst@ill.eu; Institut Laue Langevin, Grenoble, France;
- [24] T.K. Dam, C.F. Brewer; *Chem. Rev.*, **2002**, *102*, 387;

## 8. SUMMARY / ZUSAMMENFASSUNG

### Summary

In this work Polyisobutylene-*block*-poly(methacrylic acid) (PIB<sub>*x*</sub>-*b*-PMAA<sub>*y*</sub>) diblock copolymers with low polydispersity index (PDI) were studied according to their self-assembly in aqueous solutions. A wide range of hydrophobic PIB and hydrophilic PMAA block lengths were synthesized via combination of cationic and anionic polymerization. Investigations of the micellization in aqueous solutions by means of Small Angle Neutron Scattering (SANS) and Dynamic Light Scattering (DLS) point to an interesting dynamic behavior of such micelles reacting to an external stimulus of changes in pH from 10 to 5. The response is not only related to a change of the degree of neutralization of the PMAA block and therewith to a denser packing of these blocks in the corona. Quantitative evaluation of the SANS curves shows a change of the size of the hydrophobic core formed by the PIB blocks, due to a change of the aggregation numbers,  $\overline{N_{agg}}$ .

From cryogenic Transmission Electron Microscopy (cryo-TEM) images, a spherical shape of the micelles is clearly seen. This allows us to evaluate the SANS data using a model of a spherical particle with arms protruding into the solvent. Evaluation of the SANS curves evidences changes in the aggregation number,  $\overline{N_{agg}}$ , with pH and with ionic strength. In agreement with the theory for dynamic micelles with ionic blocks, an increase of pH leads to increasing charge on the arms formed by a weak polyacid. The corresponding repulsion increases the area at the core-corona interface, leading to decreasing values of  $\overline{N_{agg}}$  with rising pH. An increase in ionic strength has an opposite effect, resulting in higher  $\overline{N_{agg}}$  upon more pronounced screening of the charges of the PMAA blocks.

DLS measurements also show the response of the corona of the micelle on external stimuli such as changes in pH or ionic strength. The PMAA block stretches with rising number of charges. This leads to an increasing hydrodynamic radius,  $R_h$ . Here the hydrophilic block dominates the response of the micellar aggregate.

Potentiometric titrations demonstrate an effect of the ionic strength on the apparent  $pK_a$  value, shifting it to lower values with increasing  $c_{NaCl}$ , while the length of the hydrophilic block seems to play a minor role.

Concerning the evaluation of the Critical Micelle Concentration,  $cmc$ , of different diblock copolymers, the PIB block determines the properties of the micellar assemblies. The  $cmc$  clearly depends on the length of the hydrophobic PIB block. The

longer the block is, the lower the  $cmc$  is found to be.

In addition to the study of the pure  $PIB_x-b-PMAA_y$  micelles, a detailed investigation of water-soluble IPECs formed by  $PIB_x-b-PMAA_y$  with quaternized poly(4-vinyl pyridine) (P4VPQ) is presented. The complexes have a core-shell-corona structure. Based on cryo-TEM images, a spherical shape of the Interpolyelectrolyte Complexes (IPECs) can be concluded. Slight differences in the overall shape of the complexed micelle give an indication on the proposed structure.

The process of formation of complexes can be subdivided in a kinetically driven and a thermodynamically driven process. Upon addition of the polycation solution to the micellar  $PIB_x-b-PMAA_y$  solution, first an increase in turbidity of the solution can be observed. In this kinetically driven regime, large assemblies of micelles are formed. With time, these aggregates are equilibrating toward the thermodynamically more stable species of a single micelle with a complexed shell formed around the hydrophobic PIB core. The formation process can also be seen by means of SANS, leading to higher scattering intensity with increasing ratio of positive and negative charges of the polyelectrolyte species,  $Z$ .

Besides, SANS was used to follow the salt-induced dissociation of the complex. Increasing the ionic strength of the IPEC solution leads to a release of the polycation, starting from about 0.2 M NaCl. Beyond 0.5 M NaCl, almost no difference in scattering behavior of the IPEC solution compared to pure micellar solution can be stated. This strongly suggests a total dissociation of the IPEC. By means of titration with a sodium-selective electrode, the decrease of the activity of the  $Na^+$  ions can be explained by substitution of the polycation due to Manning condensation. After complete dissociation of the IPEC, the activity of the IPEC solution, upon addition of further NaCl, goes comparable to the behavior of a background solution.

Additionally a new diblock copolymer, namely Polyisobutylene-*block*-poly(acrylic acid) ( $PIB_x-b-PAA_y$ ), was synthesized via combination of cationic and anionic polymerization. For this polymer, the influence of the point of time of addition of salt to an aqueous solution was investigated. By means of cryo-TEM of samples with CsCl as added salt, no effect on the shape of the particles formed in solution could be obtained, whether the salt was added before dissolution (BD) or after dissolution of the polymer (PD). For the BD samples, a relatively high polydispersity of the particles can be seen from cryo-TEM images. By means of SANS it can be stated, that for both pathways of preparation of samples almost no difference in scattering behavior can be observed.

Investigations on polymer samples with NaCl in  $H_2O$  solutions revealed an unexpected behavior of the polymer. Here, samples dissolved before addition of salt contain spherical micelles whereas for samples with salt added before dissolution of the diblock copolymer non-equilibrium structures are obtained. Additionally, for the latter samples, the sedimentation of a certain part of the polymer is another

indication on larger aggregates, which are partially insoluble. For the PD samples, spherical micelles with a core-corona structure are visible in cryo-TEM images. Their PDI is relatively low. This suggests that interparticle exchange of unimers between the micelles is possible, at least before addition of the NaCl.

Additionally it turned out, that samples in D<sub>2</sub>O result in smaller aggregates compared to H<sub>2</sub>O samples. For the latter one the difference in size of the assemblies formed for PD and BD samples is much more pronounced than for D<sub>2</sub>O samples.

Furthermore, it was shown, that changing the counterion to the "harder" Na<sup>+</sup> in H<sub>2</sub>O does not allow the formation of equilibrium structures for BD samples, as seen from the non-spherical structure in cryo-TEM images. Hence it can be concluded that the PIB<sub>*x*</sub>-*b*-PAA<sub>*y*</sub> solution behavior strongly depends on the treatment and way of preparation of the sample. Therefore it depends on the addition of salt, nature of counterion and solvent, whether the equilibrium state of the solution can be obtained.

Compared to the results obtained from investigations on PIB<sub>*x*</sub>-*b*-PMAA<sub>*y*</sub>, the PIB<sub>*x*</sub>-*b*-PAA<sub>*y*</sub> copolymer behaves totally different. Especially the effect of the point of time of addition of salt is unexpected, as for PIB<sub>*x*</sub>-*b*-PMAA<sub>*y*</sub> solutions always equilibrated spherical particles were obtained.

The explanation for this phenomenon might be the missing  $\alpha$ -methyl group of the new polymer, which was already found to have an influence, e.g. in potentiometric titrations. More detailed investigations about the various opportunities of influencing the structures of the new polymer are beyond the scope of this thesis.

## Zusammenfassung

In dieser Arbeit wurden lineare Blockcopolymere, Polyisobutylen-*block*-poly(methacrylsäure) (PIB<sub>x</sub>-*b*-PMAA<sub>y</sub>), mit enger Molekulargewichtsverteilung untersucht, die in wässrigen Lösungen selbst aggregieren. Dazu wurden Polymere durch Kombination von kationischer und anionischer Polymerisation mit verschiedensten Blocklängen des hydrophoben PIB und des hydrophilen PMAA synthetisiert. Untersuchungen der Mizellbildung durch Kleinwinkelneutronenstreuung (SANS) und Dynamische Lichtstreuung (DLS) deuten ein interessantes dynamisches Verhalten derartiger Mizellen an, die auf äußere Veränderungen, z.B. des pH-Wertes von 10 auf 5, reagieren. Die Veränderung beschränkt sich nicht nur auf den Neutralisationsgrad des PMAA-Blockes und damit auf eine dichtere Packung der Mizellarme in der Korona. Die quantitative Auswertung der SANS-Kurven ergab, dass der hydrophobe Kern, der aus PIB besteht, durch eine Änderung der Aggregationszahl,  $\overline{N_{agg}}$ , die Größe ändert.

Cryo-Transmissionselektronenmikroskopiebilder (Cryo-TEM) zeigen kugelförmige Mizellen. Daher konnten die SANS-Daten durch Anwendung eines Modells kugelförmiger Teilchen mit in das Lösungsmittel hineinragenden Armen ausgewertet werden. Dadurch konnten die Änderungen der Aggregationszahl,  $\overline{N_{agg}}$ , mit dem pH-Wert und mit der Ionenstärke bewiesen werden. In Übereinstimmung mit der Theorie von dynamischen Mizellen mit ionischen Blöcken führt eine pH-Erhöhung zu steigender Ladungsdichte in den Armen, die aus einer schwachen Polysäure aufgebaut sind. Die damit einhergehende Abstoßung vergrößert den Platzbedarf pro Molekül an der Kern-Korona-Grenzfläche, wodurch die  $\overline{N_{agg}}$  mit steigendem pH sinkt. Eine ansteigende Ionenstärke hat durch größere Ladungsabschirmung in der PMAA-Kette den entgegengesetzten Effekt.

Auch DLS-Messungen zeigen eine Reaktion der Mizellkorona auf externe Stimuli wie Änderungen des pH-Wertes oder der Ionenstärke. Der PMAA-Block ist umso gestreckter, je höher die Ladungsdichte ist. Das führt zu einem Anstieg des hydrodynamischen Radius,  $R_h$ . Dabei dominiert der hydrophile Block die Mizellantwort.

Potentiometrische Titrations zeigen ebenfalls Auswirkungen der Ionenstärke auf den apparenten  $pK_a$ -Wert. Er wird mit steigender  $c_{NaCl}$  kleiner, während die PMAA-Blocklänge eine untergeordnete Rolle zu spielen scheint. Auch die kritische Mizellbildungskonzentration,  $cmc$ , wird hauptsächlich von der Länge des PIB-Blocks bestimmt. Sie wird mit zunehmendem PIB-Anteil kleiner.

Es wurden zudem detaillierte Untersuchungen von wasserlöslichen Interpolyelektrolytkomplexen (IPECs) durchgeführt, die aus PIB<sub>x</sub>-*b*-PMAA<sub>y</sub> durch Komplexbildung mit quaternisiertem Poly(4-vinylpyridin) (P4VPQ) hergestellt wurden. Es wurden Komplexe mit Kern-Schale-Korona Struktur erhalten. Cryo-TEM-Bilder zeigen kugelförmige IPECs. Unterschiede im Vergleich mit Bildern reiner Mizellen geben einen Hinweis auf die vorgeschlagene Struktur.

Der Prozess der Komplexbildung kann in einen kinetisch kontrollierten und einen thermodynamisch kontrollierten Prozess unterteilt werden. Durch Zugabe von Polykationlösung zu mizellarem  $\text{PIB}_x\text{-}b\text{-PMAA}_y$  wird anfangs eine Erhöhung der Trübung der Lösung beobachtet. Während dieser kinetisch kontrollierten Phase bilden sich größere Aggregate von Mizellen. Mit der Zeit equilibrieren sich diese Aggregate zu Gunsten von thermodynamisch stabileren separierten Mizellen, deren Kern vom hydrophoben Komplex umgeben ist. Der Prozess der Komplexbildung kann auch mittels SANS verfolgt werden. Hier resultiert er in Mizellen, deren Streuintensität umso höher ist, je größer das Ladungsverhältnis  $+/- (Z)$  ist.

Mit Hilfe von SANS wurde die salzinduzierte Dissoziation der Komplexe verfolgt. Eine Erhöhung der Ionenstärke der IPEC-Lösung hat eine Freisetzung des Polykations zur Folge. Dieser Vorgang beginnt ab einer Konzentration von etwa 0.2 M NaCl. Über 0.5 M NaCl verändert sich das Streuverhalten der IPEC-Lösung im Vergleich zur reinen Mizellösung kaum mehr. Das deutet stark auf eine komplette Dissoziation des Komplexes hin. Bei Titrationen konnte mit Hilfe einer  $\text{Na}^+$ -selektiven Elektrode eine Verringerung der Aktivität der  $\text{Na}^+$ -Ionen festgestellt werden. Dies lässt sich durch Substitution des Polykations durch  $\text{Na}^+$ -Ionen auf Grund von Manning-Kondensation erklären. Nach kompletter Dissoziation des Komplexes ist die Veränderung der Aktivität der IPEC-Lösung bei weiterer NaCl-Zugabe mit dem Verhalten der Hintergrundmessung vergleichbar.

Der Vergleich verschiedener Techniken zeigt, dass der Startpunkt der Komplexdissoziation bei Ionenstärken von etwa 0.2 M konstatiert werden kann. Unabhängig von sowohl der PIB- als auch der PMAA-Blocklänge ist die Dissoziation des IPECs bei  $c_{\text{NaCl}} \sim 0.5$  M vollständig abgeschlossen.

Darüberhinaus wurde ein neues Zweiblockcopolymer, Polyisobutylen-*block*-poly(acrylsäure) ( $\text{PIB}_x\text{-}b\text{-PAA}_y$ ) durch Kombination von lebend-kationischer und lebend-anionischer Polymerisations synthetisiert. Für dieses Polymer wurde der Einfluss des Zeitpunktes der Salzzugabe zu wässrigen Lösungen untersucht. Auf cryo-TEM-Aufnahmen von Proben, zu denen CsCl als Salz zugegeben wurde, konnte kein Einfluss des Salzes auf die Struktur der Teilchen in Lösung beobachtet werden, unabhängig davon, ob das Salz vor dem Auflösen (BD) oder nach dem Auflösen (PD) des Polymers zugegeben wurde. Für BD-Proben sieht man in Cryo-TEM Bildern eine relativ hohe Polydispersität der Aggregate. Mit Hilfe von SANS konnte gezeigt werden, dass die Strukturkurven der Proben beider Probenpräparationswege sich kaum unterscheiden.

Untersuchungen von Polymerproben mit NaCl als zugesetztem Salz in  $\text{H}_2\text{O}$  zeigen ein unerwartetes Verhalten. Hier bilden sich kugelförmige Mizellen in Proben, bei denen das Salz nach dem Lösen des Polymers zugegeben wurde, während sich in Proben, bei denen das Salz vor dem Lösen des Zweiblocks zugegeben wurde, große, schlecht definierte Strukturen ausbilden, die sich nicht im Gleichgewicht

befinden. Zusätzlich ist die Sedimentation von Teilen des Polymers ein weiterer Hinweis auf größere Aggregate, die teilweise unlöslich sind. Cryo-TEM Bildern zu Folge sind für PD-Proben kugelförmige Mizellen mit Kern-Korona Struktur erkennbar, deren Polydispersität sehr gering ist. Das lässt vermuten, dass der Austausch von Unimern zwischen den Aggregaten zumindest vor der Zugabe von Salz möglich ist.

Zudem zeigte sich, dass sich in D<sub>2</sub>O-Proben kleinere Aggregate ausbilden als in H<sub>2</sub>O-Proben. Für letztere sind außerdem die Größenunterschiede für PD- und BD-Proben weitaus ausgeprägter als für D<sub>2</sub>O-Proben.

Des Weiteren wurde gezeigt, dass ein Austausch des Gegenions zum "härteren" Na<sup>+</sup> für BD-Proben die Ausbildung von Gleichgewichtsstrukturen unmöglich macht, was man an Cryo-TEM-Bildern von mizellaren Teilchen mit unregelmäßigen Strukturen sieht.

Daher kann auf eine starke Abhängigkeit der PIB<sub>x</sub>-b-PAA<sub>y</sub>-Struktur von der Probenherstellung und -behandlung geschlossen werden. Es hängt von der Salzzugabe, dem Gegenion sowie dem Lösungsmittel ab, ob die Lösungen den Gleichgewichtszustand erreichen.

Im Vergleich zu den Untersuchungen zu mit PIB<sub>x</sub>-b-PMAA<sub>y</sub> verhält sich das PIB<sub>x</sub>-b-PAA<sub>y</sub> Blockcopolymer gänzlich unterschiedlich. Speziell die Auswirkung des Zeitpunktes der Salzzugabe ist unerwartet, zumal für PIB<sub>x</sub>-b-PMAA<sub>y</sub>-Lösungen immer sich im Gleichgewicht befindliche Strukturen erhalten wurden. Die Erklärung dieses Phänomens ist in der fehlenden  $\alpha$ -Methylgruppe des Polymers zu sehen, deren Einfluss schon in früheren Arbeiten bei potentiometrischen Titrations beobachtet wurde. Detailliertere Untersuchungen der zahlreichen Möglichkeiten, die Strukturen dieses neuen Polymers zu beeinflussen, übersteigen den Rahmen dieser Doktorarbeit.

## 9. ACKNOWLEDGMENT

Die vorliegende Arbeit wurde in der Zeit von August 2003 bis Juni 2007 am Lehrstuhl Makromolekulare Chemie II der Universität Bayreuth unter der Leitung von Prof. Dr. Axel H.E. Müller durchgeführt. Desgleichen möchte ich mich dafür bedanken, dass er es mir ermöglicht hat, bei zahlreichen internationalen Konferenzen, nicht nur im Rahmen des Marie-Curie RTN und des PolyAmphi Networks, mich mit wissenschaftlichen Beiträgen zu präsentieren.

Des weitern möchte ich mich bei Prof. Dr. Michael Gradzielski bedanken, der mich durch seine Diskussionsbereitschaft bei physiko-chemischen Fragestellungen unterstützt hat.

Mein Dank gilt beiden Professoren für die Bereitstellung dieses interessanten Themas und die Betreuung bei der Durchführung dieser Arbeit.

Zudem gilt mein Dank allen Mitarbeitern am Lehrstuhl "Makromolekulare Chemie II" für ihre Hilfsbereitschaft, die gute Zusammenarbeit und das angenehme Arbeitsklima während der gesamten Zeit. Weiterhin gilt mein Dank Sandrine Tea, Felix Schacher, Roland Walker und Ivan Grishagin, die durch ihre Praktika zum Gelingen dieser Arbeit mit beigetragen haben.

Meinen Eltern, die mir den nötigen Rückhalt gaben, danke ich für die finanzielle Unterstützung während meines gesamten Studiums. Ebenso möchte ich mich bei meiner Freundin bedanken, die mir in schwierigen Zeiten gleichermaßen den nötigen privaten Rückhalt gegeben hat.

## 10. LIST OF PUBLICATIONS

X. Andre, M. Burkhardt, M. Drechsler, P. Lindner, M. Gradzielski, A.H.E. Müller; **Schizophrenic micelles from a poly(acrylic acid)-block-poly (N,N-diethyl acrylamide) copolymer**, *PMSE Preprints*, **2007**, 96, 560-561

O. Colombani, M. Ruppel, M. Burkhardt, M. Drechsler, M. Schumacher, M. Gradzielski, R. Schweins, A.H.E. Müller; **Structure of Micelles of Poly(n-butyl acrylate) - block-poly(acrylic acid) Diblock Copolymers in Aqueous Solution**, *Macromolecules*, **2007**, 40, 4351-4362

A.H.E. Müller, O. Colombani, M. Burkhardt, M. Drechsler, M. Fink, M. Ruppel, M. Gradzielski, D.V. Pergushov; **Micellisation of block and graft copolymers of n-butyl acrylate and acrylic acid**, *Abstracts of Papers, 231st ACS National Meeting, Atlanta, GA, United States, March 26-30, 2006*, **2006**, COLL-387

S. Muthukrishnan, M. Zhang, M. Burkhardt, M. Drechsler, H. Mori, A.H.E. Müller; **Molecular Sugar Sticks: Cylindrical Glycopolymer Brushes**, *Macromolecules*, **2005**, 38, 7926-7934

D.V. Pergushov, M. Burkhardt, I.V. Grishagin, I.A. Babin, E.V. Remizova, M. Gradzielski, A.B. Zezin, V.A. Kabanov, A.H.E. Müller; **Interpolyelectrolyte complexes based on micelles of ionic amphiphilic diblock copolymers**, *Abstracts of Papers, 231st ACS National Meeting, Atlanta, GA, United States, March 26-30, 2006*, **2006**, COLL-317

D.V. Pergushov, M. Gradzielski, M. Burkhardt, E.V. Remizova, A.B. Zezin, V.A. Kabanov, A.H.E. Müller; **Novel "core-shell-corona" architectures via complexation of micelles of ionic amphiphilic diblock copolymers with oppositely charged polyelectrolytes**, *Polymer Preprints*, **2004**, 45, 236-237

P. Petrov, M. Bozukov, M. Burkhardt, S. Muthukrishnan, A.H.E. Müller, C.B. Tsvetanov; **Stabilization of polymeric micelles with a mixed poly(ethylene oxide)/poly(2-hydroxyethyl methacrylate) shell by formation of poly (pentaerythritol tetraacrylate) nano networks within the micelles**, *Journal of*

---

*Materials Chemistry*, **2006**, 16, 2192-2199

M. Schumacher, M. Ruppel, M. Burkhardt, M. Drechsler, O. Colombani, R. Schweins, A.H.E. Müller; **Novel class of organic-inorganic nanohybrids from functionalized silsesquioxane-based nanoparticles and micelles of poly(n-butyl acrylate)-block-poly(acrylic acid)**, *PMSE Preprints*, **2007**, 96, 374-375

Y. Xu, H. Becker, J. Yuan, M. Burkhardt, Y. Zhang, A. Walther, S. Bolisetty, M. Ballauff, A.H.E. Müller; **Double-grafted Cylindrical Brushes: Synthesis and Characterization of Poly(lauryl methacrylate) Brushes**; *Macromol. Chem. Phys.*, **2007**, *accepted*;

M. Burkhardt, N. Martinez-Castro, S. Tea, M. Drechsler, I. Babin, I. Grishagin, R. Schweins, D.V. Pergushov, M. Gradzielski, A.B. Zezin, A.H.E. Müller; **Polyisobutylene-block-poly(methacrylic acid) Diblock Copolymers: Self-Assembly in Aqueous Media**; *Langmuir*, **2007**, *Webreleasedate* : 15 – Nov – 2007;

M. Burkhardt, M. Ruppel, M. Drechsler, R. Schweins, D.V. Pergushov, M. Gradzielski, A.B. Zezin, A.H.E. Müller; **Water-Soluble Interpolyelectrolyte Complexes of Polyisobutylene-block-Poly(methacrylic acid) Micelles: Formation and Properties**; *Langmuir*, **2007**, *accepted*;

# Erklärung

Ich bestätige hiermit, dass ich die Arbeit selbständig verfasst und keine anderen, als die von mir angegebenen Quellen und Hilfsmittel benutzt habe.

Zudem bestätige ich hiermit, dass ich nicht anderweitig mit oder ohne Erfolg versucht habe, eine Dissertation einzureichen oder mich einer Doktorprüfung zu unterziehen.

Bayreuth, den 28. Juni 2007

---

Markus Burkhardt